

Synthesis, characterization and photophysical properties of visible light excited Eu^{3+} - β -diketonate complexes

**Thesis Submitted to the
Cochin University of Science and Technology in Partial
Fulfillment of the Requirements for the Degree of**

**DOCTOR OF PHILOSOPHY
in Chemistry under the Faculty of Science**

By

Biju Francis

**Under the Supervision of
Dr. M. L. P. Reddy**



**Chemical Sciences and Technology Division
CSIR-National Institute for Interdisciplinary Science and
Technology (CSIR-NIIST), Trivandrum 695 019, Kerala**

January 2016

DECLARATION

I hereby declare that the matter embodied in the thesis entitled “**Synthesis, characterization and photophysical properties of visible light excited Eu^{3+} - β -diketonate complexes**” is the result of investigations carried out by me at the Chemical Sciences and Technology Division of the CSIR-National Institute for Interdisciplinary Science and Technology (CSIR-NIIST), Trivandrum, under the supervision of Dr. M. L. P. Reddy and the same has not been submitted elsewhere for a degree.

In keeping with the general practice of reporting scientific observations, due acknowledgement has been made wherever the work described is based on the findings of other investigators.

Biju Francis

Thiruvananthapuram

January, 2016

NATIONAL INSTITUTE FOR INTERDISCIPLINARY SCIENCE AND TECHNOLOGY (NIIST)



Council of Scientific & Industrial Research
(CSIR)
(Formerly Regional Research Laboratory)
Industrial Estate P.O., Trivandrum - 695 019
Kerala, INDIA



Dr. M. L. P. Reddy
Chief Scientist & Head (Retired)
Materials Science and Technology Division

Tel: 91-471-2515 360
Fax: +91-471-2491 712
E-mail: mlpreddy55@gmail.com

CERTIFICATE

This is to certify that the thesis entitled “**Synthesis, characterization and photophysical properties of visible light excited Eu³⁺-β-diketonate complexes**” is a genuine record of research work carried out by **Mr. Biju Francis**, under my supervision at the Chemical Sciences and Technology Division of the CSIR-National Institute for Interdisciplinary Science and Technology (CSIR-NIIST), Trivandrum, in partial fulfilment of the requirements for the degree of Doctor of Philosophy of Cochin University of Science and Technology, and further that no part thereof has been presented before for the award of any other degree. All the relevant corrections and modifications suggested by the audience and recommended by the doctoral committee of the candidate during the presynopsis seminar have been incorporated in the thesis.

Thiruvananthapuram
January 06, 2016

Dr. M. L. P. Reddy
(Supervising Guide)

ACKNOWLEDGEMENTS

I am extremely grateful to Dr. M. L. P. Reddy, my thesis supervisor, for suggesting me the research problem and for his valuable guidance, support and encouragement, leading to the successful completion of this work.

I would like to express my sincere gratitude to Prof. Dr. Christoph Janiak for his constant support, valuable guidance and inspiration during my research stays at the Heinrich Heine University, Düsseldorf

I wish to thank Dr. A. Ajayaghosh, Director, Dr. Suresh Das and Dr. B. C. Pai, former Directors, CSIR-NIIST, for providing me the necessary facilities to carry out my work.

I sincerely thank my doctoral committee member, Dr. S. Prathapan, Cochin University of Science and technology (CUSAT), for all the help and support extended to me.

I deeply express my sincere gratitude to Prof. M. V. George for his constant support and inspiration during the tenure of this work.

I would like to thank Dr. P. Prabhakar Rao, Head, MSTD, CSIR-NIIST for his helps and support. I am grateful to Dr. D. Ramaiah, former Head, Chemical Sciences and Technology Division, CSIR-NIIST, for his help and support. I am also grateful to all scientists and staffs of CSTD and MSTD for all the help and support extended to me.

I deeply express my sincere thanks to Prof. Dr. Claus A. M. Seidel and Prof. Dr. Peter Gilch, Heinrich Heine University, Düsseldorf for the fruitful discussions and help they rendered. I sincerely thank Prof. Dr. Ricardo O. Freire, Universidade Federal de Sergipe, Brazil for his valuable help in theoretical studies. I would like to express my sincere thanks to Prof. Dr. Matthias Epple and Mr. Bernhard Neuhaus, University of Duisburg-Essen, for helping me to carry out bio-imaging experiments.

My sincere thanks to Ms. Soumini Mathew, Mr. B. Adarsh, Ms. Viji, Mr. M. Kiran, Mr. M. Aswin, Mr. Robert Philip, Mr Peter Zentis, Mr. Sascha Froebel, Mr. Karsten Klauke, Ms Susann Wegner and Mr. Hajo Meyer for their help in recording various spectral and morphological data.

I thank all the members of CSTD and MSTD, in particular, Dr. S. Biju, Dr. S. Raphael, Dr. V. S. Vishnu., Dr. G. Giable, Dr. M. Balamurugan, Dr. V. Divya, Dr. S. Sarika, Dr. A. R. Ramya, Ms. M. V. Lucky, Ms. P. Aiswaria, Ms. J. Sheethu, Mr. M. Bejoy, Mr. T. M. George, Ms. T. V. Usha Gangan, Ms. Anaswara, Mr. Ajay Kumar and Mr. Sreenath for their help and cooperation. I also thank all the former and present colleagues in my division for their help and support.

The support and companionship of the technical staffs and my dear friends at Heinrich Heine University, Düsseldorf, are also kindly acknowledged which made my stay memorable and comfortable at Heinrich Heine University, Düsseldorf.

Special thanks to Mr. Christian Heering, Mr. Gamall Makhloufi, Mr. Martin Davi, and Mr. Simon for the timely helps, companionship and support.

I always cherish the sincere support and help of my friends and senior colleagues Dr. Jubi John, Dr. Anas, Dr. Pratheesh, Dr. Praveen and Dr. Jatish for their care, loving companionship and ardent support.

I cannot forget the companionship of my dear friends Sinu, Rethesh, Vinayak, Rony, Krishnan, Jithesh, Shahul, Sankar, Deepak and Ajesh, for their love, care, companionship and support.

Special thanks to Mrs. Akkamma, Mrs. Valsala and Mrs. Daisy for preparing nice food for me during the period of my stay at CSIR-NIIST.

Words are inadequate to thank my dear Kunji for her love, fun, care, support and companionship.

I sincerely thank Dr. G. Devikarani, Dr. K. P. Subhash Chandran, Dr. K. S. Vijayalakshmi Amma, and all faculty members of Sri Vyasa N.S.S. College, Wadakkanchery for their encouragement and support.

I owe a lot to my family members and friends who encouraged and helped me at every stage of my personal and academic life, and longed to see this achievement come true.

I sincerely thank the Department of Science and Technology (DST), CSIR and DAAD for the financial support.

Above all, I bow before the Almighty for all his blessings.

Biju Francis

PREFACE

The fascinating photoluminescence properties of trivalent europium (Eu^{3+}) coordination compounds have aroused tremendous interest in recent years due to their potential applications ranging from biomedical analysis to material science. The Eu^{3+} ions have excellent luminescent features such as long-lived excited-state lifetimes (μs – ms range) and narrow, easily recognizable line-like red emission bands with large Stokes shifts. A big challenge in the chemistry of lanthanide ions is to develop luminescent europium complexes that can be sensitized by visible-light. This field has become much more important because of the demand for less-harmful labelling reagents in the life sciences and low-voltage-driven pure-red emitters in optoelectronic. Thus, the primary objective of the present research work is to design and develop novel visible-light sensitized Eu^{3+} - β -diketonate complexes with impressive photophysical properties.

The thesis comprises of four chapters which are presented as independent units and therefore the structure formulae, schemes, figures and references are numbered chapterwise. The introductory chapter highlights a background sketch of the use of β -diketonates as antenna ligands for Eu^{3+} ion, the recent developments in visible light excitable Eu^{3+} - β -complexes and an overview of the various methods of synthesis of Eu^{3+} -based silica hybrid materials, their photophysical properties and possible applications.

The second chapter deals with the synthesis, characterization and photophysical properties of a series of Eu^{3+} -complexes prepared with novel carbazole-based fluorinated β -diketones, namely, 4,4,5,5,5-pentafluoro-3-hydroxy-1-(9-phenyl-9H-carbazol-2-yl)pent-2-en-1-one (**L1**) and 4,4,5,5,5-pentafluoro-3-hydroxy-1-(9-(4-methoxyphenyl)-9H-carbazol-2-yl)pent-2-en-1-one (**L2**) as primary ligands and a bidentate phosphine oxide molecule, 4,5-bis(diphenylphosphino)-9,9-dimethylxanthene oxide (**DDXPO**) as ancillary

ligand. Using the Sparkle/PM3 model the molecular geometries of the designed complexes are optimized and the luminescent parameters are calculated by the LUMPAC software. The results demonstrated that suitably expanded π -conjugation in the developed Eu^{3+} -carbazole based β -diketonate complexes dramatically red-shifted the excitation maximum to the visible region ($\lambda_{ex, max} = 420 \text{ nm}$) with an impressive overall quantum yield (34–42%). The triplet state energy levels of **L1** and **L2** in the complexes are higher than that of the lowest excited level of Eu^{3+} ion, $^5\text{D}_0$, so the photoluminescence mechanism of the Eu^{3+} complexes was proposed as a ligand-sensitized luminescence process. The predicted luminescent parameters from the Sparkle/PM3 structures are in good agreement with the experimental data.

In the third chapter, a novel approach was developed for the design of visible light excitable luminescent silica nanoparticles, **Eu(L2)₃(DPOXPO)**, by the copolymerization of the silylated-bidentate phosphine oxide-based Eu^{3+} - β -diketonate conjugate, tetraethyl orthosilicate and (3-aminopropyl) triethoxysilane in a water-in-oil reverse microemulsion. The nanoparticles (35 nm) exhibit bright red luminescence with impressive quantum yield (38%) and long excited state lifetime (537 μs) values, when excited at 400 nm under physiological pH conditions. The nanoparticles were also successfully employed for the cell uptake studies with HeLa cells. The developed nanoparticles have excellent biocompatibility, monodispersability in aqueous dispersion and efficient luminescence under visible-light excitation and hence may find potential use in life sciences for bio-imaging applications.

The fourth chapter presents the synthesis, characterization and photophysical investigations of a novel fluorinated β -diketonate ligand and its corresponding Eu^{3+} ternary complex, **Eu(BBPPF)₃(DDXPO)**. Photoluminescence measurement results indicated that the europium(III) ternary complex exhibits intense red emission under UV irradiation with a solid-state quantum yield of 39%. An organic-inorganic mesoporous hybrid material, **Eu(BBPPF-Si)₃(DDXPO)/MCM-41**, was also constructed by linking

the developed **Eu(BBPPF)₃(DDXPO)** complex to the hexagonal mesoporous MCM-41. β -Diketonate grafted to the coupling agent 3-(triethoxysilyl)propyl isocyanate was used as the precursor for the preparation of hybrid material. **Eu(BBPPF-Si)₃(DDXPO)/MCM-41** exhibits an efficient intramolecular energy transfer process from the silylated β -diketonate to the central Eu³⁺, namely, the “antenna effect”, which favours a strong luminescence intensity (quantum yield = 43%). The excellent optical properties of the developed hybrid material suggest that it may find potential applications in various fields of optoelectronics.

In summary we have developed novel efficient visible light excitable Eu³⁺ complexes by molecular engineering. The experimental photophysical parameters of the developed complexes were compared with that derived from theoretical calculations and found in good agreement with each other. The photostability and water dispersibility of visible light excitable Eu³⁺ complex was improved by encapsulating the complex molecule into silica nanoparticles. The prepared luminescent nanoparticles were then employed for the cell uptake studies using HeLa cells. Further, we investigated the influence of a host matrix on the optical properties of a Eu³⁺- β -diketonate complex by incorporating it into mesoporous MCM-41.

ABBREVIATIONS

1. CHCl_3 Chloroform
2. CH_3CN Acetonitrile
3. CH_2Cl_2 Dichloromethane
4. CH_3OH Methanol
5. CIE Commission internationale de l'éclairage
6. DLS Dynamic Light Scattering
7. DMF *N,N'*-dimethylformamide
8. DMSO Dimethyl sulphoxide
9. DSC Differential Scanning Calorimeter
10. EtOH Ethanol
11. Eu^{3+} Trivalent Europium ion
12. FAB-MS Fast Atom Bombardment Mass Spectrometer
13. FT-IR Fourier Transform Infra-Red
14. ILCT Intraligand Charge Transfer
15. ISC Inter System Crossing
16. KBr Potassium bromide
17. K_2CO_3 Potassium carbonate
18. La^{3+} Trivalent Lanthanum ion
19. LMCT Ligand-to-Metal Charge Transfer
20. Ln^{3+} Trivalent Lanthanide ion
21. Lu^{3+} Trivalent Lutetium ion
22. MD Magnetic Dipole
23. MLCT Metal-to-Ligand Charge Transfer
24. NMR Nuclear Magnetic Resonance
25. OLED Organic Light Emitting Diode

26.	PL	Photoluminescence
27.	PMMA	poly(methyl methacrylate)
28.	ppm	Parts per million
29.	S ₁	Singlet
30.	SEM	Scanning Electron Microscopy
31.	Tb ³⁺	Trivalent Terbium ion
32.	T ₁	Triplet
33.	TEM	Transmission Electron Microscopy
34.	TGA	Thermogravimetric analysis
35.	UV-vis	Ultra Violet-visible
36.	Xe	Xenon
37.	XRD	X-Ray Diffraction

CONTENTS

	Page
Chapter 1 Ligand Sensitized Lanthanide Luminescence: An Overview	1-41
1.1. Abstract	1
1.2. Introduction	2
1.3. History and Significance of Europium	5
1.4. β -diketonates as antenna ligands for Eu^{3+} ion	6
1.5. Visible light excitable Eu^{3+} complexes	8
1.5.1. Visible light excitation <i>via</i> ancillary ligand modifications	8
1.5.2. Visible light excitation <i>via</i> β -diketonate ligand modifications	12
1.6. Eu^{3+} complexes-based luminescent silica hybrid materials	16
1.6.1 Sol-gel hybrid materials <i>via</i> doping or impregnation	16
1.6.2. Sol-gel hybrid materials <i>via</i> covalent attachment	17
1.6.3. Mesoporous silica hybrid materials	21
1.7. Applications of Eu^{3+} complexes based luminescent silica hybrid materials	24
1.7.1. Bio-imaging	24
1.7.2. Temperature imaging	27
1.7.3. White light generation	29
1.7.4 Sensing	31
1.7.5. Luminescent solar concentrators	33
1.8. Problem statements and objectives of the thesis	35
1.9. References	37
Chapter 2 Achieving Visible Light Excitation in Carbazole Based Eu^{3+}-β-diketonate Complexes <i>via</i> Molecular Engineering	42-80
2.1. Abstract	42
2.2. Introduction	43

2.3.	Experimental section	45
2.4.	Results and discussion	55
2.4.1.	Synthesis and characterization of ligands and Ln ³⁺ complexes	55
2.4.2.	Thermal behaviour of the complexes	57
2.4.3.	Molecular structures of the complexes by Sparkle/PM3 model	58
2.4.4.	Photophysical properties	63
2.4.5.	Comparison of experimental and theoretical luminescent parameters	74
2.5.	Conclusions	76
2.6.	References	78
Chapter 3	Amine Functionalized Silica Nanoparticles Incorporating Covalently Linked Visible Light Excitable Eu³⁺ Complexes: Synthesis, Characterization and Cell Uptake Studies	81-107
3.1.	Abstract	81
3.2.	Introduction	82
3.3.	Experimental section	85
3.4.	Results and discussion	92
3.4.1.	Synthesis and characterisation of DPOXPO and Eu ³⁺ complex	92
3.4.2.	Synthesis and characterisation of Si-DPOXPO and Eu(L2)₃(Si-DPOXPO)	93
3.4.3.	Synthesis and characterisation of nanoparticles	94
3.4.4.	Photophysical properties	97
3.4.5.	Cell uptake studies	102
3.4.6.	Cell viability studies	103
3.5.	Conclusions	104
3.6.	References	105
Chapter 4	Highly Efficient Luminescent Hybrid Materials Covalently Linking with Eu³⁺ Complexes via a Novel Fluorinated β-diketonate Ligand	108-141
4.1.	Abstract	108

4.2.	Introduction	109
4.3.	Experimental section	111
4.4.	Results and discussion	118
4.4.1.	Synthesis and characterization of HBBPPF and Eu^{3+} complex	118
4.4.2.	Synthesis and characterization of SiBBPPF-Na and hybrid material	120
4.4.3.	Photophysical properties	128
4.4.4.	Intramolecular energy transfer in Eu^{3+} complexes	134
4.5.	Conclusions	138
4.6.	References	139
	Summary of the Thesis	142
	Papers Presented at Conferences	143
	List of Publications	144

Chapter 1

Ligand Sensitized Lanthanide Luminescence: An Overview

1.1. *Abstract*

Ligand-sensitized luminescent Eu^{3+} complexes are of considerable importance because their unique optical properties find potential applications in various fields of optoelectronics and biochemistry. The development of such complexes for practical use requires the design of visible light excitable Eu^{3+} complexes with high luminescence quantum yields and lifetimes. Additional favorable properties such as high optical transparency, biocompatibility, hydrophilicity and easy surface functionalization, which are inherent to silica, have been realized in the developed Eu^{3+} complexes by employing sol-gel derived silica as the encapsulating matrix. The synergy between the intrinsic characteristics of silica matrices and the attractive optical properties of Eu^{3+} complexes gives rise to several luminescent hybrid materials with excellent properties. This chapter presents a background sketch of the use of β -diketonates as antenna ligands for Eu^{3+} ion, the recent developments in visible light excitable Eu^{3+} - β -complexes and an overview of the various methods of synthesis of Eu^{3+} -based silica hybrid materials, their photophysical properties and possible applications. Lastly, the problem statements and objectives of the thesis are formulated.

1.2. Introduction

Trivalent lanthanide ions (Ln^{3+}) are characterized by the gradual filling of their 4f orbitals from $4f^0$ (for La^{3+}) to $4f^{14}$ (for Lu^{3+}). These 4f orbitals are shielded from their external environment by the outer filled 5s and 5p orbitals.¹ So the optical properties of these Ln^{3+} ions, which arise due to the intra 4f-4f transitions, are somewhat independent of their external environment.² The Ln^{3+} ions have excellent luminescence features like long-lived excited-state lifetimes (μs – ms range) and narrow, easily recognizable sharp emission bands with large Stokes shifts.³ These exceptional optical properties of Ln^{3+} ions make them suitable for a variety of photonic applications ranging from biomedical analysis (fluoroimmunoassays and cellular imaging)⁴⁻⁷ to materials science (organic light emitting diodes and solar cells)⁸⁻¹¹ (Figure 1.1). Nevertheless, they exhibit very small molar absorption coefficients (less than $10 \text{ M}^{-1}\text{cm}^{-1}$) because of the parity forbidden intra 4f-4f transitions. Fortunately, this weak absorbance can be overcome by coordinating Ln^{3+} ions with suitable organic ligands with high molar absorption coefficients, which upon irradiation, absorb energy and transfer the absorbed energy to the metal center, thereby populating the Ln^{3+} excited levels.¹ This process was first observed by Weissman *et al.* in 1942 and later, in 1990, Lehn and co-workers coined the term “antenna effect” for this process (Figure 1.2).^{7, 12-14}

The important criteria to be satisfied by an organic molecule to act as an efficient antenna ligand for a particular Ln^{3+} ion are as follows (i) it should contain enough number of ligand binding sites to coordinate with Ln^{3+} ions (ii) its molar absorption coefficient should be high ($> 10^4 \text{ M}^{-1}\text{cm}^{-1}$) (iii) it should have a minimum number of high frequency oscillators such as $-\text{OH}$ or $-\text{NH}$ groups and most importantly, (iv) its

triplet state energy should match well with the emitting excited state energy of the corresponding Ln^{3+} ion.¹ According to Latva's empirical rule, this energy gap should be around $2000\text{-}4000\text{ cm}^{-1}$ for Eu^{3+} and $2500\text{-}4500\text{ cm}^{-1}$ for Tb^{3+} .¹⁵

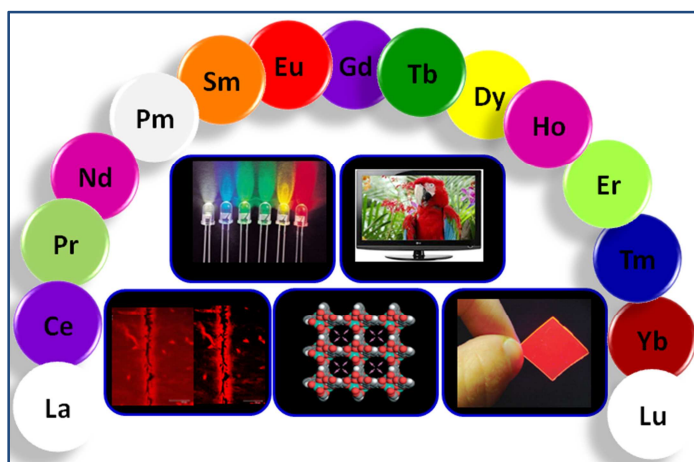


Figure 1.1. Lanthanide elements and some applications of lanthanide luminescence.

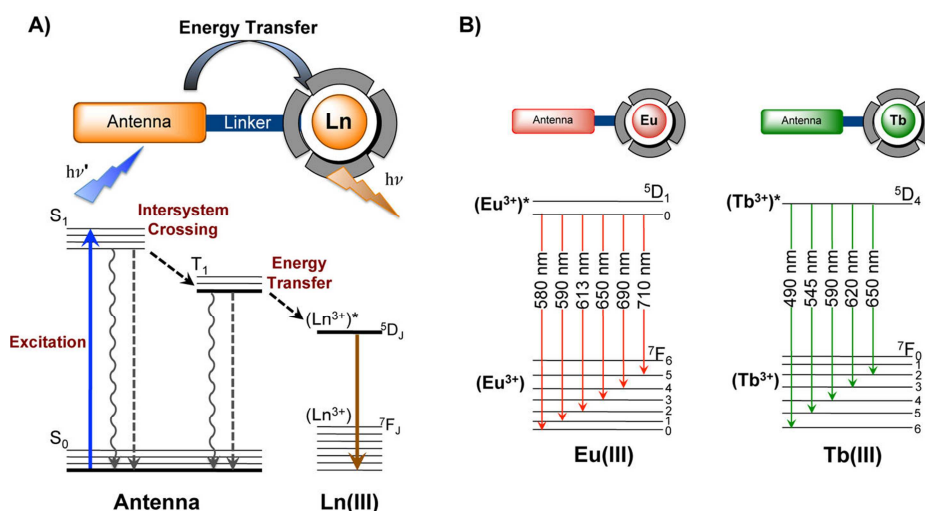


Figure 1.2. (A) The antenna effect and the mechanism of energy transfer from an organic ligand to the Ln^{3+} ion. (B) Luminescent 4f-4f transitions of Eu^{3+} and Tb^{3+} ions. Picture taken from reference 7.

Crosby and Whan proposed the commonly accepted mechanism of energy transfer from an organic ligand to the Ln^{3+} ion.¹⁶⁻¹⁸ Upon irradiation with UV or visible light, the organic ligands of the Ln^{3+} complex get excited to a vibrational level of first

excited singlet state ($S_0 \rightarrow S_1$). The molecule then undergoes fast internal conversion to lower vibrational levels of S_1 state. The excited singlet state may deactivate radiatively to the ground state ($S_1 \rightarrow S_0$, molecular fluorescence) or may undergo nonradiative intersystem crossing to the triplet state, T_1 . The triplet state, T_1 , may then radiatively deactivate to the ground state, S_0 ($T_1 \rightarrow S_0$, molecular phosphorescence) or may undergo nonradiative transition to an excited state of Ln^{3+} ion. Finally, from the excited state of the Ln^{3+} ion, the complex may deactivate radiatively to the ground state by its characteristic line-like emission bands or may undergo nonradiative transitions to the ground state (Figure 1.2). The photoluminescence of Ln^{3+} complexes is efficient only if the molecular fluorescence, phosphorescence or nonradiative transitions are minimized. The efficiency of photoluminescence can be expressed in terms of luminescence quantum yield, Φ , which is defined as the ratio of the number of photons emitted to the number of photons absorbed per unit time,¹⁹

$$\Phi = \frac{\text{Number of photons emitted}}{\text{Number of photons absorbed}}$$

For luminescent Ln^{3+} complexes, the overall luminescence quantum yield, Φ_{overall} , upon the excitation of the organic ligands can be determined by the ligand sensitization efficiency, η_{sens} , and the intrinsic quantum yield, Φ_{Ln} , of the Ln^{3+} ion:

$$\Phi_{\text{overall}} = \eta_{\text{sens}} \Phi_{\text{Ln}}$$

Φ_{Ln} is directly related to the rate constants for radiative deactivation (k_r) and nonradiative deactivation (k_{nr}), as:

$$\Phi_{\text{Ln}} = \frac{k_r}{k_r + k_{nr}}$$

The factor k_r is temperature independent. Back energy transfer from Ln^{3+} ion to the ligand and matrix vibrations (-OH or -NH) are the main processes contributing to k_{nr} .

1.3. History and Significance of Europium

In 1885, Sir William Crookes recorded the first signal from element 63 as he observed an unusual red line at 609 nm in the emission spectrum of a samarium sample.²⁰ In 1893, a French chemist, Paul-émile LeCoq de Boisbaudran, confirmed the existence of this band and detected a further green band at 535 nm.²⁰ However, the discovery of europium is credited to Eugène-Anatole Demarçay, who, in 1896, determined the presence of a new rare-earth element between samarium and gadolinium.²⁰ He isolated it in 1901, and proposed the name europium, with symbol 'Eu' for the new element. The most important sources of europium are the minerals bastnäsite, monazite, loparite and xenotime. Like other lanthanides, the most stable oxidation state of europium is +3, but +2 oxidation state is also present in some europium compounds. In 1906, French chemist Georges Urbain observed a bright red emission for yttrium oxide doped with europium. Thus europium found its place as an active component in red phosphorescent materials. Europium is also being used as a blue emitter since the divalent form, Eu^{2+} , emits in the blue region. Eu^{3+} (red), Tb^{3+} (green) and Eu^{2+} (blue) based phosphors can convert UV radiation into visible light.⁸ These phosphors are being used in various potential applications such as the cathode-ray tube or plasma-display panels, X-ray intensifying screens, etc. Recently, they have also been used in energy-saving fluorescent lamps and light emitting diodes.⁸ The amazing luminescence properties of Eu^{3+} ions make them ideal candidates as components in highly sensitive applications such as security inks, bar codes and

counterfeiting tags. When the European Union introduced its single currency, Euro, in 2002, they used a Eu^{3+} phosphor, believed to be a Eu^{3+} - β -diketonate complex, as an anticounterfeiting ink which gives an orange-red emission under UV irradiation (Figure 1.3).¹¹ There have also been some speculations that the greenish-blue emission observed under UV irradiation of the Euro notes is due to the presence of a Eu^{2+} phosphor.²⁰ Moreover, europium based compounds have widely been employed in many highly sensitive biomedical analyses and bio-imaging applications.⁴⁻⁶

Eu^{3+} ion is also interesting from a theoretical point of view. On account of its $4f^6$ configuration, the degeneracies of the $^{2S+1}L_J$ levels may partly or completely change due to the crystal-field perturbation induced by the host matrix.²¹ Furthermore, Eu^{3+} compounds can be used as spectroscopic probes for site symmetry determination by ascertaining the number of lines corresponding to the $^5D_0 \rightarrow ^7F_J$ transitions in the emission spectrum or the $^7F_0 \rightarrow ^5D_J$ transitions in the absorption spectrum.



Figure 1.3. Fifty Euro note illuminated at 365 nm.

1.4. β -diketonates as antenna ligands for Eu^{3+} ion

β -diketonates are the most important class of ligands for Eu^{3+} ions because of the close match in the energy of their triplet state with the emitting state, 5D_0 , of Eu^{3+} ion.¹⁹ These ligands contain negatively charged binding site that results in the

formation of neutral, 3:1 ligand-europium complexes. β -Diketonate ligands with aromatic substituents exhibit strong absorption over a substantial wavelength range, which is one of the main criteria to be satisfied by an organic ligand to act as an efficient antenna ligand for Ln^{3+} ions. The synthesis, photophysical properties and applications of Eu^{3+} - β -diketonate complexes are well documented in various review articles.^{6, 7, 22, 23} Figure 1.4 displays some of the most commonly used β -diketonate ligands for Eu^{3+} ion.¹⁹

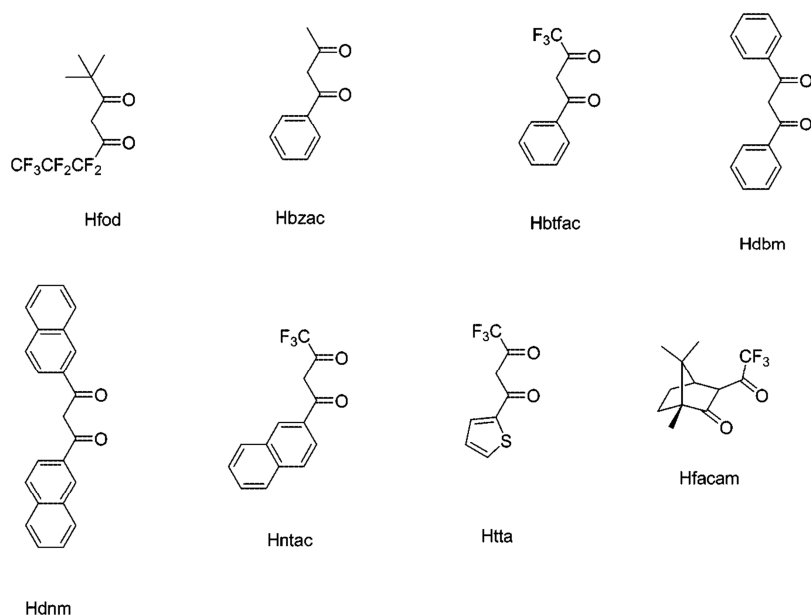


Figure 1.4. Molecular structure of some β -diketonate ligands for Eu^{3+} ion.

Because of the high coordination number of Eu^{3+} ion (usually 8 or 9), it is very difficult to isolate the Eu^{3+} - β -diketonate complexes in anhydrous forms. Generally, in addition to the organic ligand, water or other solvent molecules will also be present in the coordination sphere of Eu^{3+} ions. The presence of these solvent molecules with high frequency oscillators such as $-\text{OH}$ or $-\text{NH}$ groups will effectively quench the Eu^{3+} luminescence by the activation of nonradiative decay pathways. It is well known that the replacement of the solvent molecules with certain

ancillary ligands such as bidentate nitrogen donor ligands or phosphine oxides (Figure 1.5) will result in the enhancement of luminescence intensities and lifetimes of Eu^{3+} complexes.²⁴ These ancillary ligands not only saturate the coordination sphere of Eu^{3+} ion, but also give additional rigidity to the resulting complexes.

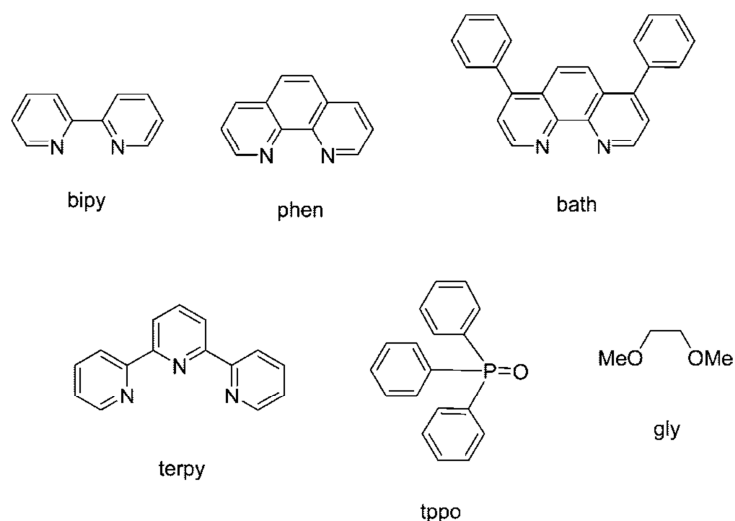


Figure 1.5. Molecular structure of some ancillary ligands for Eu^{3+} ion.

1.5. Visible light excitable Eu^{3+} complexes

Despite the attractive optical properties of Eu^{3+} - β -diketonate complexes, the excitation wavelengths of most them are in the UV region, which in turn limits their practical use in various biological applications. UV irradiation is harmful for living tissues and the pump sources for UV excitation are comparatively costly. When compared to UV irradiation, visible light excitation reduces the background fluorescence of the biomaterial, causes less photodecomposition of the emitting species, allows better tissue penetration, is less harmful to the biological tissues and is a cheaper excitation source.²⁵ Hence the development of visible light excitable Eu^{3+} complexes has become much more relevant. Usually two approaches are implemented to achieve visible light excitation in Eu^{3+} complexes. One is to

introduce 4d or 5d transition metal complexes such as Ir(III) or Pt(II) complexes in to Eu^{3+} complexes, which can transfer energy to the Eu^{3+} ion. However, the luminescence efficiencies of these systems, which are based on the $^3\text{MMLCT}$ (metal-metal-to-ligand charge transfer) or $^3\text{MLCT}$ (metal-to-ligand charge transfer) is usually very low.²⁶ Another approach, that which is employed in this work, is the expansion of the π -conjugation of the system by the modification of the organic ligands.

1.5.1 Visible light excitation in Eu^{3+} complexes via ancillary ligand modifications

In 1994, Bunzli and co-workers reported mixed Eu^{3+} complexes of some β -diketonates and o-phenanthroline, which displayed absorption bands in the near UV region, 380–400 nm, but exhibited very low luminescence quantum yields upon ligand excitation.²⁷ Then in 1999, Werts and co-workers mixed Michler's ketone [4,4'-bis(*N,N*-dimethylamino)benzophenone] and $\text{Eu}(\text{fod})_3$ [europium-tris(6,6,7,7,8,8-heptafluoro-2,2-dimethyloctane-3,5-dione)] in benzene, and observed a red glow under daylight illumination.²⁸ The excitation and emission spectra of the resulting complex, MK- $\text{Eu}(\text{fod})_3$, demonstrated that the red glow is due to the characteristic sharp emission bands of Eu^{3+} ion and the excitation spectra extends well beyond 450 nm, with a maxima at around 414 nm, indicating that the compound can be excited by visible light (Figure 1.6). The complex exhibited a luminescence quantum yield of 17% in aerated solution and 20% after deoxygenation, at an excitation wavelength of 420 nm. Here the authors predicted a triplet pathway mechanism for the sensitization of Eu^{3+} ions by Michler's ketone.

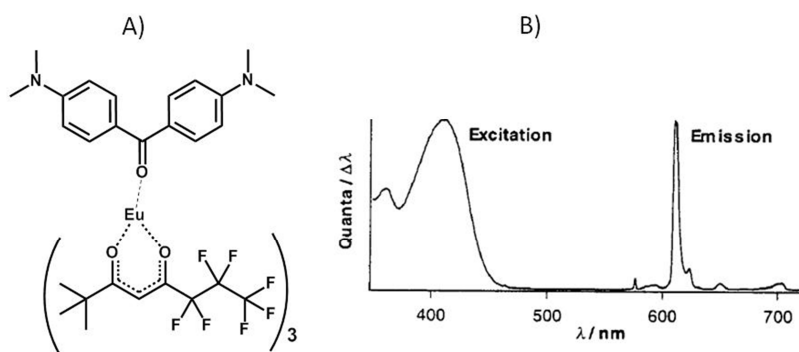


Figure 1.6. (A) Molecular structure of MK-Eu(fod)₃. (B) luminescence excitation ($\lambda_{em} = 612$ nm) and emission ($\lambda_{ex} = 450$ nm) spectra of a solution of 10^{-5} M Michler's ketone and 10^{-4} M Eu(fod)₃ in benzene. Picture taken from reference 28.

In 2004, Wang and co-workers demonstrated the singlet pathway mechanism for the first time in a visible-light-sensitized europium tris-thenoyltrifluoroacetato-2-(*N,N*-diethylanilin-4-yl)-4,6-bis(3,5-dimethyl-pyrazol-1-yl)-1,3,5-triazine complex [Eu(tta)₃(dpbt)] (Figure 1.7. (A)).²⁹ The ancillary ligand, 2-(*N,N*-diethylanilin-4-yl)-4,6-bis(3,5-dimethyl-pyrazol-1-yl)-1,3,5-triazine (dpbt), was responsible for the visible light excitation of the complex. Coordination of the ligand dpbt to Eu³⁺ ion resulted in a red shift in the dpbt ligand charge-transfer (CT) absorption band from 387 nm to 406 nm. Upon selective excitation of the ligand CT band at room temperature, the emission spectrum of Eu(tta)₃(dpbt) complex displayed a broad band centered at 430 nm, from the coordinated dpbt ligand, and the characteristic emission peaks of the ⁵D₀ → ⁷F_J transitions of the Eu³⁺ ion. Here, the overall luminescence quantum yields for the emissions from the Eu³⁺ ion and the coordinated ligand in toluene were determined as 52% and 27%, respectively ($\lambda_{ex} = 402$ nm). Later they modified the dpbt ligand by replacing four methyl groups with hydrogen atoms and synthesized the corresponding Eu³⁺ complex, Eu(tta)₃(bpt), where bpt is 2-(*N,N*-diethylanilin-4-yl)-4,6-bis(pyrazol-1-yl)-1,3,5-triazine (Figure 1.7. (B)).³⁰ The excitation window of the new complex was much broader

than that of $\text{Eu}(\text{tta})_3(\text{dpbt})$ with a red edge extending up to 450 nm in a dilute toluene solution (1.0×10^{-5} M) and 500 nm in a more concentrated toluene solution (1.0×10^{-2} M). Upon visible-light excitation ($\lambda_{\text{ex}} = 410$ nm) at 295 K, the authors also observed a 23% enhancement in the overall luminescence quantum yield of $\text{Eu}(\text{tta})_3(\text{bpt})$ complex. Ziessel and co-workers also designed a series of visible light sensitized Eu^{3+} complexes, using tta as primary ligand and new ancillary ligands based on neutral tridentate heteroaromatic coordinating units.³¹ Shi and co-workers developed a tetrakis Eu^{3+} complex, $\text{Eu}(\text{tta})_4(\text{DEASPI})$, where DEASPI is [trans-4-[p-(N,N-diethylamino)styryl]-N-methylpyridinium cation].³² When excited at 485 nm, the complex exhibited a broad ligand band at around 580 nm along with the characteristic emission peaks of Eu^{3+} ion.

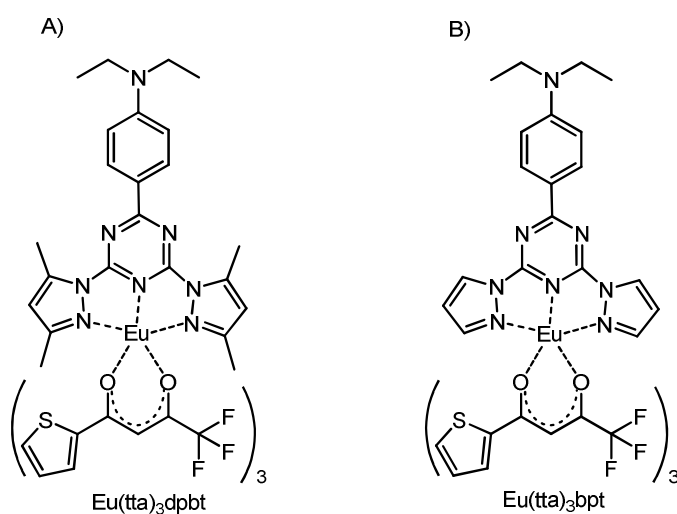


Figure 1.7. Molecular structure of Eu^{3+} complexes (A) $\text{Eu}(\text{tta})_3\text{dpbt}$ and (B) $\text{Eu}(\text{tta})_3\text{bpt}$. References 29,30.

While these reported Eu^{3+} complexes could achieve visible light excitation, some of them were stable only in solvents like benzene and toluene. Also some of the above mentioned adducts could not be obtained in the solid state and had to be made *in situ*. These factors significantly limited their practical applicability.

1.5.2 Visible light excitation in Eu^{3+} complexes via β -diketonate ligand modifications

In 2004, Van Deun and co-workers developed a visible light excitable Eu^{3+} complex, $\text{Eu}(\text{PHN})_3(\text{H}_2\text{O})(\text{DMF})$, using 9-hydroxyphenal-1-one (HPHN) as the antenna ligand (Figure 1.8).³³ Even though the complex exhibited the characteristic emission bands of Eu^{3+} ion when excited at 458 nm, the luminescence quantum yield and the excited state lifetime of this complex were found to be very low. The authors pointed out two possible reasons for the low quantum yield value: (i) the close matching of the triplet energy of the ligand with the emitting Eu^{3+} ion which causes back energy transfer from Eu^{3+} ion to the ligand and (ii) the poor shielding of the europium ion from the external environment.

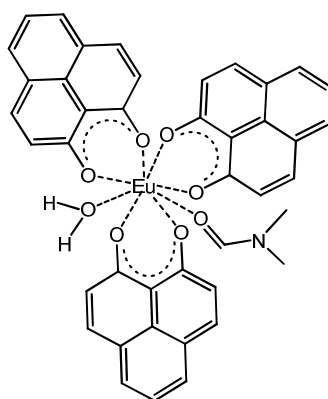


Figure 1.8. Molecular structure of $\text{Eu}(\text{PHN})_3(\text{H}_2\text{O})(\text{DMF})$. Reference 33.

Carbazole-based ligands are widely acknowledged for their role as visible light sensitized antenna molecules for the Eu^{3+} ion by virtue of their modest cost, excellent hole transporting properties, easily tunable optoelectronic properties and their high chemical and environmental stabilities.³⁴ In 2009, Gong and co-workers reported two novel carbazole-based β -diketonate ligands, 2-(4'4'4'-trifluoro-1'3'-dioxobutyl)-carbazole (2-T-FDBC) and 2,7-bis(4'4'4'-trifluoro-1'3'-dioxobutyl)-carbazole (2,7-

BTFDBC) and their corresponding Eu^{3+} complexes [$\text{Eu}(2\text{-TFDBC})_3(\text{phen})$, $\text{Eu}(2,7\text{-BTFDBC})_3(\text{phen})_2$] using 1,10-phenanthroline as ancillary ligand (Figure 1.9).³⁵ Compared to the excitation spectra of their previously reported similar β -diketonate complexes, linked at 3- and 6- positions in the carbazole ring,^{36, 37} the excitation spectra of the newly developed Eu^{3+} complexes exhibited a red shift of around 30 nm and extended up to 500 nm, because of their increased π -conjugation. Further, because of this increased π -conjugation, the excitation spectra of $\text{Eu}_2(2,7\text{-BTFDBC})_3(\text{phen})_2$ exhibited a larger red shift than $\text{Eu}(2\text{-TFDBC})_3(\text{phen})$ complex. The solid state luminescence quantum yields were recorded as 28% for $\text{Eu}(2\text{-TFDBC})_3(\text{phen})$ and 10% for $\text{Eu}_2(2,7\text{-BTFDBC})_3(\text{phen})_2$. The predicted reason for the decrease in the quantum yield of $\text{Eu}_2(2,7\text{-BTFDBC})_3(\text{phen})_2$ complex was the concentration quenching arising from the metal-metal centres being in close proximity. Later, by introducing an electron donating methoxy group in the 7-position of the carbazole ring of $\text{Eu}(2\text{-TFDBC})_3(\text{phen})$, they successfully increased the electron density of the complex and thereby improved the excitation band intensity in the blue region.³⁸ A 60% enhancement in the integrated emission intensity of the new complex, $\text{Eu}(\text{EMOCTFBD})_3(\text{phen})$, was observed when compared to the complex $\text{Eu}(2\text{-TFDBC})_3(\text{phen})$. Further, a bright red-emitting diode was fabricated by coating the new Eu^{3+} complex, onto a ~ 460 nm-emitting InGaN chip. Here also, introducing a $-\text{CF}_3$ group on the 7-position of the carbazole skeleton in $\text{Eu}(2\text{-TFDBC})_3(\text{phen})$, improved the luminescence quantum yield of the corresponding Eu^{3+} complex, $\text{Eu}(\text{ETFMCTFBD})_3(\text{phen})$, to 34%.³⁹ Yuan and co-workers synthesized a new visible light excitable Eu^{3+} complex, BHHBB– Eu^{3+} –BPT (BHHBB: 1,2-bis[4'-(1'',1'',1'',2'',2'',3'',3''-heptafluoro-4'',6''-hexanedion-6''-yl)-

benzyl]-benzene; BPT: 2-(N,N-diethylanilin-4-yl)-4,6-bis(pyrazol-1-yl)-1,3,5-triazine), and used it for cell imaging applications.⁴⁰

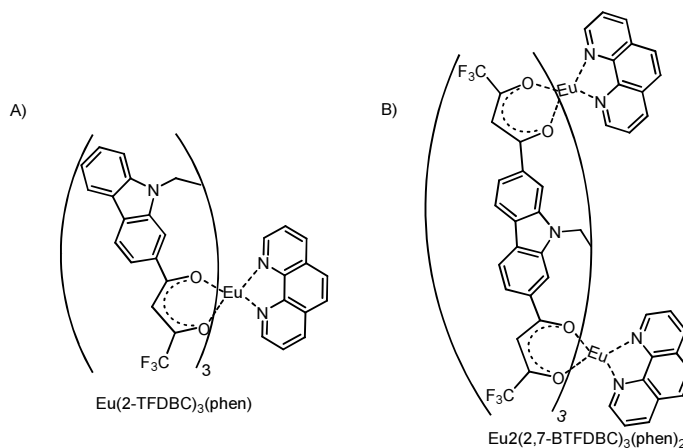


Figure 1.9. Molecular structures of (A) $\text{Eu}(\text{2-TFDBC})_3(\text{phen})$ and (B) $\text{Eu}(\text{2,7-BTFDBC})_3(\text{phen})_2$. Reference 35.

In 2011, Reddy and co-workers investigated the effect of π -conjugation on the excitation spectra of a series of Eu^{3+} complexes by introducing phenyl, naphthyl and biphenyl groups in to the 3-position of a fluorene based β -diketonate ligand.²⁶ The complex with biphenyl substituted ligand exhibited a remarkable red shift in the excitation window, which extended up to 500 nm. They also reported a high solid state luminescence quantum yield of 43% at an excitation wavelength of 440 nm. In 2013, they developed a visible light excitable Eu^{3+} complex, $\text{Eu}(\text{pfppd})_3(\text{tpy})$, using a highly fluorinated fluorene based β -diketone, 4,4,5,5,5-pentafluoro-3-hydroxy-1-(phenanthren-3-yl)pent-2-en-1-one (Hpfppd), as the primary ligand and 2,2':6,6''-terpyridine as the ancillary ligand (Figure 1.10. (A)).⁴¹ They reported the highest solid state luminescence quantum yield (75%) of Eu^{3+} complex under blue light excitation (415 nm). Further, they employed this Eu^{3+} complex for live cell imaging in rat embryonic heart cell line, H9c2, and it showed mitochondria specific localization (Figure 1.10. (B)).⁴² Very recently, they developed a series of visible

light excitable Eu^{3+} complexes using three novel aminophenyl based polyfluorinated β -diketonates, namely, 1-(4-aminophenyl)-4,4,5,5,5-pentafluoro-3-hydroxypent-2-en-1-one (HAPFP), 1-(4-(dimethylamino)phenyl)-4,4,5,5,5-pentafluoro-3-hydroxypent-2-en-1-one (HDMAPFP) or 1-(4-(diphenylamino)phenyl)-4,4,5,5,5-pentafluoro-3-hydroxypent-2-en-1-one (HDPAPFP) as the primary ligands and a bidentate phosphine oxide molecule, 4,5-bis(diphenylphosphino)-9,9-dimethylxanthene oxide (DDXPO) as the ancillary ligand.⁴³ The Eu^{3+} complex with DPAPFP ligand as primary ligand and DDXPO as neutral donor, exhibited intense red emission under blue light excitation ($\lambda_{ex} = 400 \text{ nm}$) with a luminescence quantum yield of 40 % and an excited state lifetime of 551 μs . The conjugation between nitrogen lone pair electrons and the phenyl π -electrons in the DPAPFP ligand was put forward as the reason for the red shift in the excitation window. Recently, Borisov and co-workers developed a visible light excitable Eu^{3+} complex using 8-hydroxyphenalenone as the primary ligand.⁴⁴ The absorption spectrum of the complex exhibited several bands in the blue region which enabled the visible light excitation. The authors reported a luminescence quantum yield of 20% for the Eu^{3+} complex and successfully employed the developed complex for sensing of oxygen.

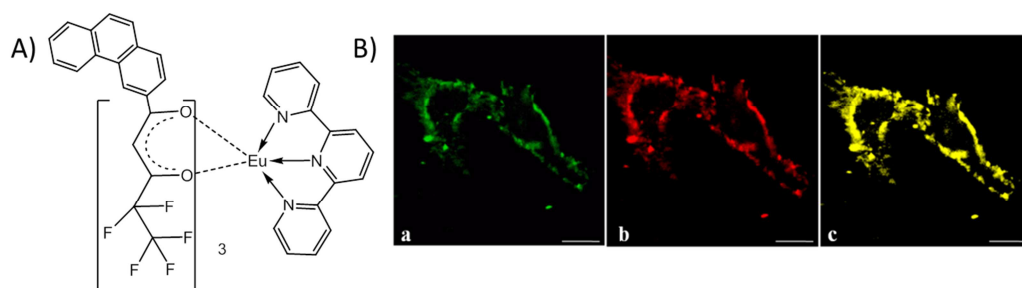


Figure 1.10. (A) Molecular Structure of $\text{Eu}(\text{pfppd})_3(\text{tpy})$. (B) (a) Image of H9c2 cells after incubation of Mitochondria tracker CellLight™ Mitochondria-GFP BacMam 2.0. (b) Image of H9c2 cells after incubation of 30 μM concentration of $\text{Eu}(\text{pfppd})_3(\text{tpy})$ complex. (c) Merged image. Scale bars- 25 μm . Picture taken from reference 42.

1.6. Eu^{3+} complexes based luminescent silica hybrid materials

Low thermal and photo stabilities, poor mechanical processabilities and hydrophobicities of Eu^{3+} - β -diketonate complexes limit their practical applicability in various optoelectronic applications. Several research groups demonstrated that by incorporating these Eu^{3+} complexes into rigid matrices, one could overcome the aforementioned limitations.^{19, 45, 46} So the study of Eu^{3+} complexes in hybrid materials is not only of fundamental concern, also these materials find potential use in various optoelectronic applications such as solid state lighting, bio-imaging studies, drug delivery etc. In Eu^{3+} - β -diketonate-based luminescent hybrid materials, a Eu^{3+} - β -diketonate complex is incorporated in a host matrix such as sol-gel derived materials, mesoporous materials, polymer matrices etc. by impregnation, doping or covalent attachment. Because of their attractive characteristics such as high biocompatibility, chemical inertness, optical transparency, high water dispersibility and easy surface functionalization strategies silica is considered as one of the best host matrices for Eu^{3+} complexes.⁴⁷⁻⁴⁹ Moreover, encapsulation into silica matrices usually improves the chemical and photo stabilities of the loaded Eu^{3+} complexes.⁵⁰

1.6.1. Sol-gel hybrid materials *via* doping or impregnation

The approach of embedding Eu^{3+} - β -diketonate complex into a silica glass matrix was first reported by Matthews and Knobbe.⁵¹ The authors incorporated Eu^{3+} - β -diketonate complexes, $[\text{Eu}(\text{tta})_3(\text{H}_2\text{O})_2]$ and $(\text{pipH})[\text{Eu}(\text{tta})_4]$ into silica sol-gel glass prepared by the hydrolysis and condensation of TEOS. They investigated the photophysical properties of the resulting hybrid materials and observed that the spontaneous emission cross sections, a measure of the radiative emission intensity of

a given sample volume, were 14 and 16 times larger for the tris and tetrakis chelates, respectively, than the EuCl_3 doped silica gel material when excited at the ${}^7\text{F}_0 \rightarrow {}^5\text{D}_2$ transition. The quantum efficiencies of the gels doped with Eu^{3+} complexes doped gels were determined to be between 15% and 23%. Later the authors studied the effect of concentration of dopants on the Eu^{3+} luminescence in hybrid materials.⁵² In 1997, Yan and co-workers doped $\text{Eu}(\text{dbm})_3(\text{phen})$ complex into silica glass and observed a longer excited state life time for this hybrid material compared to the pure solid complex.⁵³ Legendziewicz and co-workers incorporated several Eu^{3+} - β -diketonate complexes into silica gel glasses and reported that the Eu^{3+} complexes retained their optical properties in the hybrid materials.⁵⁴ Tanner developed a luminescent hybrid material by incorporating $\text{Eu}(\text{tta})_3(\text{phen})$ into a silica/polymer mixed host matrix and observed a better thermal stability for the hybrid material.⁵⁵ Fan and co-workers reported a hybrid material which was made by the dip-coating of a sol co-doped with EuCl_3 and tta ligand.⁵⁶

The luminescent silica hybrid materials prepared by the doping or impregnation of Eu^{3+} complexes usually present problems such as leaching out of the samples from host matrix, crystallization of complex molecules in the host matrix leading to a loss of transparency of the resulting hybrid material, long drying methods to reduce the cracking of the silica gel glasses and poor mechanical properties of the hybrid materials which have not been heat treated.¹⁹

1.6.2. Sol-gel hybrid materials *via* covalent attachment

Compared to other preparation methods like impregnation and doping, covalent linking of Eu^{3+} complexes to silica matrices reduces the risk of the molecules being leached out from the hybrid materials. Furthermore, it improves the homogeneity of

the hybrid materials, avoids clustering of Eu^{3+} complexes and allows more loading concentrations.¹⁹ Covalent attachment of Eu^{3+} complexes to various silica host matrices can be done using organically modified silicates (ormosils). These ormosils usually give better mechanical processabilities than the silica sol-gel glasses. The covalent linking of Eu^{3+} complexes on to sol-gel derived silica matrices was first reported by Franville and co-workers in 1998. They used organically modified derivatives of dipicolinic acid as the antenna ligands for Eu^{3+} ion.⁵⁷ The Eu^{3+} complex incorporated luminescent hybrid materials were prepared by the hydrolysis and condensation of the organically modified silicates of dipicolinic acid using TEOS as a precursor for the silica shell formation. They observed around 150 °C enhancement in the thermal stability of the hybrid material compared to the pure Eu^{3+} complex. The authors also noted that the developed hybrid material retained the optical properties of the parent Eu^{3+} complex. Subsequently they studied the effect of different substituents on the luminescence properties of Eu^{3+} complexes based hybrid silica gel materials and compared these properties with their parent Eu^{3+} complexes.⁵⁸ Even though the hybrid materials retained the optical properties of their parent Eu^{3+} complexes, the authors observed a slight decrease in the excited state lifetimes of the hybrid materials compared to their parent complexes, which was ascribed to a possible quenching by $-\text{OH}$ or silanol groups. The most noticeable effect of the host silica matrix was a broadening of the Eu^{3+} emission peaks. Here, the substituents also shifted the excitation window towards longer wavelengths. Zhang and co-workers described the preparation of hybrid materials using a modified 2,2'-bipyridine-4,4'-dicarboxylic acid ligand as the antenna molecule for Eu^{3+} and Tb^{3+} ions and investigated their luminescence properties (Figure 1.11).⁵⁹ The authors

could observe only minor differences between the optical properties of the hybrid materials and their parent complexes. Here also, a decrease in the excited state lifetimes of the hybrid materials was detected compared to that of pure organic complexes. Menu and co-workers grafted silylated 2,2'-bipyridine derivatives to silica nanoparticles and the reaction of $\text{Eu}(\text{tmhd})_3$ with these silica nanoparticles resulted in the formation of luminescent hybrid material.⁶⁰ Binnemans and co-workers covalently attached $\text{Eu}(\text{tta})_3(\text{phen})$ complex to silica matrix using functionalized 1,10-phenanthroline, phen-Si (Figure 1.12).⁶¹ The authors observed that the covalent grafting of the $\text{Eu}(\text{tta})_3(\text{phen})$ complex to silica matrix had a limited influence on its optical properties. In a subsequent work, the authors used a 2-substituted imidazo[4,5-f]-1,10-phenanthroline molecule as ancillary ligand for $\text{Eu}(\text{tta})_3$ complex instead of phen-Si ligand and synthesized the corresponding luminescent thin films by spin-coating on a quartz plate or on a silicon wafer.⁴⁶ Liu and Yan grafted a Eu^{3+} complex to silica gel matrix using 3-alkyl-4-amino-5-ylsulfanyl-1,2,4-triazole derivatives and reported a luminescence quantum efficiency of 4.59% and lifetime of 202 μs for the resulted hybrid material.⁶² Jiang and co-workers reported luminescent hybrid films using N-(3-propyltriethoxysilane)-4-carboxyphthalimide as the precursor and obtained a luminescence lifetime as high as 1.2 ms.⁶³ Nassar and co-workers made the first attempt to introduce a substituted silyl group on the 2-position of acetyl acetone or dibenzoylmethane and used this for the synthesis of hybrid materials.⁶⁴ Later, Malta and co-workers followed the same method to prepare luminescent hybrid materials.⁶⁵ They replaced the coordinated water molecules by 1,10-phenanthroline and thereby improved the luminescence intensities of the hybrid materials. Carlos and co-workers prepared luminescent

1.6.3. Mesoporous silica hybrid materials

In 1992, researchers at the Mobil Corporation developed mesoporous silica materials with very narrow pore diameters, approximately 2-10 nm.⁶⁸ These materials are characterized by large surface areas, well ordered pore systems, and well-defined pore radii distributions. The pores of these mesoporous materials are large enough to accommodate Eu^{3+} complexes. The development of luminescent hybrid porous materials with large surface areas is currently an area of extensive research. Several luminescent Eu^{3+} complexes have been incorporated into the micropores of mesoporous silica materials such as MCM-41, MCM-48, SBA-15 etc.^{19, 69-72}

Xu and co-workers encapsulated $[\text{Eu}(\text{tta})_4]^{-}(\text{C}_5\text{H}_5\text{NC}_{16}\text{H}_{33})^{+}$ complex into modified MCM-41.⁷³ The authors noticed a remarkable enhancement in the intensity of the hypersensitive, ${}^5\text{D}_0 \rightarrow {}^7\text{F}_2$ transition and obtained high colour purity for the hybrid material. The intensity ratio $I({}^5\text{D}_0 \rightarrow {}^7\text{F}_2)/I({}^5\text{D}_0 \rightarrow {}^7\text{F}_1)$ for the hybrid material with modified MCM-41 was found to be very high (almost $+\infty$) when compared to that in hybrid material with unmodified MCM-41 (5.5). The authors proposed the reduced pore size of modified MCM-41 (14.26 Å) when compared to the larger pore size of unmodified MCM-41 (29.31 Å) as the reason for this intensity increase. Inside the pores of modified MCM-41, the symmetry of the Eu^{3+} complex was decreased, which resulted in an increase in the intensity of induced electric dipole transition ${}^5\text{D}_0 \rightarrow {}^7\text{F}_2$. The authors also obtained a long luminescence lifetime value for the hybrid material (2.18 ms) compared to the pure $[\text{Eu}(\text{tta})_4]^{-}(\text{C}_5\text{H}_5\text{NC}_{16}\text{H}_{33})^{+}$ powder (0.84 ms). The photostability of the Eu^{3+} complex was also found to have improved after encapsulation into the modified MCM-41. In a subsequent study, they modified MCM-41 with aminopropyltriethoxysilane (APTES) or *N*-[(3-

triethoxysilyl)propyl]ethylenediamine (TEPED) and encapsulated $\text{Eu}(\text{DBM})_3(\text{phen})$ complex into these modified MCM-41 hosts.⁷⁴ They reported intensity ratios, $I(^5\text{D}_0 \rightarrow ^7\text{F}_2)/I(^5\text{D}_0 \rightarrow ^7\text{F}_1)$, which are much lower (2.7 for APTES modified hybrid and 1.7 for TEPED modified hybrid) than that reported for the $[\text{Eu}(\text{tta})_4]^- (\text{C}_5\text{H}_5\text{NC}_{16}\text{H}_{33})^+$ complex. Here also, the luminescence lifetime of the hybrid materials were found to have improved after encapsulation into the modified MCM-41 host matrices. Franville and co-workers prepared hybrid materials by impregnating $\text{Eu}(\text{DBM})_3(\text{H}_2\text{O})_2$ into the mesopores of cubic MCM-48.⁷⁵ The luminescence decay profiles of the Eu^{3+} emission were found to be multi-exponential in hybrids with high $\text{Eu}(\text{DBM})_3(\text{H}_2\text{O})_2$ concentration but single exponential in diluted hybrid material. Here, the excitation maxima of the hybrid materials were blue shifted compared to that of pure $\text{Eu}(\text{DBM})_3(\text{H}_2\text{O})_2$ complex. Fernandes *et al.* immobilized $[\text{Eu}(\text{thd})_3]$ and $[\text{Eu}(\text{dbm})_3]$ complexes into MCM-41 and investigated the optical properties of the resulting hybrid materials.⁷⁶ The luminescence characteristics of the Eu^{3+} complexes were altered after incorporation into host MCM-41, but they observed a ligand-to-metal energy transfer in the hybrid materials. In a subsequent study, they improved the thermal stabilities and optical properties of these hybrid materials by using 1,10-phenanthroline or 2,2'-bipyridine as ancillary ligands for the Eu^{3+} ion.⁷⁷ Very recently, Nunes and co-workers prepared a highly efficient luminescent hybrid material by impregnating a Eu^{3+} complex into MCM-41 and achieved a luminescence quantum yield of 31%.⁷⁸ Suwen *et al.* incorporated $\text{Eu}(\text{tta})_3(\text{TPPO})_2$ and $\text{Eu}(\text{BA})_3(\text{TPPO})_2$ complexes into the channels of SBA-15 and observed improved thermal and photo stabilities.⁷⁹ The $^5\text{D}_0 \rightarrow ^7\text{F}_2$ transition bands became broader in the hybrid materials than in the pure Eu^{3+} complexes. Zhang and co-

workers covalently grafted 1,10-phenanthroline on the surface of MCM-41 and synthesized the corresponding Eu^{3+} complex.⁸⁰ The red emission of Eu^{3+} ions was weak and a blue emission of 1,10-phenanthroline dominated the emission spectrum of the hybrid material. Subsequently, the authors developed red luminescent hybrid materials by the covalent linking of $\text{Eu}(\text{tta})_3(\text{phen})$ complex with SBA-15 (Figure 1.13).^{81, 82} The integrated emission intensity of the new hybrid material was about six times higher than that of their previously prepared hybrid material without tta ligand. Also the blue emission of 1,10-phenanthroline was completely absent, which indicated an efficient energy transfer from the ligands to the Eu^{3+} ions in the new hybrid materials. Yan and co-workers modified β -diketonates by introducing substituted silyl derivatives on 2-position and used then as antenna ligands for Eu^{3+} ion.⁸³ Then they covalently linked this to SBA-15 and developed luminescent hybrid materials. The hybrid materials exhibited improved optical properties and thermal stabilities compared to their precursor complexes.

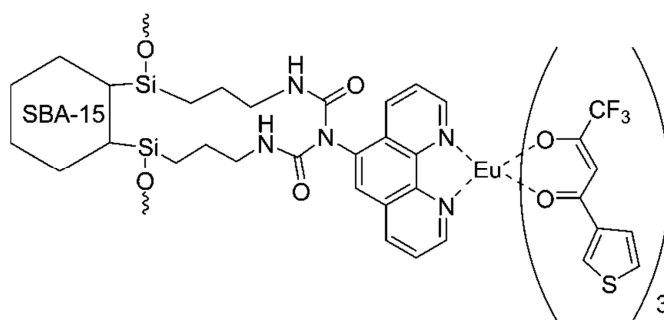


Figure 1.13. $\text{Eu}(\text{tta})_3(\text{phen})$ complex covalently attached to SBA-15 matrix. Reference 81.

Reddy and co-workers designed a hybrid material by covalently linking Eu^{3+} complex to the hexagonal channels of MCM-41 *via* a modified β -diketonate ligand, SiPFNP-Na (Figure 1.14).⁸⁴ The developed hybrid material, $\text{Eu}(\text{PFNP-Si})_3(\text{bath})/\text{MCM-41}$, exhibited efficient intramolecular energy transfer from the silylated

β -diketonate ligand to the Eu^{3+} ion, with a luminescence quantum efficiency of 81% and overall quantum yield of 43%. Later the authors developed a visible light excitable Eu^{3+} complex, $\text{Eu}(\text{BFPD})_3(\text{phen})$, and covalently incorporated this complex into the mesopores of MCM-41.⁸⁵ The resulting hybrid material, $\text{Eu}(\text{SiBFPD})_3(\text{Phen})/\text{MCM-41}$, showed better thermal stability compared to the precursor Eu^{3+} complex. The excitation band of the hybrid material extended up to 500 nm and the authors reported a high overall luminescence quantum yield of 30%.

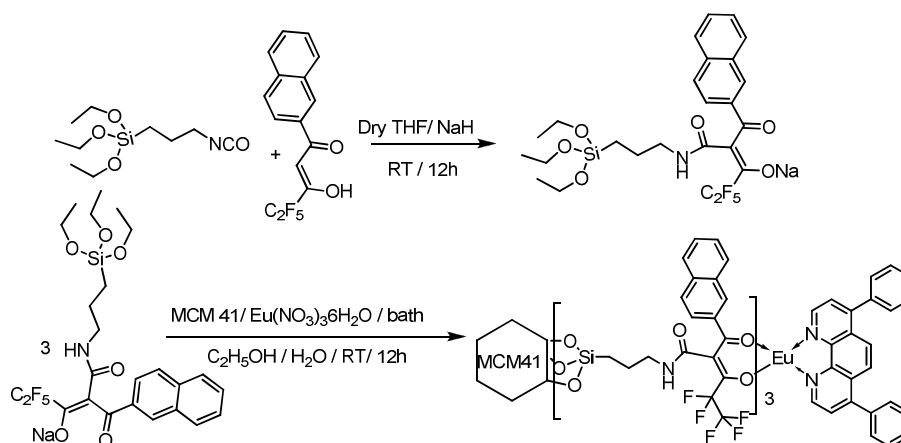


Figure 1.14. Synthesis procedure for the ligand SiPFNP-Na and hybrid $\text{Eu}(\text{PFNP-Si})_3(\text{bath})/\text{MCM-41}$. Reference 84.

1.7. Applications of Eu^{3+} complexes based luminescent silica hybrid materials

The applications of the hybrid materials are not yet fully explored. Some of the possible applications are briefly described below.

1.7.1. Bio-imaging

In 2008, Yuan and co-workers prepared Eu^{3+} - β -diketonate-based silica nanoparticles (Figure 1.15.) and used this for the time-gated luminescence imaging of an environmental pathogen, *Giardia lamblia* (Figure 1.16).⁸⁶ They introduced a substituted silyl group to a fluorinated biphenyl-based β -diketonate ligand and

synthesized the corresponding Eu^{3+} ternary complex, APS-CDHH- Eu^{3+} -DPBT, using DPBT as ancillary ligand. The nanoparticles were prepared in a water-in-oil reverse microemulsion by the hydrolysis and copolymerization of TEOS with APS-CDHH- Eu^{3+} -DPBT, conjugate. Later, the authors developed visible light excitable luminescent nanoparticles with an excitation maximum at 406 nm following the same methodology.⁸⁷ The newly developed nanoparticles exhibited fine monodispersity in aqueous solutions, a remarkable luminescence quantum yield of 66% and an excited state lifetime of 389 μs . The authors used the developed nanoparticles for the highly specific and sensitive imaging of *Giardia lamblia*. In a subsequent study, the authors synthesized a new visible light-excited tetradentate β -diketonate- Eu^{3+} -BPT ternary complex (BHHD- Eu^{3+} -BPT) and used this for the synthesis of nanoparticles.⁸⁸ The nanoparticles were prepared by the copolymerization of modified Eu^{3+} complex, IPTES-BHHD- Eu^{3+} -BPT conjugate, TEOS and APTES in a water-in-oil reverse microemulsion. The nanoparticles exhibited strong visible light-excited luminescence and a long excited state lifetime. The authors used these nanoparticles as biolabels for streptavidin labeling and for the time-gated luminescence detection of the environmental pathogens, *cryptosporidium muris* and *cryptosporidium parvium*. In 2012, Rocha and co-workers developed a non-toxic bimodal MRI-optical probe, $\text{SiO}_2@\text{APS/DTPA:Ln}$ ($\text{Ln} = \text{Eu}^{3+}$, Tb^{3+} and Gd^{3+}).⁸⁹ They used mouse macrophage cell line (RAW 264.7 cells) in order to evaluate the usefulness of the developed nanoparticles as bimodal agents for MRI and optical imaging. The nanoparticles were rapidly and efficiently taken up by RAW 264.7 cells, and exhibited both, an increased contrast for the T_1 -weighted MRI images of cellular pellets, and a potential for optical tracking by fluorescence.

Ribeiro and co-workers prepared luminescent silica-based nanoparticles SiO₂-[Eu(tta)₃(Bpy-Si)], and successfully employed it as a luminescent label for the imaging of *Pseudomonas aeruginosa* biofilms.⁹⁰ Further, they functionalized these nanoparticles with a specific monoclonal antibody and subsequently used this for the selective imaging of *Escherichia coli* bacteria.

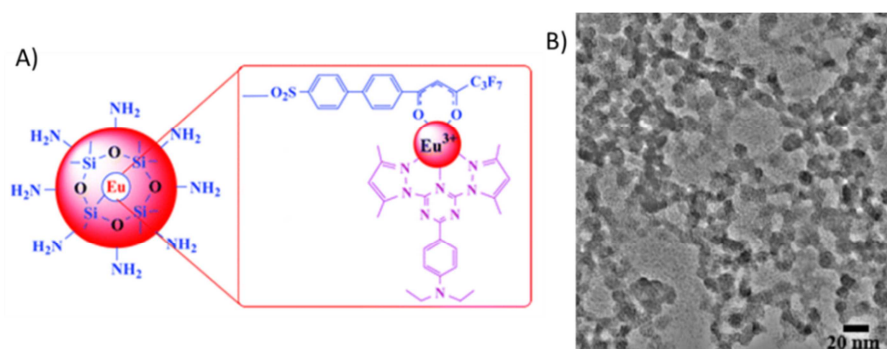


Figure 1.15. (A) Schematic of APS-CDHH-Eu³⁺-DPBT-based nanoparticle. (B) TEM image of the nanoparticles. Pictures taken from reference 86.

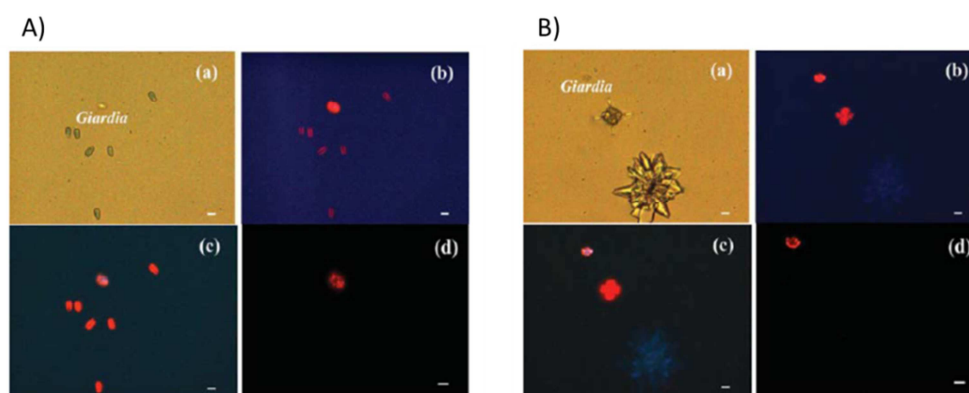


Figure 1.16. (a) Bright-field, (b) luminescence ($\lambda_{ex} = 330-380$ nm), (c) luminescence ($\lambda_{ex} = 380-420$ nm) and (d) time-gated luminescence ($\lambda_{ex} = 330-380$ nm) images of *Giardia lamblia* stained by the nanoparticle-labeled streptavidin in water samples containing green algae (A) and inert particles (B). Picture taken from reference 86.

Very recently, Wu *et al.* prepared a stable, water soluble and highly luminescent nano system, Ir-Eu-MSN, (MSN = mesoporous silica nanoparticles, Ir-Eu = [Ir(dfppy)₂(pic-OH)]₃Eu·2H₂O, dfppy = 2-(2,4-difluorophenyl)pyridine, pic-OH = 3-

hydroxy-2-carboxypyridine) with the excitation window extending up to 470 nm and a high luminescence quantum yield of 55.2% (Figure 1.17).⁹¹ The developed nanoparticles were used for luminescence imaging in living cells at an excitation wavelength of 458 nm and were successfully applied for high-contrast luminescent lymphatic imaging *in vivo* under low power density excitation of 5 mW cm⁻².

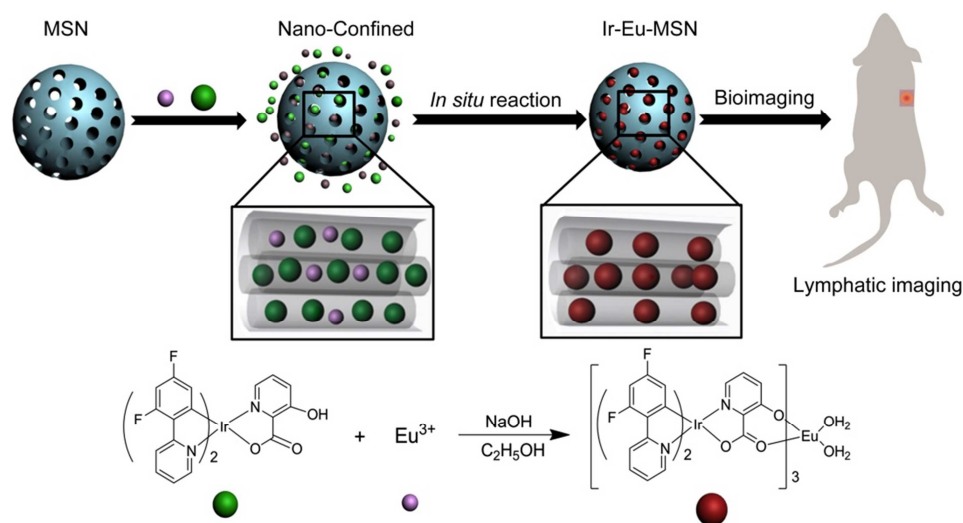


Figure 1.17. Schematic illustration of the construction of Ir-Eu-MSN nanosystem via nano-confined systems for lymphatic imaging *in vivo*. Picture taken from reference 91.

1.7.2. Temperature imaging

Wolfbeis and co-workers designed novel photostable luminescent hybrid nanoparticles of about 20-30 nm diameter, from a visible-light sensitized Eu³⁺- β -diketonate complex, Eu-DT (Figure 1.18).⁹² The developed hybrid material displayed strong temperature dependence for both luminescence intensity and lifetime over the physiological range (25-45 °C) and the authors used this nanomaterial for the imaging and sensing of temperature. The sensitivity of the developed nanoparticles towards temperature was investigated both in terms of luminescence intensity and lifetime. The authors found that the luminescence intensity decreased by 3.07% per °C on increasing temperature from 25 to 45 °C and the lifetime dropped rapidly with

the increase of temperature and a temperature sensitivity of 2.2% °C was obtained in the physiological temperature.

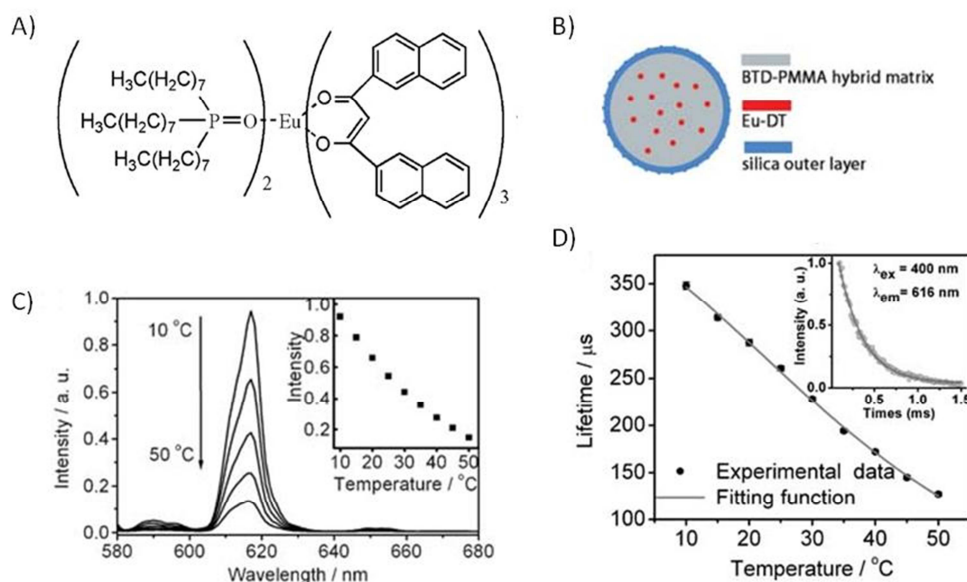


Figure 1.18. (A) Molecular structure of the temperature probe Eu-DT. (B) Schematic of the cross section of sensor nanoparticles. The probe Eu-DT is randomly incorporated in the core, which is covered with a silica shell. (C) Temperature-dependent luminescence intensity data at 616 nm ($\lambda_{ex} = 400$ nm). Inset shows the corresponding calibration plot. (D) Temperature-dependent luminescence lifetime data. Luminescence decay corresponds to single-exponential function is given in the inset. Pictures taken from reference 92.

Carlos's group explored the use of ligand sensitized luminescence of Eu^{3+} complexes for the imaging and sensing of temperature.^{93, 94} In 2010, they developed a self-referencing, $\text{Eu}^{3+}/\text{Tb}^{3+}$ luminescent nanothermometer, allowing the absolute temperature measurement in 10-300 K temperature range, with a high sensitivity of 4.9 per K.⁹⁵ The developed nanothermometer exhibited high photostability in long-term use. Recently, the authors prepared two ratiometric nanothermometers based on a magnetic core coated with a silica shell co-doped with β -diketonate complexes of Eu^{3+} and Tb^{3+} ions.⁹⁶ They used TEOS as the precursor for silica shell formation.

They detected a maximum relative sensitivity of $1.5\% \text{ K}^{-1}$ at 293 K and a spatio-temporal resolution of $64 \times 10^{-6} \text{ m}/150 \times 10^{-3} \text{ s}$.

1.7.3. White light generation

Several attempts have been made by different research groups to obtain white light emission using luminescent lanthanide-based hybrid materials.⁹⁷⁻⁹⁹ Zhao *et al.* prepared mesophase silicate thin films which exhibited multicolour photoluminescence and white light emission, using tetramethylorthosilicate (TMOS) as the silica film precursor (Figure 1.19).⁹⁸ The authors used Eu^{3+} and Tb^{3+} ions as the red and green components, and 1,10-phenanthroline as the photosensitizer as well as blue component. By changing the ratios of Ln^{3+} ions and 1,10-phenanthroline they fine-tuned the colour of the films in the whole visible region. They determined the luminescence quantum yields of these thin films and found them to be between 4.3% to 35.2%. The authors successfully developed white light emitting films with a CIE (x, y) colour coordinates of 0.3648, 0.3799 and an absolute quantum yield of 9.0% by varying the ratios of the dopants as well as the excitation wavelengths. In 2007, Armelao and co-workers anchored highly stable Eu^{3+} and Tb^{3+} complexes onto a single SiO_2 transparent layer, which resulted in luminescent films of about 40 nm thickness.⁹⁹ A dipartite ligand, consisting of 1,4,7,10-tetraazacyclododecane-1,4,7-triacetic acid (DO3A) acting as a chelating “cage” and an acetophenone unit functionalized with propyl-hydroxy group acted as the antenna ligand. The obtained films were optically homogeneous and the authors could easily tune the colour from red to green through yellow (Figure 1.20). Later, in 2010, the authors developed white luminescent silica single layers using, 10-[(4-methoxybenzoyl)methyl]-1,4,7,10-tetraazacyclododecane-1,4,7-triacetic acid-based Eu^{3+} and Tb^{3+} complexes

as the red and green components, respectively and 9H-carbazole-9-ethanol (Cz) as the blue emitting component.^{22, 100} The white luminescent silica film exhibited a CIE (x, y) coordinates of 0.32, 0.37 and a luminescence quantum yield of 6.0%. Huo and co-workers developed red and green luminescent hybrid materials by incorporating Eu^{3+} and Tb^{3+} complexes into mesoporous materials.¹⁰¹ After heat treatment at 500 °C for 3 hours, the hybrid materials exhibited white light emission with the CIE (x, y) coordinates that matched well with that of the pure white (x = 0.33, y = 0.33) light.



Figure 1.19. Full-colour mesophase silicate thin film. Picture taken from reference 98.

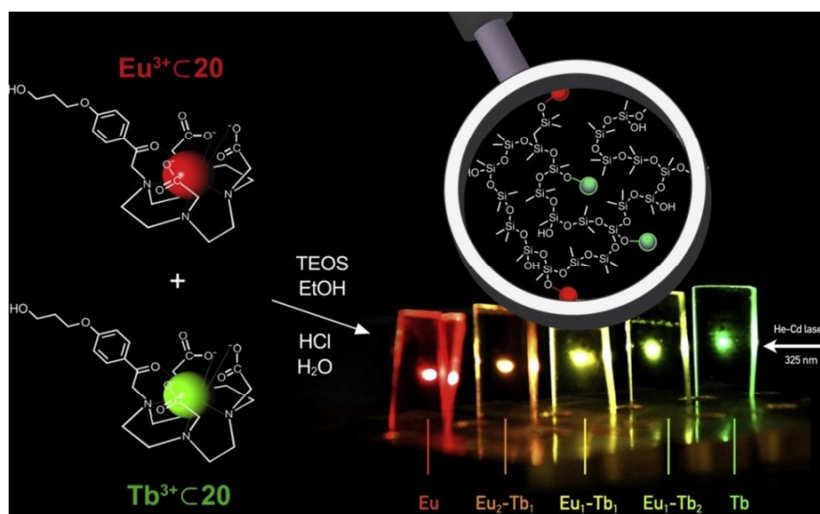


Figure 1.20. Colours emitted by silica layers containing different ratios of Eu^{3+} and Tb^{3+} complexes. Picture taken from reference 99

1.7.4. Sensing

In 2009, Lu and co-workers developed the first Eu^{3+} -based luminescent nanoparticle sensor for rapid and ultrasensitive detection of calcium dipicolinate (CaDPA), which is the main constituent of anthracis spores, in aqueous solution (Figure 1.21).¹⁰² First, the authors prepared uniform fluorescein isothiocyanate (FITC) dye-doped silica nanoparticles and subsequently functionalized the surface of the nanoparticles with 3-aminopropyltriethoxysilane. Ethylenediamine tetraacetic acid dianhydride (EDTAD) was then covalently attached onto the surface of the amine functionalized FITC-doped silica nanoparticles. Subsequent addition of EuCl_3 resulted in the formation of the complex, $\text{Eu}(\text{EDTA})(\text{H}_2\text{O})_3$, on the surface of the nanoparticles and the authors used this hybrid material as the sensor for CaDPA. Here, FITC acted as a non-interfering reference dye which enabled the ratiometric detection of CaDPA. Upon exposure of the sensor to CaDPA, water molecules were excluded from the coordination sphere of Eu^{3+} and the resulting complex, $\text{Eu}(\text{EDTA})(\text{DPA})$, effectively minimized the nonradiative quenching of Eu^{3+} emission, and thereby enhanced the overall quantum yield of the hybrid material. With this luminescent sensor, the authors could achieve a fast detection of CaDPA, with a limit of detection (LOD) of 0.2 nM. Li and co-workers prepared luminescent core-shell hybrid materials by incorporating a tta based Eu^{3+} complex into zeolite and subsequent encapsulation into silica shell using TEOS.¹⁰³ The luminescent hybrid material was then functionalized with silylated Tb^{3+} complex and used for the luminescence sensing of dipicolinic acid (DPA). The addition of DPA to the final hybrid material resulted in an enhancement in Tb^{3+} emission intensity, whereas the Eu^{3+} emission intensity remained the same. The authors could detect the presence of DPA at a concentration

of 0.05 μM . In a subsequent study, the authors developed another luminescent hybrid material and used it as a ratiometric luminescent sensor for DPA using Eu^{3+} emission as the sensing tool.¹⁰⁴

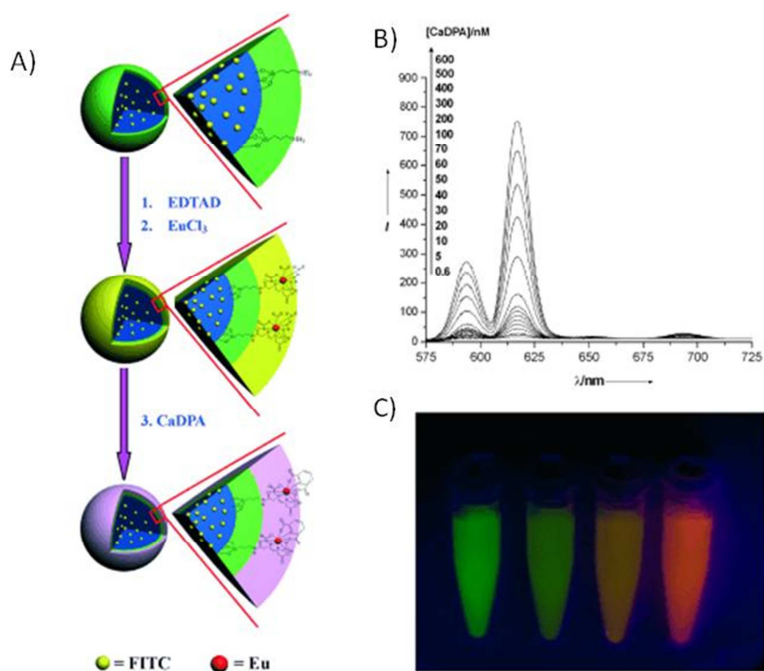


Figure 1.21. (A) Schematic representation of synthesis strategy for nanoparticle sensor. (B) Fluorescence response of sensor nanoparticle upon addition of different concentrations of CaDPA. (C) Visual fluorescence colour changes of nanoparticle sensor upon addition of different concentrations of CaDPA (from left to right: 0, 25 μM , 50 μM , 100 μM). Picture taken from reference 102.

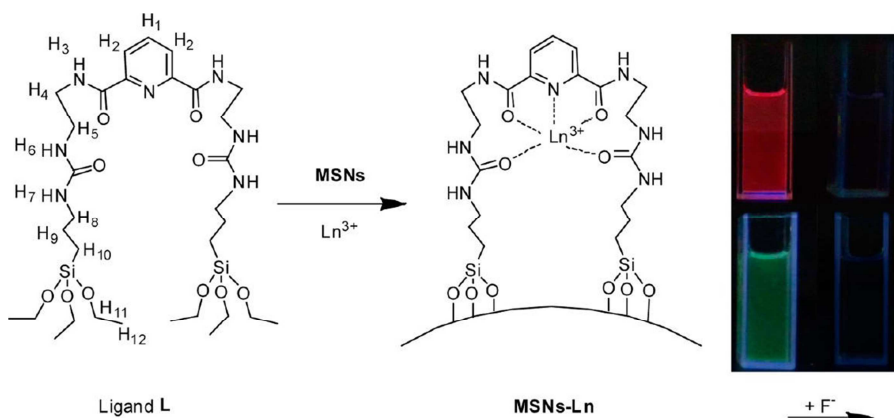


Figure 1.22. Schematic representation of MSNs-Eu and MSNs-Tb. Photo: MSNs-Eu (top) and MSNs-Tb (bottom) in DMSO excited by UV light at 254 and 365 nm with (right) and without (left) fluoride (10^{-5} M). Picture taken from reference 105.

Recently, Wang and co-workers demonstrated the successful sensing of fluoride ion using Eu^{3+} and Tb^{3+} complexes modified mesoporous silica nanopores, MSNs-Eu and MSNs-Tb.¹⁰⁵ The developed nanopores exhibited significant properties such as high thermal stability, large specific surface area and a low detection limit (2.5×10^{-8} M for MSNs-Eu and 3.4×10^{-8} M for MSNs-Tb) specific for the fluoride ion (Figure 1.22). The intensities of Eu^{3+} and Tb^{3+} emissions were found decrease with the increasing concentration of F^- ions. According to the authors, the hydrogen bonding between F^- and $-\text{NH}$ group of the organic ligand changes the coordination conformation which in turn affects the energy transfer efficiency from the ligand to the Ln^{3+} ions.

1.7.5. Luminescent solar concentrators

The utilization of Eu^{3+} complex based hybrid materials in luminescent solar concentrators (LSCs) is in its primary experimental stage and extensive study and considerable basic knowledge are required before its adoption into commercial use. Machida and co-workers developed transparent films from ormosil sol solutions doped with $[\text{Eu}(\text{phen})_2]\text{Cl}_3$ complex by dip-coating.¹⁰⁶ LSC panels were prepared by coating the developed film and the authors observed 10-15% enhancement in the photovoltaic current of the corresponding crystalline silicon solar cells when compared to the corresponding uncoated LSCs. In 2011, Carlos and co-workers prepared luminescent bridged silsesquioxanes (M5-Eu and M6-Eu) by the hydrolysis and condensation of the new urea-bipyridine derived bridged organosilanes in presence of Eu^{3+} salts.¹⁰⁷ The authors processed the developed silsesquioxane, M6-Eu, as thin films by spin-coating on glass substrates. The resulting thin layer (~ 54 nm) of Eu^{3+} containing silica coated glass plates exhibited a high absolute

luminescence quantum yield of 34% and the authors successfully employed the developed hybrid material as new LSCs with an optical conversion efficiency of $\sim 4\%$. In a subsequent study, the authors synthesized a highly luminescent Eu^{3+} complex using tta as primary ligand and 5,6-epoxy-5,6-dihydro-[1,10]phenanthroline (ephen) as the ancillary ligands.¹⁰⁸ Using tri-urea-propyltriethoxysilane (t-UPTES) as the precursor, the authors developed organic-inorganic hybrid materials as a monolith (MtU5Eu-II) and as a thin film (FtU5Eu-II), with luminescence quantum yields of 66% and 48%, respectively. FtU5Eu-II was then used as a LSC which exhibited an optical conversion efficiency of $\sim 9\%$ and the authors also verified a boost up of 0.5% in the Si-photovoltaic cell output.

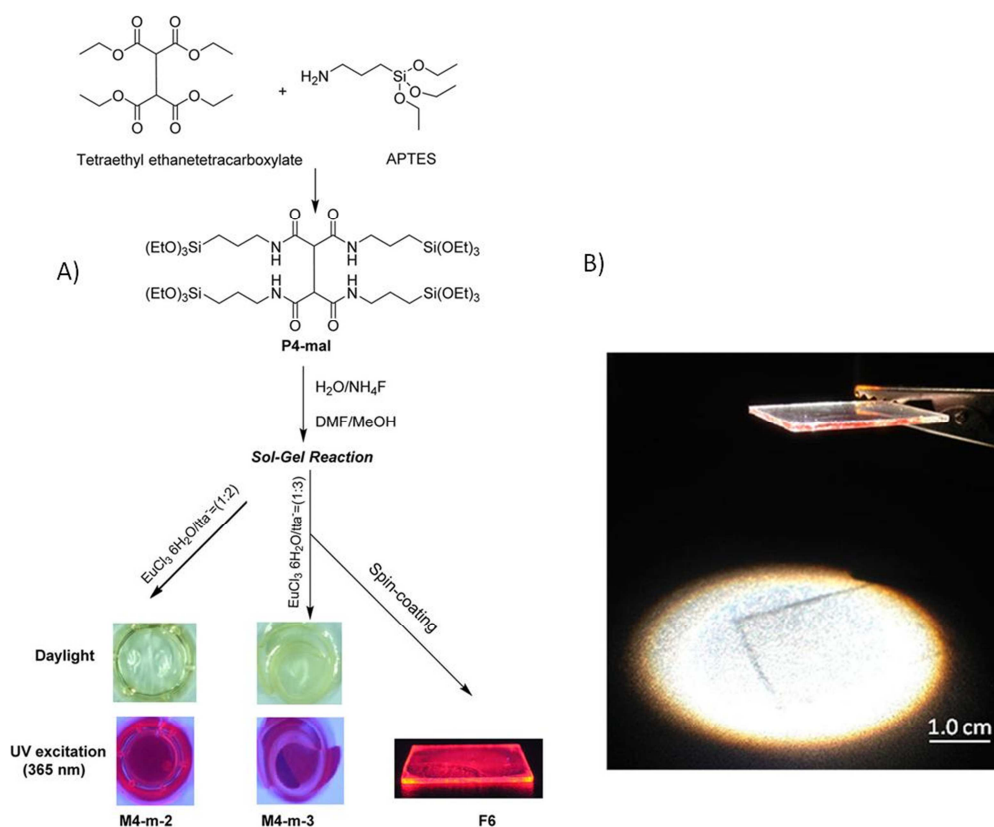


Figure 1.23. (A) Representation of the Synthesis Route of P4-m, M4-m-2, M4-m-3 and F6; Photographs Acquired under Daylight Illumination and UV Exposure (Spectroline ENF- 280C/FE). (B) Photo of F6 under AM1.5G illumination. Picture taken from reference 109.

In 2015, they synthesized a new ethane tetracarboxamide-based organosilane (P4-mal), and employed it for the development of luminescent bridged silsesquioxanes (M4-m-2 and M4-m-3) containing different amounts of tta-based Eu^{3+} complex.¹⁰⁹ Glass plate spin-coated with thin films (~200-400 nm) of this hybrid material was prepared (F6), which exhibited a high luminescence quantum yield of 60% (Figure 1.23). The thin films were then tested as planar LSCs and the optimized device showed an optical conversion efficiency of 12.3%. Very recently, the same group developed a Eu^{3+} -based luminescent hybrid material and used it as LSC which displayed an optical conversion efficiency of 20.7% and a power conversion efficiency of 2.5%, which are among the highest values reported so far for UV-absorbing devices.¹¹⁰

1.8. Problem statements and objectives of the thesis

As mentioned above, Eu^{3+} - β -diketonate complexes are one of the most extensively studied and explored lanthanide complexes due to their interesting luminescence properties such as sharp red emission bands with high colour purity, long luminescence lifetimes, large Stokes shifts and high luminescence efficiencies. Despite all these attractive optical properties, the excitation window of most of the Eu^{3+} - β -diketonate complexes are in the UV region, which limit their practical use in various biological applications.

Reddy and co-workers demonstrated that by extending the π -conjugation of organic ligands, one could shift the excitation wavelength of these Eu^{3+} complexes towards the visible region.^{26, 43} Gong and co-workers prepared visible light excitable Eu^{3+} complexes by introducing alkyl groups on the nitrogen atom of carbazole-based

β -diketonate ligands.^{35, 38, 39, 111} Raj *et al.* developed a highly efficient Eu^{3+} ternary complex, using a carbazole-based β -diketonate ligand as primary ligand and a bidentate phosphine oxide molecule as the ancillary ligand.¹¹² However, the excitation window of this reported complex was in the UV region which restricted their use in biological applications. Consequently, the primary objective of the present study is to design and develop visible-light excitable Eu^{3+} - β -diketonate complexes by engineering organic ligands with extended π -conjugation.

Further obstacles which limit the practical use of these Eu^{3+} - β -diketonate complexes as bio-probes are their poor water solubilities and low photostabilities. Several groups have employed Eu^{3+} - β -diketonate complexes in bio-imaging studies, albeit in presence of organic solvents.^{42, 113} This brings us to the next objective of the investigation - improving the aqueous dispersibility and photostability of the loaded species for their use as bio-probes by encapsulating these complex molecules into silica nanoparticles.

Lastly, we investigate the influence of a host matrix on the optical properties of the Eu^{3+} - β -diketonate complexes. The incorporation of dye molecules in to mesoporous materials have shown to usually improve their mechanical processabilities, thermal and photo stabilities, and optical properties.^{19, 45} The mesopores of MCM-41 are about 2-10 nm and are large enough to accommodate the Eu^{3+} - β -diketonate complexes.¹¹⁴ Therefore, our next objective is to develop a novel luminescent hybrid material by incorporating Eu^{3+} - β -diketonate complexes into the mesopores of MCM-41 and to investigate their photophysical properties.

The subsequent chapters in this thesis are a detailed and systematic approach to the realization of each of these above objectives.

1.9. References

1. J.-C. G. Bunzli and C. Piguet, *Chem. Soc. Rev.*, 2005, **34**, 1048-1077.
2. E. G. Moore, A. P. S. Samuel and K. N. Raymond, *Acc. Chem. Res.*, 2009, **42**, 542-552.
3. G. F. de Sá, O. L. Malta, C. de Mello Donegá, A. M. Simas, R. L. Longo, P. A. Santa-Cruz and E. F. da Silva Jr, *Coord. Chem. Rev.*, 2000, **196**, 165-195.
4. S. V. Eliseeva and J.-C. G. Bunzli, *Chem. Soc. Rev.*, 2010, **39**, 189-227.
5. C. P. Montgomery, B. S. Murray, E. J. New, R. Pal and D. Parker, *Acc. Chem. Res.*, 2009, **42**, 925-937.
6. J.-C. G. Bünzli, *Chem. Rev.*, 2010, **110**, 2729-2755.
7. M. C. Heffern, L. M. Matosziuk and T. J. Meade, *Chem. Rev.*, 2014, **114**, 4496-4539.
8. J. Kido and Y. Okamoto, *Chem. Rev.*, 2002, **102**, 2357-2368.
9. H. Kataoka, S. Omagari, T. Nakanishi and Y. Hasegawa, *Opt. Mat.*, 2015, **42**, 411-416.
10. Y. Hasegawa and T. Nakanishi, *RSC Adv.*, 2015, **5**, 338-353.
11. J.-C. G. Bunzli and S. V. Eliseeva, *Chem. Sci.*, 2013, **4**, 1939-1949.
12. S. I. Weissman, *J. Chem. Phys.*, 1942, **10**, 214-217.
13. J.-M. Lehn, *Angew. Chem. Int. Ed.*, 1990, **29**, 1304-1319.
14. N. Sabbatini, M. Guardigli and J.-M. Lehn, *Coord. Chem. Rev.*, 1993, **123**, 201-228.
15. M. Latva, H. Takalo, V.-M. Mikkala, C. Matachescu, J. C. Rodríguez-Ubis and J. Kankare, *J. Lumin.*, 1997, **75**, 149-169.
16. G. A. Crosby, R. E. Whan and R. M. Alire, *J. Chem. Phys.*, 1961, **34**, 743-748.
17. G. A. Crosby, R. E. Whan and J. J. Freeman, *J. Phys. Chem.*, 1962, **66**, 2493-2499.
18. R. E. Whan and G. A. Crosby, *J. Mol. Spectrosc.*, 1962, **8**, 315-327.
19. K. Binnemans, *Chem. Rev.*, 2009, **109**, 4283-4374.
20. J.-C. Bunzli, *Nat Chem*, 2010, **2**, 696-696.
21. K. Binnemans, *Coord. Chem. Rev.*, 2015, **295**, 1-45.
22. L. Armelao, S. Quici, F. Barigelletti, G. Accorsi, G. Bottaro, M. Cavazzini and E. Tondello, *Coord. Chem. Rev.*, 2010, **254**, 487-505.
23. J.-C. G. Bünzli, *Coord. Chem. Rev.*, 2015, **293-294**, 19-47.
24. D. B. Ambili Raj, S. Biju and M. L. P. Reddy, *Dalton Trans.*, 2009, 7519-7528.
25. M. L. P. Reddy, V. Divya and R. Pavithran, *Dalton Trans.*, 2013, **42**, 15249-15262.
26. V. Divya, R. O. Freire and M. L. P. Reddy, *Dalton Trans.*, 2011, **40**, 3257-3268.
27. J.-C. G. Bünzli, E. Moret, V. Foiret, K. J. Schenk, M. Wang and L. Jin, *J. Alloys Compd.*, 1994, **207-208**, 107-111.
28. M. H. V. Werts, M. A. Duin, J. W. Hofstraat and J. W. Verhoeven, *Chem. Commun.*, 1999, 799-800.
29. C. Yang, L.-M. Fu, Y. Wang, J.-P. Zhang, W.-T. Wong, X.-C. Ai, Y.-F. Qiao, B.-S. Zou and L.-L. Gui, *Angew. Chem. Int. Ed.*, 2004, **43**, 5010-5013.
30. F. Xue, Y. Ma, L. Fu, R. Hao, G. Shao, M. Tang, J. Zhang and Y. Wang, *Phys. Chem. Chem. Phys.*, 2010, **12**, 3195-3202.
31. P. Kadjane, L. Charbonnière, F. Camerel, P. Lainé and R. Ziessel, *J. Fluoresc.*, 2008, **18**, 119-129.

32. M. Shi, C. Ding, J. Dong, H. Wang, Y. Tian and Z. Hu, *Phys. Chem. Chem. Phys.*, 2009, **11**, 5119-5123.
33. R. V. Deun, P. Nockemann, P. Fias, K. V. Hecke, L. V. Meervelt and K. Binnemans, *Chem. Commun.*, 2005, 590-592.
34. B. Francis, C. Heering, R. O. Freire, M. L. P. Reddy and C. Janiak, *RSC Adv.*, 2015, **5**, 90720-90730.
35. P. He, H. H. Wang, S. G. Liu, J. X. Shi, G. Wang and M. L. Gong, *Inorg. Chem.*, 2009, **48**, 11382-11387.
36. P. He, H. Wang, S. Liu, W. Hu, J. Shi, G. Wang and M. Gong, *J. Electrochem. Soc.*, 2009, **156**, E46-E49.
37. P. He, H. Wang, S. Liu, J. Shi, G. Wang and M. Gong, *Electrochem. Solid-State Lett.*, 2009, **12**, B61-B64.
38. P. He, H. H. Wang, H. G. Yan, W. Hu, J. X. Shi and M. L. Gong, *Dalton Trans.*, 2010, **39**, 8919-8924.
39. P. He, H. H. Wang, S. G. Liu, J. X. Shi and M. L. Gong, *Applied Physics B*, 2010, **99**, 757-762.
40. L. Tian, Z. Dai, Z. Ye, B. Song and J. Yuan, *Analyst*, 2014, **139**, 1162-1167.
41. V. Divya and M. L. P. Reddy, *J. Mater. Chem. C*, 2013, **1**, 160-170.
42. V. Divya, V. Sankar, K. G. Raghu and M. L. P. Reddy, *Dalton Trans.*, 2013, **42**, 12317-12323.
43. T. V. Usha Gangan and M. L. P. Reddy, *Dalton Trans.*, 2015, **44**, 15924-15937.
44. S. M. Borisov, R. Fischer, R. Saf and I. Klimant, *Adv. Funct. Mater.*, 2014, **24**, 6548-6560.
45. L. D. Carlos, R. A. S. Ferreira, V. d. Z. Bermudez and S. J. L. Ribeiro, *Adv. Mater.*, 2009, **21**, 509-534.
46. P. Lenaerts, A. Storms, J. Mullens, J. D'Haen, C. Görller-Walrand, K. Binnemans and K. Driesen, *Chem. Mater.*, 2005, **17**, 5194-5201.
47. A. Burns, H. Ow and U. Wiesner, *Chem. Soc. Rev.*, 2006, **35**, 1028-1042.
48. O. S. Wolfbeis, *Chem. Soc. Rev.*, 2015, **44**, 4743-4768.
49. C. Caltagirone, A. Bettoschi, A. Garau and R. Montis, *Chem. Soc. Rev.*, 2015, **44**, 4645-4671.
50. S. Bonacchi, D. Genovese, R. Juris, M. Montalti, L. Prodi, E. Rampazzo and N. Zaccheroni, *Angew. Chem. Int. Ed.*, 2011, **50**, 4056-4066.
51. L. Matthews and E. T. Knobbe, *Chem. Mater.*, 1993, **5**, 1697-1700.
52. L. R. Matthews, X.-j. Wang and E. T. Knobbe, *J. Non-Cryst. Solids*, 1994, **178**, 44-51.
53. B. Yan, H.-j. Zhang, S.-b. Wang and J.-z. Ni, *Mater. Chem. Phys.*, 1997, **51**, 92-96.
54. W. Strek, J. Sokolnicki, J. Legendziewicz, K. Maruszewski, R. Reisfeld and T. Pavich, *Opt. Mat.*, 1999, **13**, 41-48.
55. P. A. Tanner, B. Yan and H. Zhang, *J. Mater. Sci.*, 2000, **35**, 4325-4328.
56. X. Hao, X. Fan and M. Wang, *Thin Solid Films*, 1999, **353**, 223-226.
57. A. C. Franville, D. Zambon, R. Mahiou, S. Chou, Y. Troin and J. C. Cousseins, *J. Alloys Compd.*, 1998, **275-277**, 831-834.
58. A.-C. Franville, D. Zambon, R. Mahiou and Y. Troin, *Chem. Mater.*, 2000, **12**, 428-435.

59. H. Li, J. Yu, F. Liu, H. Zhang, L. Fu, Q. Meng, C. Peng and J. Lin, *New J. Chem.*, 2004, **28**, 1137-1141.
60. S. Cousinié, M. Gressier, C. Reber, J. Dexpert-Ghys and M.-J. Menu, *Langmuir*, 2008, **24**, 6208-6214.
61. K. Binnemans, P. Lenaerts, K. Driesen and C. Gorller-Walrand, *J. Mater. Chem.*, 2004, **14**, 191-195.
62. J. L. Liu and B. Yan, *J. Phys. Chem. C*, 2008, **112**, 14168-14178.
63. D. Dong, S. Jiang, Y. Men, X. Ji and B. Jiang, *Adv. Mater.*, 2000, **12**, 646-649.
64. E. J. Nassar, O. A. Serra and I. L. V. Rosa, *J. Alloys Compd.*, 1997, **250**, 380-382.
65. R. F. de Farias, A. P. S. de Freitas, M. F. Belian, O. L. Malta, G. F. de Sá and S. Alves Jr, *J. Alloys Compd.*, 2008, **459**, 543-547.
66. X. Guo, H. Guo, L. Fu, H. Zhang, L. D. Carlos, R. Deng and J. Yu, *J. Photochem. Photobiol. A*, 2008, **200**, 318-324.
67. X.-F. Qiao and B. Yan, *Inorg. Chem.*, 2009, **48**, 4714-4723.
68. C. T. Kresge, M. E. Leonowicz, W. J. Roth, J. C. Vartuli and J. S. Beck, *Nature*, 1992, **359**, 710-712.
69. J. Feng and H. Zhang, *Chem. Soc. Rev.*, 2013, **42**, 387-410.
70. S. Gago, J. A. Fernandes, J. P. Rainho, R. A. Sá Ferreira, M. Pillinger, A. A. Valente, T. M. Santos, L. D. Carlos, P. J. A. Ribeiro-Claro and I. S. Gonçalves, *Chem. Mater.*, 2005, **17**, 5077-5084.
71. P. Escribano, B. Julian-Lopez, J. Planelles-Arago, E. Cordocillo, B. Viana and C. Sanchez, *J. Mater. Chem.*, 2008, **18**, 23-40.
72. B. Yan, *RSC Adv.*, 2012, **2**, 9304-9324.
73. Q. Xu, L. Li, B. Li, J. Yu and R. Xu, *Microporous Mesoporous Mater.*, 2000, **38**, 351-358.
74. L. Fu, Q. Xu, H. Zhang, L. Li, Q. Meng and R. Xu, *Materials Science and Engineering: B*, 2002, **88**, 68-72.
75. Q. G. Meng, P. Boutinaud, A. C. Franville, H. J. Zhang and R. Mahiou, *Microporous Mesoporous Mater.*, 2003, **65**, 127-136.
76. A. Fernandes, J. Dexpert-Ghys, C. Brouca-Cabarrecq, E. Philippot, A. Gleizes, A. Galarneau and D. Brunel, in *Stud. Surf. Sci. Catal.*, eds. G. G. R. Aiello and F. Testa, Elsevier, 2002, vol. Volume 142, pp. 1371-1378.
77. A. Fernandes, J. Dexpert-Ghys, A. Gleizes, A. Galarneau and D. Brunel, *Microporous Mesoporous Mater.*, 2005, **83**, 35-46.
78. M. R. Felicio, T. G. Nunes, P. M. Vaz, A. M. P. Botas, P. Ribeiro-Claro, R. A. S. Ferreira, R. O. Freire, P. D. Vaz, L. D. Carlos, C. D. Nunes and M. M. Nolasco, *J. Mater. Chem. C*, 2014, **2**, 9701-9711.
79. S. Li, H. Song, W. Li, S. Lu and X. Ren, *J. Nanosci. Nanotechnol.*, 2008, **8**, 1272-1278.
80. H. R. Li, J. Lin, L. S. Fu, J. F. Guo, Q. G. Meng, F. Y. Liu and H. J. Zhang, *Microporous Mesoporous Mater.*, 2002, **55**, 103-107.
81. C. Peng, H. Zhang, J. Yu, Q. Meng, L. Fu, H. Li, L. Sun and X. Guo, *J. Phys. Chem. B*, 2005, **109**, 15278-15287.
82. X. Guo, H. Guo, L. Fu, R. Deng, W. Chen, J. Feng, S. Dang and H. Zhang, *J. Phys. Chem. C*, 2009, **113**, 2603-2610.

83. Y. Li, B. Yan and H. Yang, *J. Phys. Chem. C*, 2008, **112**, 3959-3968.
84. D. B. Ambili Raj, S. Biju and M. L. P. Reddy, *J. Mater. Chem.*, 2009, **19**, 7976-7983.
85. V. Divya, S. Biju, R. L. Varma and M. L. P. Reddy, *J. Mater. Chem.*, 2010, **20**, 5220-5227.
86. J. Wu, G. Wang, D. Jin, J. Yuan, Y. Guan and J. Piper, *Chem. Commun.*, 2008, 365-367.
87. J. 389 msWu, Z. Ye, G. Wang, D. Jin, J. Yuan, Y. Guan and J. Piper, *J. Mater. Chem.*, 2009, **19**, 1258-1264.
88. L. Tian, Z. Dai, L. Zhang, R. Zhang, Z. Ye, J. Wu, D. Jin and J. Yuan, *Nanoscale*, 2012, **4**, 3551-3557.
89. S. L. C. Pinho, H. Faneca, C. F. G. C. Geraldés, M.-H. Delville, L. D. Carlos and J. Rocha, *Biomaterials*, 2012, **33**, 925-935.
90. A. P. Duarte, L. Mauline, M. Gressier, J. Dexpert-Ghys, C. Roques, J. M. A. Caiut, E. Deffune, D. C. G. Maia, I. Z. Carlos, A. A. P. Ferreira, S. J. L. Ribeiro and M.-J. Menu, *Langmuir*, 2013, **29**, 5878-5888.
91. Y. Wu, M. Shi, L. Zhao, W. Feng, F. Li and C. Huang, *Biomaterials*, 2014, **35**, 5830-5839.
92. H. Peng, M. I. J. Stich, J. Yu, L.-n. Sun, L. H. Fischer and O. S. Wolfbeis, *Adv. Mater.*, 2010, **22**, 716-719.
93. D. Ananias, F. A. A. Paz, D. S. Yufit, L. D. Carlos and J. Rocha, *J. Am. Chem. Soc.*, 2015, **137**, 3051-3058.
94. P. P. Lima, F. A. A. Paz, C. D. S. Brites, W. G. Quirino, C. Legnani, M. Costa e Silva, R. A. S. Ferreira, S. A. Júnior, O. L. Malta, M. Cremona and L. D. Carlos, *Org. Electron.*, 2014, **15**, 798-808.
95. C. D. S. Brites, P. P. Lima, N. J. O. Silva, A. Millán, V. S. Amaral, F. Palacio and L. D. Carlos, *Adv. Mater.*, 2010, **22**, 4499-4504.
96. C. D. S. Brites, P. P. Lima, N. J. O. Silva, A. Millan, V. S. Amaral, F. Palacio and L. D. Carlos, *Nanoscale*, 2013, **5**, 7572-7580.
97. K. O. Iwu, P. C. R. Soares-Santos, H. I. S. Nogueira, L. D. Carlos and T. Trindade, *J. Phys. Chem. C*, 2009, **113**, 7567-7573.
98. D. Zhao, S. J. Seo and B. S. Bae, *Adv. Mater.*, 2007, **19**, 3473-3479.
99. L. Armelao, G. Bottaro, S. Quici, M. Cavazzini, M. C. Raffo, F. Barigelletti and G. Accorsi, *Chem. Commun.*, 2007, 2911-2913.
100. L. Armelao, G. Bottaro, S. Quici, C. Scalera, M. Cavazzini, G. Accorsi and M. Bolognesi, *ChemPhysChem*, 2010, **11**, 2499-2502.
101. D. Zhang, D. Tang, X. Wang, Z.-a. Qiao, Y. Li, Y. Liu and Q. Huo, *Dalton Trans.*, 2011, **40**, 9313-9319.
102. K. Ai, B. Zhang and L. Lu, *Angew. Chem. Int. Ed.*, 2009, **48**, 304-308.
103. H. Li, W. Cheng, Y. Wang, B. Liu, W. Zhang and H. Zhang, *Chem. Eur. J.*, 2010, **16**, 2125-2130.
104. Y. Wang, Y. Yue, H. Li, Q. Zhao, Y. Fang and P. Cao, *Photochem. Photobiol. Sci.*, 2011, **10**, 128-132.
105. Z. Zhou, Y. Zheng and Q. Wang, *Inorg. Chem.*, 2014, **53**, 1530-1536.
106. K. Machida, H. Li, D. Ueda, S. Inoue and G. Adachi, *J. Lumin.*, 2000, **87-89**, 1257-1259.

107. J. Graffion, X. Cattoën, M. Wong Chi Man, V. R. Fernandes, P. S. André, R. A. S. Ferreira and L. D. Carlos, *Chem. Mater.*, 2011, **23**, 4773-4782.
108. M. M. Nolasco, P. M. Vaz, V. T. Freitas, P. P. Lima, P. S. Andre, R. A. S. Ferreira, P. D. Vaz, P. Ribeiro-Claro and L. D. Carlos, *J. Mater. Chem. A*, 2013, **1**, 7339-7350.
109. V. T. Freitas, L. Fu, A. M. Cojocariu, X. Cattoën, J. R. Bartlett, R. Le Parc, J.-L. Bantignies, M. Wong Chi Man, P. S. André, R. A. S. Ferreira and L. D. Carlos, *ACS Applied Materials & Interfaces*, 2015, **7**, 8770-8778.
110. S. F. H. Correia, P. P. Lima, P. S. André, M. R. S. Ferreira and L. A. D. Carlos, *Sol. Energy Mater. Sol. Cells*, 2015, **138**, 51-57.
111. P. He, H. Wang, S. Liu, J. Shi, G. Wang and M. Gong, *J. Phys. Chem. A*, 2009, **113**, 12885-12890.
112. D. B. A. Raj, B. Francis, M. L. P. Reddy, R. R. Butorac, V. M. Lynch and A. H. Cowley, *Inorg. Chem.*, 2010, **49**, 9055-9063.
113. Z.-J. Hu, X.-H. Tian, X.-H. Zhao, P. Wang, Q. Zhang, P.-P. Sun, J.-Y. Wu, J.-X. Yang and Y.-P. Tian, *Chem. Commun.*, 2011, **47**, 12467-12469.
114. F. Hoffmann, M. Cornelius, J. Morell and M. Fröba, *Angew. Chem. Int. Ed.*, 2006, **45**, 3216-3251.

Chapter 2

Achieving Visible Light Excitation in Carbazole Based Eu^{3+} - β -diketonate Complexes via Molecular Engineering

2.1. Abstract

*In this chapter, we present the synthesis, characterization and photophysical properties of a series of Eu^{3+} complexes prepared with novel carbazole-based fluorinated β -diketonates, namely, 4,4,5,5,5-pentafluoro-3-hydroxy-1-(9-phenyl-9H-carbazol-2-yl)pent-2-en-1-one (**L1**) and 4,4,5,5,5-pentafluoro-3-hydroxy-1-(9-(4-methoxyphenyl)-9H-carbazol-2-yl)pent-2-en-1-one (**L2**) as primary ligands and a bidentate phosphine oxide molecule, 4,5-bis(diphenylphosphino)-9,9-dimethylxanthene oxide (**DDXPO**) as ancillary ligand. Using the Sparkle/PM3 model the molecular geometries of the designed complexes are optimized and the luminescent parameters are calculated by the LUMPAC software. The results demonstrated that suitably expanded π -conjugation in the developed Eu^{3+} complexes dramatically red-shifted the excitation maxima to the visible region ($\lambda_{\text{ex,max}} = 420$ nm) with impressive quantum yields (34-42%). The triplet state energy levels of **L1** and **L2** in the complexes are higher than that of the excited emitting level of Eu^{3+} ion, $^5\text{D}_0$, so the photoluminescence mechanism of the Eu^{3+} complexes was proposed as a ligand-sensitized luminescence process. The predicted luminescent parameters from the Sparkle/PM3 structures are in good agreement with the experimental data.*

2.2. Introduction

Capitalizing on the unique and appealing spectroscopic characteristics of Eu^{3+} ions, its complexes have been utilized for a myriad of applications in domains as diverse as biomedical analysis (fluoroimmunoassays, FRET microscopy and cellular imaging),¹⁻⁵ sensing (pH, temperature, pathogens and toxic gases/ions)⁶⁻¹¹ and materials science (organic light emitting diodes and solar cells).¹²⁻¹⁹ The advantageous features of Eu^{3+} ions include long excited-state lifetimes (μs – ms range) and narrow, easily recognizable line-like emission bands with large Stokes shifts.²⁰⁻²⁴ The major obstacle in adopting Eu^{3+} for relevant applications arises due to its weak absorbance (molar absorption coefficients less than $10 \text{ L mol}^{-1} \text{ cm}^{-1}$) because of the parity forbidden intra 4f-4f transitions.²⁵⁻²⁷ Fortunately, this handicap is easily overcome by coordinating Eu^{3+} ions to suitable organic ligands which upon irradiation, absorb energy and transfer this energy to the metal center by the “antenna effect”.²⁸⁻³¹ Carbazole-based ligands are widely acknowledged for their role as antenna molecules for the Eu^{3+} ion by virtue of their modest cost, excellent hole transporting properties, easily tunable optoelectronic properties and their high chemical and environmental stabilities.³²⁻³⁴

There is a rapidly increasing demand for less-harmful biomarkers in life sciences and low-voltage-driven emitters in optoelectronics.³⁵⁻³⁷ Owing to this scenario, the development of visible light excitable europium complexes has received great attention in the past decade.³⁸⁻⁴³ Visible light is less harmful to biological tissues, allowing deep penetration, causing less background fluorescence and, thus, minimizing the interferences from biological

samples.^{44, 45} Gong and co-workers reported visible light excitable Eu^{3+} complexes using carbazole-based ligands by substituting the hydrogen atom on nitrogen with alkyl groups.⁴⁶ Also by introducing a $-\text{CF}_3$ group in the carbazole skeleton, they improved the luminescence quantum yield of the Eu^{3+} complexes to 34%.⁴⁷ Recently, our group reported a highly luminescent Eu^{3+} complex, $\text{Eu}(\text{CPFHP})_3(\text{DDXPO})$, (henceforth, referred to as complex **A**) using a carbazole-based fluorinated β -diketonate as the primary ligands and a phosphine oxide molecule as the neutral donor (Figure 2.1).⁴⁸ However, the excitation window of the reported complex was in the UV region ($\lambda_{ex,max} = 390$ nm), which limited its use in biological applications.

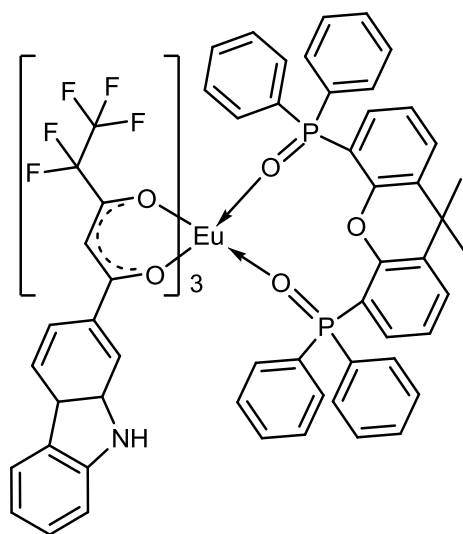


Figure 2.1. Chemical structure of $\text{Eu}(\text{CPFHP})_3(\text{DDXPO})$ (**A**).

Along the lines of the foregoing results, we have, in the present study, tuned the physical properties of carbazole-based fluorinated β -diketonate complexes into promising candidates for biological applications by extending the π -conjugation of the ligand, thus, decreasing the band gap of the complexes and

consequently shifting the excitation wavelength to the lower energy visible region. A series of new Eu^{3+} antenna complexes, which contain highly conjugated carbazole-based β -diketonates, **L1** (Scheme 2.1) and **L2** (Scheme 2.1) were synthesized. Here, 4,5-bis(diphenylphosphino)-9,9-dimethylxanthene oxide (**DDXPO**) has been chosen as the ancillary ligand. The newly synthesized Eu^{3+} complexes are characterized using various spectroscopic methods and their photophysical properties are investigated. From the photoluminescence studies we confirm that extension of π -conjugation in the organic ligand shifts the excitation window of the corresponding Eu^{3+} complexes towards the visible region. Also by introducing an electron donating $-\text{OCH}_3$ group, we improve the overall luminescence quantum yield and the luminescence lifetime values of Eu^{3+} complexes to 42% and 828 μs respectively, from 28% and 702 μs in the reference complex **A**. The molecular geometries of the designed complexes are optimized by the Sparkle/PM3 model and their spectroscopic parameters are theoretically calculated using the LUMPAC software.⁴⁹ Theoretical calculations of the photophysical properties of the complexes are in good agreement with the experimental values.

2.3. Experimental section

2.3.1. Materials and Instrumentation. Europium(III) nitrate pentahydrate (99.9% purity), gadolinium(III) nitrate hexahydrate (99.9% purity), 2-acetylcarbazole (98% purity), iodobenzene (98% purity), 4-iodoanisole (98% purity), copper(I) iodide, potassium phosphate tribasic (98% purity),

ethylpentafluoropropionate (98% purity) and sodium hydride (60% dispersion in mineral oil) were procured from Sigma-Aldrich. L-Proline (99% purity) was purchased from Alfa-Aesar. All the other chemicals used were of analytical reagent grade and were used without subsequent purification. Solvents were dried using standard methods. The bidentate phosphine oxide, 4,5-bis(diphenylphosphino)-9,9-dimethylxanthene oxide (**DDXPO**), was synthesized according to the method described in our earlier publication.⁵⁰

Perkin-Elmer Series 2 Elemental Analyser 2400 was used to record the C, H, and N elemental analyses. The FT-IR spectra were taken using KBr pellets on a Perkin-Elmer Spectrum One FT-IR spectrometer operating between 4000 and 450 cm⁻¹. The ¹H NMR (500 MHz), ¹³C NMR (125.7 MHz) and ³¹P NMR (202.44 MHz) spectra of the new compounds were recorded in chloroform-d solution using a Bruker 500 MHz NMR spectrometer. The chemical shifts are reported in parts per million relative to tetramethylsilane (SiMe₄) for ¹H NMR and ¹³C NMR spectra. The mass spectra were recorded using a JEOL JSM 600 fast atom bombardment (FAB) high resolution mass spectrometer (FAB-MS), and a TG/DTA-6200 instrument (SII Nano Technology Inc., Japan) was used to perform the thermogravimetric analyses. UV-visible absorption spectra were recorded with a Shimadzu, UV-2450 UV-vis spectrophotometer. All spectra were corrected for the background spectrum of the solvent. The absorbances of the ligands and complexes were measured in CHCl₃ solution. The solid state absorption spectra were recorded using UV-3600 UV-vis spectrophotometer, with BaSO₄ as reference. The PL spectra were recorded on a Spex-Fluorolog FL22 spectrofluorimeter equipped with a double grating 0.22 m Spex 1680 monochromator and a 450W Xe lamp as the excitation source operating

in the front face mode. The lifetime measurements were carried out at room temperature using a Spex 1040 D phosphorimeter. The overall quantum yields for the Eu^{3+} complexes were determined under ligand excitation (390-420 nm) and are based on the absolute method using a calibrated integrating sphere in a Spex-Fluorolog spectrofluorimeter.⁵¹ Xe-arc lamp was used to excite the samples placed in the sphere. The quantum yields were determined by comparing the spectral intensities of the lamp and the sample emission as reported in the literature.⁵²⁻⁵⁴ Using this experimental setup and the integrating sphere system, the solid-state fluorescence quantum yield of tris-8-hydroxyquinolinolato aluminum (Alq_3) was determined to be 40%, which is consistent with previously reported values.^{55, 56} Each sample was measured several times under slightly different experimental conditions. The estimated error for the quantum yields is ($\pm 10\%$).⁵⁷

2.3.2 Synthesis of the ligands. The ligands 4,4,5,5,5-pentafluoro-3-hydroxy-1-(9-phenyl-9H-carbazol-2-yl)pent-2-en-1-one (**L1**) and 4,4,5,5,5-pentafluoro-3-hydroxy-1-(9-(4-methoxyphenyl)-9H-carbazol-2-yl)pent-2-en-1-one (**L2**) were synthesized according to the route presented in Scheme 2.1.

2.3.2.1. Synthesis of 1-(9-phenyl-9H-carbazol-2-yl)ethanone. As shown in Scheme 2.1, the synthesis of 1-(9-phenyl-9H-carbazol-2-yl)ethanone was achieved by a typical substitution reaction. 2-Acetylcarbazole (2.3 mmol) was added to a round bottom flask containing 20 mL of anhydrous DMF. To this, K_3PO_4 (5 mmol) was added as base. 20 mol % of CuI and L-proline were added to the reaction mixture which act as catalyst and promoter respectively. The reaction mixture was refluxed for 48 h after the addition of 4-iodobenzene (2.3 mmol) at 160 °C. The resultant reaction mixture was then allowed to cool

to room temperature and poured into ice-cold water. The precipitate obtained was washed well with water, dried and purified by column chromatography (5% (v/v) ethyl acetate in hexane) to give the product as a yellowish solid (Yield 75%). ^1H NMR (500 MHz, CDCl_3): δ (ppm) 8.17 (s, 2H), 8.02 (s, 1H), 7.91-7.89 (m, 1H), 7.63 (t, 2H, $J = 7.5$), 7.55 (d, 2H, $J = 10$), 7.52-7.25 (m, 4H), 2.66 (s, 3H). ^{13}C NMR (125 MHz, CDCl_3): δ (ppm) 197.3, 145.8, 137.1, 136.6, 134.5, 129.6, 127.1, 125.8, 121.7, 120.9, 120.1, 114.8, 111.5, 110.3, 109.8, 26.9. FAB-MS $m/z = 286.34$ ($\text{M}^+ + \text{H}$).

2.3.2.2. Synthesis of 4,4,5,5,5-pentafluoro-3-hydroxy-1-(9-phenyl-9H-carbazol-2-yl)pent-2-en-1-one (L1). The ligand, 4,4,5,5,5-pentafluoro-3-hydroxy-1-(9-phenyl-9H-carbazol-2-yl)pent-2-en-1-one, **L1**, was synthesized by a modified Claisen condensation procedure. 1-(9-phenyl-9H-carbazol-2-yl)ethanone (1 mmol) was dissolved in 20 mL of dry THF. To this, sodium hydride (2.5 mmol) was added under inert atmosphere at 0 °C and stirred for 1 h. After the reaction mixture turned orange-red, ethyl pentafluoropropionate (1.2 mmol) was added drop wise and the reaction mixture was then allowed to stir under inert atmosphere for 12 h. The reaction was then quenched with cold water, 2 M HCl (20 mL) was added, and the solution was extracted with dichloromethane (3×20 mL). The organic layer was dried over anhydrous Na_2SO_4 , filtered and the solvent was evaporated. The product was then purified by column chromatography (5% (v/v) ethyl acetate in hexane) to give the product as yellowish crystals (yield 70%). Elemental analysis (%): Calcd. for $\text{C}_{23}\text{H}_{14}\text{F}_5\text{NO}_2$ (431.36): C, 64.04; H, 3.27; N, 3.25. Found: C, 64.24; H, 3.29; N, 3.30. ^1H NMR (500 MHz, CDCl_3): δ (ppm) 15.625 (broad, enol -OH),

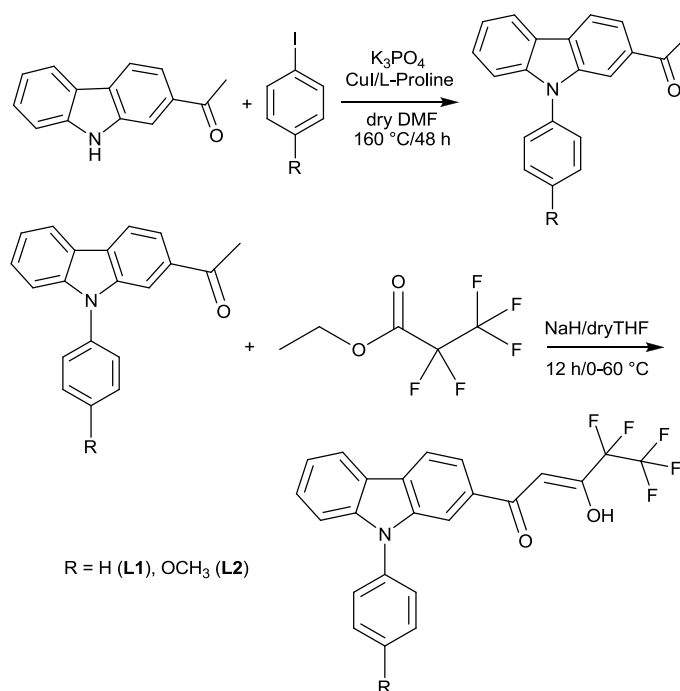
8.24-8.19 (m, 2H), 8.03 (s, 1H), 7.85 (d, 1H, $J = 10$), 7.67 (t, 2H, $J = 7.5$), 7.57-7.49 (m, 4H), 7.42 (d, 1H, $J = 10$), 7.35 (t, 1H, $J = 7$), 6.70 (s, 1H). ^{13}C NMR (125 MHz, CDCl_3): δ (ppm) 198.2, 186.8, 158.3, 142.8, 140.8, 136.8, 130.3, 130.0, 128.3, 128.1, 127.3, 122.3, 121.3, 120.8, 120.6, 119.3, 110.4, 109.8, 94.7. FT-IR (KBr) ν_{max} : 3070, 1620, 1597, 1504, 1234 cm^{-1} . FAB-MS $m/z = 432.66$ ($\text{M}^+ + \text{H}$).

2.3.2.3. Synthesis of 1-(9-(4-methoxyphenyl)-9H-carbazol-2-yl)ethanone. A

typical substitution reaction was used for the synthesis of 1-(9-(4-methoxyphenyl)-9H-carbazol-2-yl)ethanone. 2-Acetylcarbazole (2.3 mmol) was added to a round bottom flask containing 20 mL of anhydrous DMF. To this K_3PO_4 (5 mmol) was added as base. 20 mol% of CuI and L-proline were added to the reaction mixture which act as catalyst and promoter respectively. The reaction mixture was refluxed for 48 h after the addition of 4-iodoanisole (2.3 mmol) at 160 °C. The resultant reaction mixture was then allowed to cool to room temperature and poured into ice-cold water. The precipitate obtained was washed well with water, dried and purified by column chromatography (5% (v/v) ethyl acetate in hexane) to give the product as a yellowish solid (yield 73%). ^1H NMR (500 MHz, CDCl_3): δ (ppm) 8.18 (d, 2H, $J = 10$), 7.94 (s, 1H), 7.89 (d, 1H, $J = 10$), 7.48-7.43 (m, 3H), 7.35-7.29 (m, 2H), 7.14 (d, 2H, $J = 7$), 3.94 (s, 3H), 2.67 (s, 3H). ^{13}C NMR (125 MHz, CDCl_3): δ (ppm) 198.4, 159.2, 143.0, 141.1, 134.8, 129.6, 128.7, 127.4, 127.0, 122.2, 121.11, 120.2, 120.2, 120.0, 115.3, 110.1, 110.0, 55.7, 27.0. FAB-MS $m/z = 316.05$.

2.3.2.4. Synthesis of 4,4,5,5,5-pentafluoro-3-hydroxy-1-(9-(4-methoxyphenyl)-9H-carbazol-2-yl)pent-2-en-1-one (L2). The ligand

4,4,5,5,5-pentafluoro-3-hydroxy-1-(9-(4-methoxyphenyl)-9H-carbazol-2-yl)pent-2-en-1-one, **L2**, was synthesized by a modified Claisen condensation procedure. 1-(9-(4-methoxyphenyl)-9H-carbazol-2-yl)ethanone (1 mmol) was dissolved in 20 mL of dry THF. To this, sodium hydride (2.5 mmol) was added under inert atmosphere at 0 °C and stirred for 1 h. After the reaction mixture turned orange-red, ethyl pentafluoropropionate (1.2 mmol) was added drop wise and the reaction mixture was allowed to stir under inert atmosphere for 12 h. The reaction was then quenched with water, 2 M HCl (20 mL) was added, and the solution was extracted with dichloromethane (3 × 20 mL). The organic layer was dried over anhydrous Na_2SO_4 , filtered and the solvent was evaporated. The product was then purified by column chromatography (5% (v/v) ethyl acetate in hexane) to give the product as yellowish crystals (yield 70%). Elemental analysis (%): Calcd. for $\text{C}_{24}\text{H}_{16}\text{F}_5\text{NO}_3$ (461.38): C, 62.48; H, 3.50; N, 3.04. Found: C, 62.64; H, 3.59; N, 3.10. ^1H NMR (500 MHz, CDCl_3 , Figure 2.2): δ (ppm) 15.77 (broad, enol -OH), 8.23-8.19 (m, 2H), 7.95 (s, 1H), 7.84 (d, 1H, $J = 10$), 7.50 (t, 1H, $J = 7.5$), 7.45 (d, 2H, $J = 10$), 7.36-7.32 (m, 2H), 7.16 (d, 2H, $J = 10$), 6.71 (s, 1H), 3.95 (s, 3H). ^{13}C NMR (125 MHz, CDCl_3): δ (ppm) 198.4, 186.9, 159.4, 143.2, 141.1, 129.9, 129.2, 128.6, 128.1, 128.0, 122.2, 121.1, 120.2, 120.1, 120.0, 115.3, 110.3, 109.7, 93.8, 55.6. FT-IR (KBr) ν_{max} : 2949, 2837, 1618, 1595, 1520, 1233 cm^{-1} . FAB-MS $m/z = 462.36$ ($\text{M}^+ + \text{H}$).



Scheme 2.1. Synthesis of ligands **L1** and **L2**.

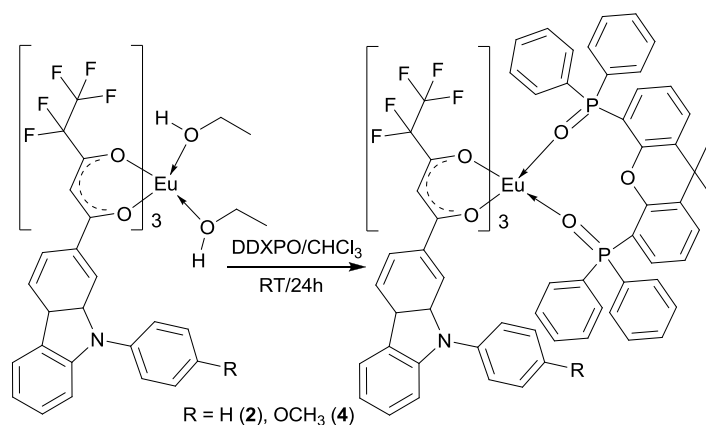
2.3.2.5. Synthesis of solvated lanthanide β -diketonate complexes: A mixture of the relevant β -diketonate ligand, **L1** or **L2**, (0.6 mmol) and NaOH (0.6 mmol) in 10 mL ethanol was stirred at room temperature for 10 min, following which a saturated ethanolic solution of $\text{Ln}(\text{NO}_3)_3 \cdot n\text{H}_2\text{O}$ (0.2 mmol) was added drop wise, and the reaction mixture stirred subsequently for 24 h (Scheme 2.2). 20 mL water was then added, and the precipitate formed was filtered off, washed again with water (3×10 mL), dried and purified by recrystallization from THF-water (10:90) mixture.

$\text{Eu}(\text{L1})_3(\text{C}_2\text{H}_5\text{OH})_2$ (**1**). Elemental analysis (%): Calcd. for $\text{C}_{73}\text{H}_{51}\text{F}_{15}\text{N}_3\text{O}_8\text{Eu}$ (1535.26): C, 57.11; H, 3.35; N, 2.74. Found: C, 57.23; H, 3.39; N, 2.75. FT-IR (KBr) ν_{max} : 3440 (br), 2957, 2934, 1607, 1514, 1234 cm^{-1} . FAB-MS m/z = 1443.36 ($\text{M}^+ - 2\text{C}_2\text{H}_5\text{OH}$), 1013.32 ($\text{M}^+ - \text{L1} - 2\text{C}_2\text{H}_5\text{OH}$), 582.84 ($\text{M}^+ - 2\text{L1} - 2\text{C}_2\text{H}_5\text{OH}$).

2.3.2.6. Synthesis of Eu^{3+} complexes 2 and 4. Complexes **2** and **4** were prepared by stirring equimolar quantities of the corresponding solvated Eu^{3+} complexes and the phosphine oxide **DDXPO** in CHCl_3 solution for 24 h at room temperature (Scheme 2.3). The products were isolated by solvent evaporation and purified by recrystallization from a chloroform-hexane mixture (20:80).

Eu(L1)₃(DDXPO) (2). Elemental analysis (%): Calcd. for $\text{C}_{108}\text{H}_{71}\text{F}_{15}\text{N}_3\text{O}_9\text{P}_2\text{Eu}$ (2053.62): C, 63.16; H, 3.48; N, 2.05. Found: C, 63.24; H, 3.53; N, 2.10. FT-IR (KBr) ν_{max} : 3060, 2970, 1617, 1516, 1502, 1214, 1151 cm^{-1} . FAB-MS $m/z = 1623.28$ ($\text{M}^+ - \text{L1}$), 1193.20 ($\text{M}^+ - 2\text{L1}$), 763.11 ($\text{M}^+ - 3\text{L1}$). ^{31}P NMR (202.44 MHz, CDCl_3): δ (ppm) -91.92 .

Eu(L2)₃(DDXPO) (4). Elemental analysis (%): Calcd. for $\text{C}_{111}\text{H}_{77}\text{F}_{15}\text{N}_3\text{O}_{12}\text{P}_2\text{Eu}$ (2143.40): C, 62.19; H, 3.62; N, 1.96. Found: C, 62.34; H, 3.59; N, 2.03. FT-IR (KBr) ν_{max} : 3070, 1616, 1504, 1234, 1150 cm^{-1} . FAB-MS $m/z = 1683.36$ ($\text{M}^+ - \text{L2}$), 1222.14 ($\text{M}^+ - 2\text{L2}$), 763.11 ($\text{M}^+ - 3\text{L2}$). ^{31}P NMR (202.44 MHz, CDCl_3): δ (ppm) -96.96 .



Scheme 2.3. Synthesis of Eu^{3+} complexes **2** and **4**.

2.3.3. Geometry optimization by Sparkle/PM3 model. Using Sparkle/PM3 model implemented in MOPAC2009 program,⁵⁸ the ground state geometries of complexes **1-4** and **A** were optimized. The high accuracy of Sparkle models in predicting the ground state geometries of lanthanide complexes has been demonstrated in previous publications.⁵⁹ The keywords used were, PM3; SPARKLE; PRECISE; BFGS; GNORM = 0.25; SCFCRT = 1.D-10 (to increase the SCF convergence criterion) and XYZ (for Cartesian coordinates).

2.3.4. Experimental Judd-Oflet parameters. The intensity parameters Ω_λ for the complexes **1-4** were determined from their emission spectra using equation (2.1):

$$\Omega_\lambda = (2\lambda + 1) \sum_t^{\lambda-1, \lambda+1(\text{odd}) \text{ or } (\text{all})} \sum_{p=t} |B_{\lambda tp}|^2 (2t + 1) \quad (2.1)$$

The $B_{\lambda tp}$ are calculated by:

$$B_{\lambda tp} = B_{\lambda tp}^{ed} + B_{\lambda tp}^{dc} \quad (2.2)$$

To know which values each parameters (λ , t and p) assume in relation to each other is a very important aspect to facilitate the application of Judd-Oflet theory. As indicated in equations (2.1) and (2.2), for example, when λ is 2, t will be equal to 1 and 3, whereas the values of p will be equal to 0, 1, ..., t .

The first term in equation (2.2), $B_{\lambda tp}^{ed}$, refers to the forced electric-dipole (ed) contribution, which is given by equation (2.3):

$$B_{\lambda tp}^{ed} = \frac{2}{\Delta E} \langle r^{t+1} \rangle \theta(t, \lambda) \gamma_p^t \quad (2.3)$$

And the second term, $B_{\lambda tp}^{dc}$, refers to the dynamic coupling (*dc*) contribution, given by equation (2.4):

$$B_{\lambda tp}^{dc} = - \left[\frac{(\lambda + 1)(2\lambda + 3)}{2\lambda + 1} \right]^{1/2} \langle r^\lambda \rangle (1 - \sigma_\lambda) \langle f \| C^{(\lambda)} \| f \rangle \Gamma_p^{-t} \delta_{t, \lambda+1} \quad (2.4)$$

Where, ΔE corresponds to the energy level difference between the ground state barycenters and the first excited state configuration of the opposite parity. The radial integrals, $\langle r^\lambda \rangle$ were taken from reference,⁶⁰ by extrapolating the quantity $\langle r^8 \rangle$. The terms $\theta(t, p)$ are numeric factors associated with each Ln^{3+} ion and are estimated from radial integrals of Hartree-Fock calculations.⁶¹ $(1 - \sigma_\lambda)$ is the shielding field due to $5s$ and $5p$ filled orbitals of Ln^{3+} ions, which have radial extensions larger than those of $4f$ orbitals. $\langle f \| C^{(\lambda)} \| f \rangle$ is a tensor operator of rank ($\lambda = 2, 4,$ and 6) with values $\langle 3 \| C^{(2)} \| 3 \rangle = -1.366$, $\langle 3 \| C^{(4)} \| 3 \rangle = 1.128$ e $\langle 3 \| C^{(6)} \| 3 \rangle = -1.270$ for Ln^{3+} ions. $\delta_{t, \lambda+1}$ is the Kronecker delta function. $B_{\lambda tp}^{dc}$ as such is equal to zero when t is different from $\lambda + 1$.

2.4. Results and discussion

2.4.1. Synthesis and characterization of ligands and Ln^{3+} complexes.

The β -diketonate ligands, **L1** and **L2**, were synthesized with an overall yield of 72% and 70%, respectively using the procedure outlined in Scheme 2.1. The synthesized ligands were well characterized by ^1H NMR, ^{13}C NMR, FT-IR and mass spectroscopic (FAB-MS) methods as well as by elemental analyses. The ^1H NMR analyses (Figure 2.2) reveal that the β -diketonate ligands **L1** and **L2** exist as enolic forms in chloroform solution. The synthesis procedures for the

lanthanide complexes **1-6**, are illustrated in Schemes 2.2 and 2.3. The synthesized complexes were characterized by FT-IR, mass spectroscopy (FAB-MS), ^{31}P NMR and elemental analyses. The FT-IR spectra of complexes **1**, **3**, **5** and **6** exhibit a broad absorption band in the $3000\text{-}3500\text{ cm}^{-1}$ region, which points to the presence of coordinated solvent molecules, while the absence of this band in complexes **2** and **4** implies that the solvent molecules are replaced by the bidentate phosphine oxide ligand. The carbonyl stretching frequencies for the β -diketonate ligands, **L1** (1597 cm^{-1}) and **L2** (1595 cm^{-1}) were shifted to higher wavenumbers in the complexes (1607 cm^{-1} in **1**; 1617 cm^{-1} in **2**; 1607 cm^{-1} in **3**; 1616 cm^{-1} in **4**; 1609 cm^{-1} in **5** and 1607 cm^{-1} in **6**), indicating the coordination of carbonyl oxygen to the Ln^{3+} cation in each case. The P=O stretching frequency of free **DDXPO** (1190 cm^{-1}) has been shifted to lower wave numbers in complex **2** (1151 cm^{-1}) and complex **4** (1150 cm^{-1}) which confirms the involvement of phosphoryl oxygen in the complex formation. The elemental analyses and FAB-MS data for the complexes **1-6** suggest that the central Ln^{3+} ion is coordinated to β -diketonate ligands in a metal-to-ligand mole ratio of 1:3. In addition to this, complexes **1**, **3**, **5** and **6** have two ethanol molecules coordinated to the metal centre satisfying the high co-ordination number of the Ln^{3+} ion. As expected in complexes **2** and **4** one molecule of the bidentate phosphine oxide, **DDXPO** replaces the solvent molecules from the coordination sphere of **1** and **3**, respectively. The presence of **DDXPO** in the coordination sphere of complexes **2** and **4** was further confirmed by the upfield shift in the ^{31}P NMR signal of complexes **2** (-91.92 ppm) and **4** (-96.96 ppm) compared to the free **DDXPO** (30.97 ppm).

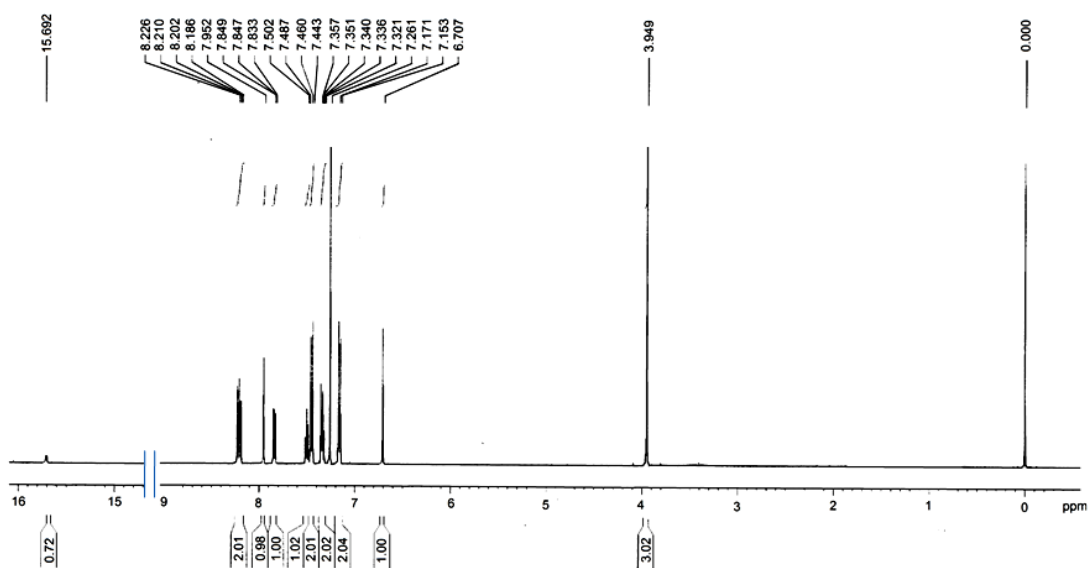


Figure 2.2. ^1H NMR spectrum of ligand L2.

2.4.2. Thermal behaviour of the complexes. In order to explore the thermal behaviour of the Eu^{3+} complexes, thermogravimetric analyses (TGA) of all the complexes were carried out under nitrogen atmosphere. The weight loss profiles for representative complexes **1**, **2** and **5** are displayed in Figure 2.3 and that of complexes **3**, **4** and **6** are given in Figure 2.4. The thermogravimetric profiles of solvated complexes (**1**, **3**, **5** and **6**) exhibit a weight loss of approximately 5% in the first step (120 to 160 °C), which corresponds to the elimination of the coordinated ethanol solvent molecules (calculated as 5.99, 5.97, 5.66, 5.64 % for **1**, **3**, **5** and **6**, respectively). Notably, complexes **2** and **4** are stable up to 325 °C, compared to our reference complex **A** (stable only up to 180 °C). The high thermal stability of complexes **2** and **4** further confirms the successful replacement of the coordinated ethanol molecules with the bidentate phosphine oxide molecule which in turn provides increased rigidity to the complexes.

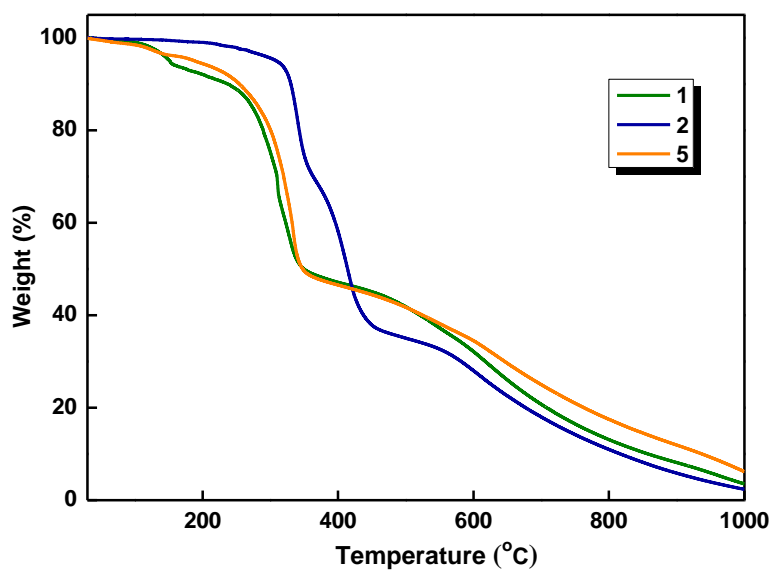


Figure 2.3. Thermogravimetric curves for complexes 1, 2 and 5.

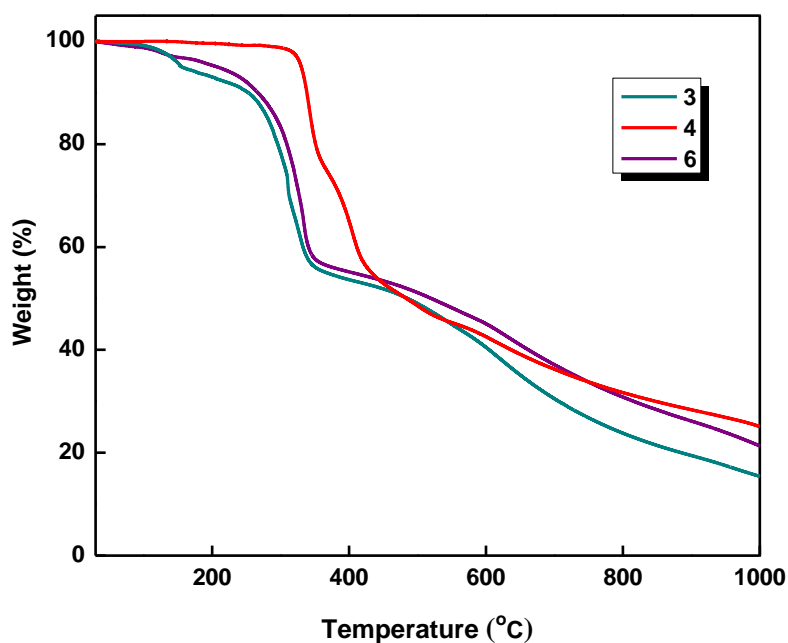


Figure 2.4. Thermogravimetric curves for complexes 3, 4 and 6.

2.4.3. Molecular structures of the complexes by Sparkle/PM3 model.

Numerous attempts to grow single crystals for the complexes 1-6 from CHCl_3 /ethanol and CHCl_3 /2-methoxy ethanol solutions were not fruitful. Hence, in the present study the molecular structures of the designed complexes

were determined using the Sparkle/PM3 model.⁶² At the outset, we verified the suitability of this model by calculating the ground state geometry of our previously reported reference complex **A** (Figure 2.1) whose crystal structure is known.⁴⁸ The geometry and spherical coordinates obtained from this calculation are compared to the reported crystal structure data (Figure 2.5 and Table 2.1) and found to be in good agreement. The optimized geometries of the complexes **1**, **2**, **3** and **4** are depicted in Figures 2.6-2.9. The calculated spherical atomic coordinates of the complexes **1-4** are summarized in Tables 2.2 and 2.3. In the solvated complexes **1** and **3** the central Ln^{3+} ions are coordinated to three β -diketonate ligands and two ethanol molecules. On the other hand, in complexes **2** and **4**, in addition to the three β -diketonate ligands, one bidentate phosphine oxide molecule is present, which replaces the two solvent molecules in the co-ordination sphere of the Eu^{3+} ions. The oxygen atom connecting the two phosphine oxide units is not involved in the coordination and consequently, the coordination number of Eu^{3+} ions in these complexes is 8. The average bond length between Eu^{3+} ion and the β -diketonate oxygen atoms in typical complex **4** is 2.469 Å, which is longer than that of Eu^{3+} and phosphoryl oxygen atoms (2.421 Å) of **DDXPO**. These trends are also in good accord with the crystal data reported for the complex **A**.

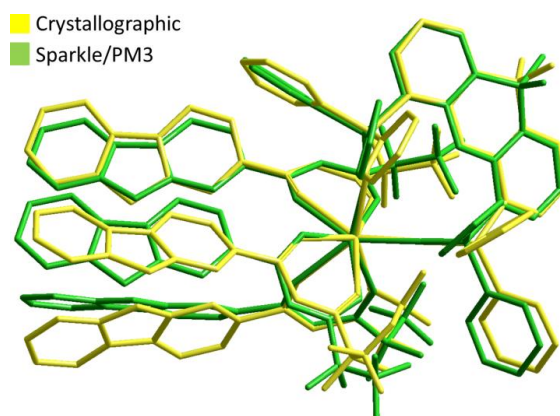


Figure 2.5. Overlay of crystal structure and Sparkle/PM3 model optimized structure of complex A.

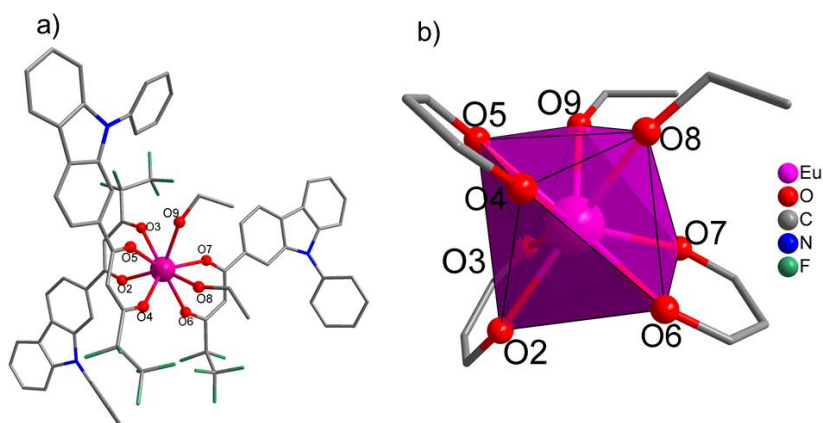


Figure 2.6. (a) The ground state geometry of the complex 1 optimized by the Sparkle/PM3 model (b) Coordination environment of complex 1. All hydrogen atoms are omitted for clarity.

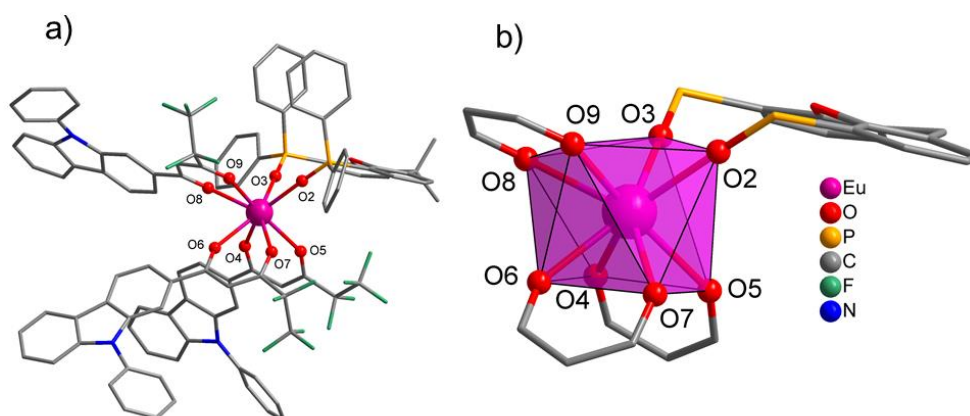


Figure 2.7. (a) The ground state geometry of the complex 2 optimized by the Sparkle/PM3 model (b) Coordination environment of complex 2. All hydrogen atoms are omitted for clarity.

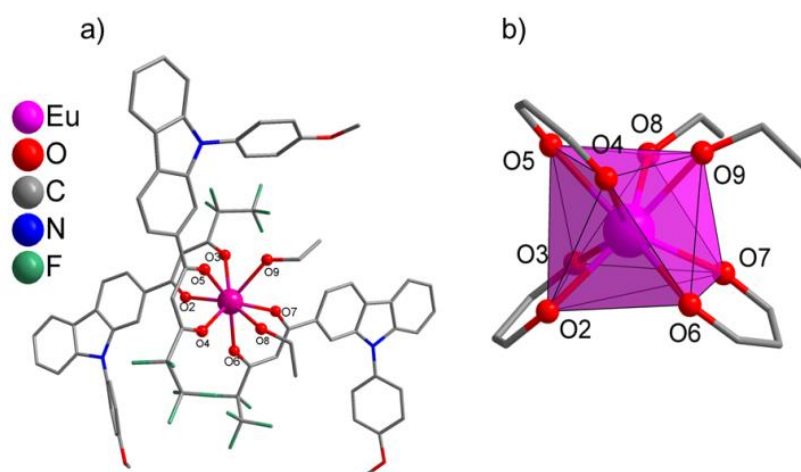


Figure 2.8. (a) The ground state geometry of the complex **3** optimized by the Sparkle/PM3 model (b) Coordination environment of complex **3**. All hydrogen atoms are omitted for clarity.

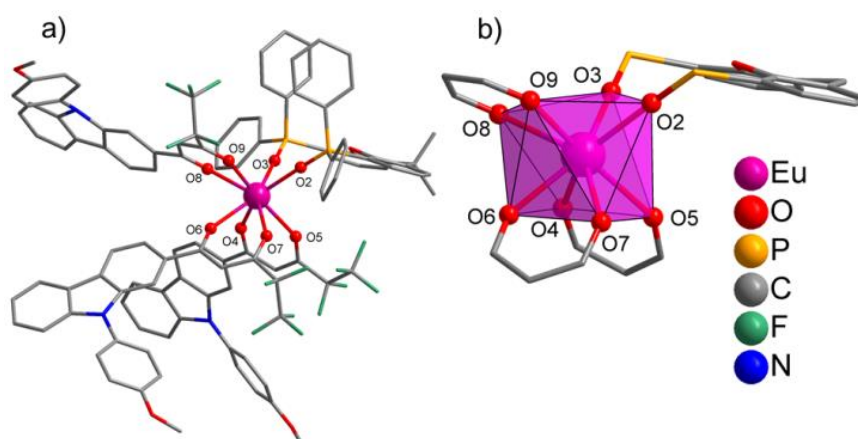


Figure 2.9. (a) The ground state geometry of the complex **4** optimized by the Sparkle/PM3 model (b) Coordination environment of complex **4**. All hydrogen atoms are omitted for clarity.

Table 2.1. Comparison of selected bond lengths (\AA) from crystal structure and Sparkle/PM3 model geometry for complex **A**

	Bond lengths (\AA)		Difference
	Crystal Structure	Sparkle/PM3 Model	
Eu-O2	2.300	2.418	0.118
Eu-O3	2.372	2.422	0.051
Eu-O4	2.399	2.469	0.071
Eu-O5	2.358	2.471	0.113

Eu-O6	2.399	2.463	0.064
Eu-O7	2.411	2.469	0.058
Eu-O8	2.344	2.474	0.129
Eu-O9	2.414	2.473	0.058
			Average 0.083

Table 2.2. Selected bond lengths (Å) for complexes 1-4 by Sparkle/PM 3 model

	1	2	3	4
Eu-O2	2.4496	2.4190	2.4506	2.4194
Eu-O3	2.4478	2.4221	2.4500	2.4224
Eu-O4	2.4574	2.4673	2.4562	2.4665
Eu-O5	2.4494	2.4721	2.4533	2.4737
Eu-O6	2.4482	2.4653	2.4482	2.4643
Eu-O7	2.4481	2.4668	2.4492	2.4674
Eu-O8	2.4481	2.4717	2.4492	2.4710
Eu-O9	2.4509	2.4712	2.4497	2.4706

Table 2.3. Selected bond angles (°) for complexes 1-4 by Sparkle/PM 3 model

	1	2	3	4
Eu-O2-O3	63.836	77.953	63.981	77.947
Eu-O2-O4	91.884	145.014	93.140	144.765
Eu-O2-O5	95.925	89.430	89.775	89.164
Eu-O2-O6	84.492	136.549	83.904	136.713
Eu-O2-O7	109.227	83.862	113.823	84.090
Eu-O2-O8	148.444	122.685	129.569	122.899
Eu-O2-O9	133.400	77.442	150.847	77.520
Eu-O3-O4	134.288	80.238	138.919	80.178
Eu-O3-O5	80.679	88.550	81.973	88.632
Eu-O3-O6	126.024	142.588	123.528	142.359
Eu-O3-O7	86.084	152.342	87.600	152.598
Eu-O3-O8	146.579	75.318	67.704	75.277
Eu-O3-O9	73.004	105.440	144.205	105.283
Eu-O4-O5	63.053	62.904	63.302	62.942

Eu-O4-O6	85.659	74.118	83.877	74.210
Eu-O4-O7	139.601	104.416	133.480	104.244
Eu-O4-O8	60.677	132.332	114.963	76.719
Eu-O4-O9	106.899	90.515	60.393	135.332
Eu-O5-O6	148.712	103.020	146.206	103.269
Eu-O5-O7	142.657	70.459	146.662	70.430
Eu-O5-O8	85.542	138.592	69.793	138.632
Eu-O5-O9	59.249	158.080	88.592	158.002
Eu-O6-O7	63.529	62.573	63.558	62.552
Eu-O6-O8	78.543	72.626	137.059	72.337
Eu-O6-O9	137.824	76.207	81.419	76.192
Eu-O7-O8	86.732	132.332	76.941	132.121
Eu-O7-O9	83.519	90.515	81.579	90.615
Eu-O8-O9	73.770	62.694	76.615	62.762

2.4.4. Photophysical properties

2.4.4.1. UV-visible absorption spectra. In Figures 2.10 and 2.11 the UV-visible absorption spectra of the free ligands and their corresponding Ln^{3+} complexes (in CHCl_3 solution, $c = 2 \times 10^{-6} \text{ mol L}^{-1}$) are depicted. The ligands **L1** and **L2** display two distinct broad bands: the band in the 315-440 nm ($\lambda_{\text{max}} = 370 \text{ nm}$) region corresponds to the electronic transitions of the enolic group of β -diketonate moiety⁴⁸ and band in the 240-270 nm region is attributable to the electronic transitions of the carbazole backbone.⁴⁷ The large molar absorption coefficients of **L1** ($3.32 \times 10^4 \text{ L mol}^{-1} \text{ cm}^{-1}$) and **L2** ($3.41 \times 10^4 \text{ L mol}^{-1} \text{ cm}^{-1}$) indicate that they have a strong ability to absorb light, which is a major criteria for an organic ligand to act as a good antenna molecule.⁶³

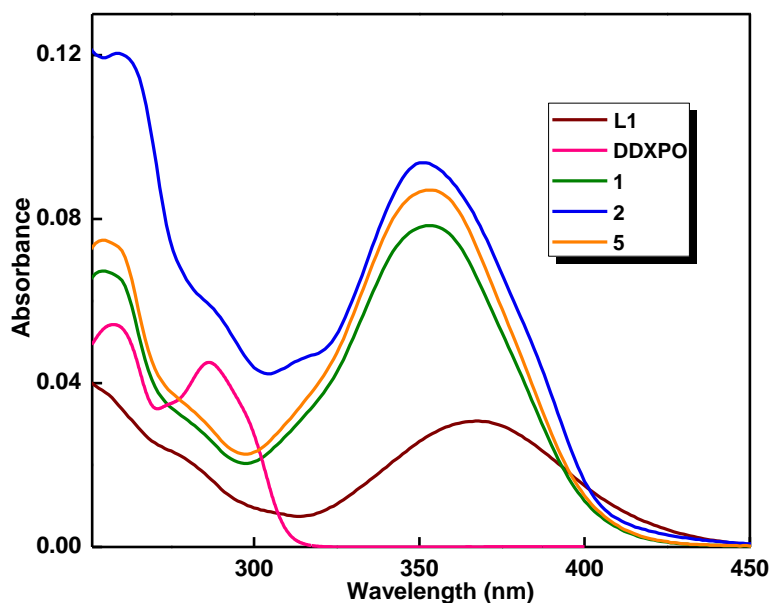


Figure 2.10. UV-vis absorption spectra of the ligands **L1** and **DDXPO** and complexes **1**, **2** and **5** in CHCl_3 solution ($c = 2 \times 10^{-6} \text{ mol L}^{-1}$).

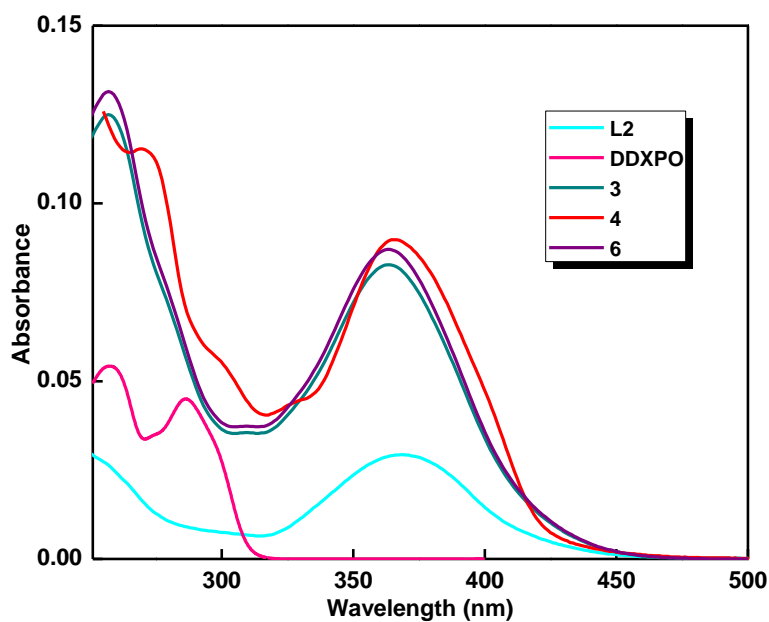


Figure 2.11. UV-vis absorption spectra of the ligands **L2** and **DDXPO** and complexes **3**, **4** and **6** in CHCl_3 solution ($c = 2 \times 10^{-6} \text{ mol L}^{-1}$).

Apart from a small blue shift observed due to the perturbation induced by metal coordination, the absorption spectra of the lanthanide complexes are similar to that of free ligands, indicating that the singlet excited states of the ligands are not significantly affected by the complexation to the Ln^{3+} ion. This

slight blue shift indicates that the electron density on the acceptor moiety (diketonate- C_2F_5) of the ligand has been perturbed by the negative charge developed at the carbonyl oxygens which resulted from deprotonation of the ligand and the presence of Ln^{3+} ions with Lewis acid character.⁶⁴ The band corresponding to the electronic transitions of the chelating phosphine oxide **DDXPO** is also observed in the absorption spectra of complexes **2** and **4** at around 280 nm. The presence of the ancillary **DDXPO** ligand not only satisfies the high coordination number of the central Eu^{3+} ion but also improves the absorbance of the complexes. The molar absorption coefficient values for the complexes **1-4** were calculated at the respective λ_{max} value and were found to be 8.65×10^4 , 9.85×10^4 , 9.05×10^4 and 9.92×10^4 $\text{L mol}^{-1} \text{cm}^{-1}$, respectively. The magnitudes of these absorbance values are approximately three times higher than that of the β -diketonate ligands, and this trend is compatible with the presence of three β -diketonate ligands in each complex.

2.4.4.2. Solid state absorption spectra of the complexes. To find out the effect of increased conjugation of organic ligands on the absorption spectra of the complexes, we recorded the solid state absorption spectra of complexes **2** and **4** and compared them with that of reference complex **A** (Figure 2.12). It is clear from the normalized spectra that the absorption maxima of the complexes **2** and **4** have been extended towards the visible region (410 and 420 nm, respectively) when compared to complex **A** (390 nm). By replacing the hydrogen atom of the carbazole nitrogen atom with a phenyl group we have successfully extended the π -conjugation of the molecule, which in turn shifts the absorption maximum of complex **1** towards visible region (from 390 to 410

nm). Moreover the introduction of an electron donating methoxy group on the phenyl moiety further red shifts the absorption window towards 420 nm.

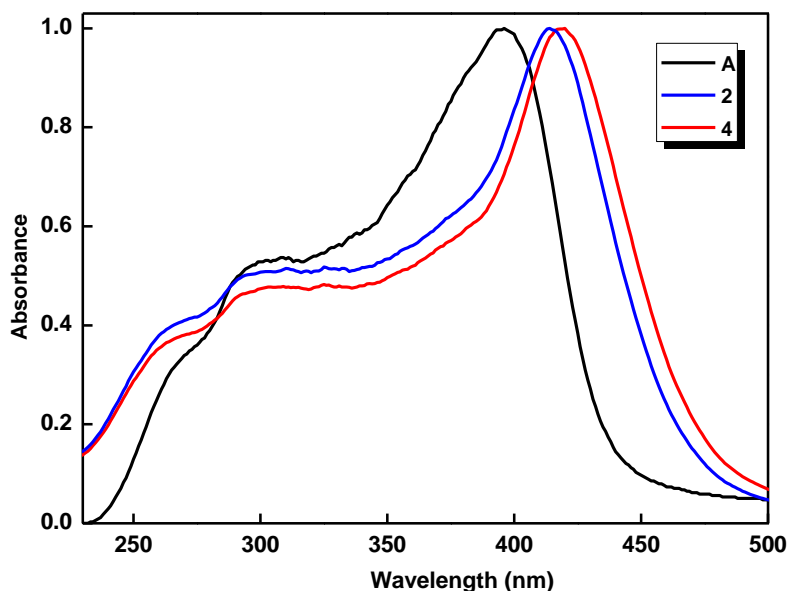


Figure 2.12. Normalized solid state UV-vis absorption spectra of complexes **A**, **2** and **4**.

2.4.4.3. Steady state photoluminescence studies. The room temperature solid state excitation and emission spectra of complexes **1-4** are given in Figure 2.13. The excitation spectra of the complexes **1-4** were recorded by monitoring the intense $^5\text{D}_0 \rightarrow ^7\text{F}_2$ transition of the Eu^{3+} ion at 612 nm. Even though some sharp excitation bands due to the metal absorptions are present, the excitation spectra mainly exhibit a broad band between 250-500 nm region, which corresponds to the electronic transitions of the antenna ligands. Compared to the ligand absorption bands, the metal absorption peaks are weaker, which indicates that the sensitization via ligand excited states is more efficient than the direct excitation of the Eu^{3+} absorption bands. The normalized excitation and emission spectra of the complexes **A**, **2** and **4** are depicted in Figure 2.14. The replacement of the hydrogen on the carbazole nitrogen with a phenyl ring

in **L1** has increased the π -conjugation in the molecule, which remarkably extends the excitation window of complexes **1** and **2** to the visible region ($\lambda_{ex,max}$ up to 410 nm). Moreover the introduction of an electron donating – OCH_3 group in **L2** increases the electron density in the molecule which further red shifts the excitation window of the corresponding Eu^{3+} complexes (complexes **3** and **4**) more towards the visible region ($\lambda_{ex,max}$ up to 420 nm). The room temperature emission spectra of Eu^{3+} complexes **1-4** exhibit the characteristically intense transitions of the Eu^{3+} ion upon excitation at 400 nm.⁶⁵ As shown in Figures 2.13 and 2.14, the radiative transitions from the excited $^5\text{D}_0$ state to the different J levels of the lower ^7F state were observed in the emission spectrum. Maximum peak intensities at 580, 592, 612, 652, and 702 nm were recorded for the $J = 0, 1, 2, 3$ and 4 transitions respectively.⁶⁶ The most intense transition is observed at 612 nm, corresponding to the hypersensitive $^5\text{D}_0 \rightarrow ^7\text{F}_2$ transition and indicates that the coordination sphere of the Eu^{3+} ion is devoid of a center of symmetry. Moreover, the existence of a single chemical environment around the Eu^{3+} ion is evident from the single sharp peak corresponding to the $^5\text{D}_0 \rightarrow ^7\text{F}_0$ transition at 580 nm.⁶⁶ The absence of broad ligand emission bands in the emission spectra of all the complexes indicates the effective sensitization of the Eu^{3+} ion by the coordinated β -diketonate ligands. From the solid state luminescence studies of complexes **1-4** (Figure 2.13) it is clear that the displacement of the solvent molecules from the coordination spheres of the complexes $\text{Eu}(\mathbf{L1})_3(\text{C}_2\text{H}_5\text{OH})_2$ (**1**) and $\text{Eu}(\mathbf{L2})_3(\text{C}_2\text{H}_5\text{OH})_2$ (**3**) by the chelating phosphine oxide **DDXPO** in **2** and **4** significantly improves the luminescence intensity.

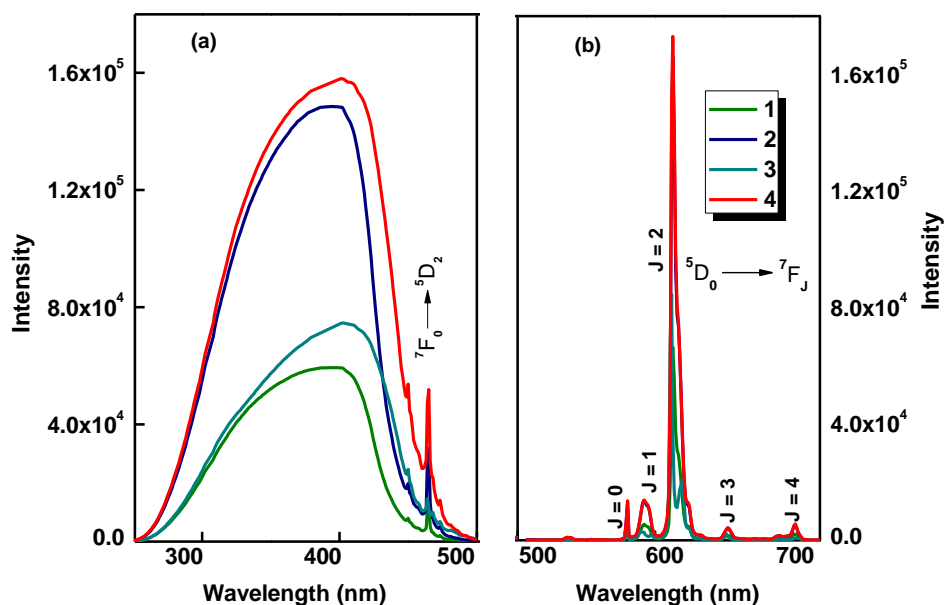


Figure 2.13. Solid-state room-temperature (a) excitation ($\lambda_{em} = 612$ nm) and (b) emission ($\lambda_{ex} = 400$ nm) spectra for complexes 1-4

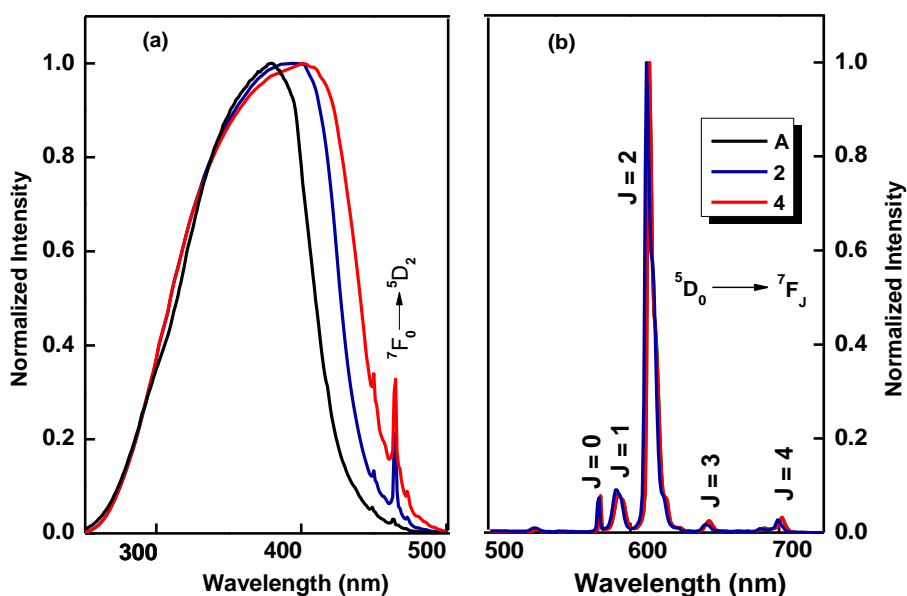


Figure 2.14. Normalized solid state room-temperature (a) excitation ($\lambda_{em} = 612$ nm) and (b) emission ($\lambda_{ex} = 400$ nm) spectra of complexes A, 2 and 4

2.4.4.4. Luminescence decay profiles. The luminescence decay times (τ) for complexes **1-4** were recorded at room temperature at an excitation wavelength of 400 nm and monitored at the most intense emission line at 612 nm and are depicted in Figures 2.15 and 2.16.

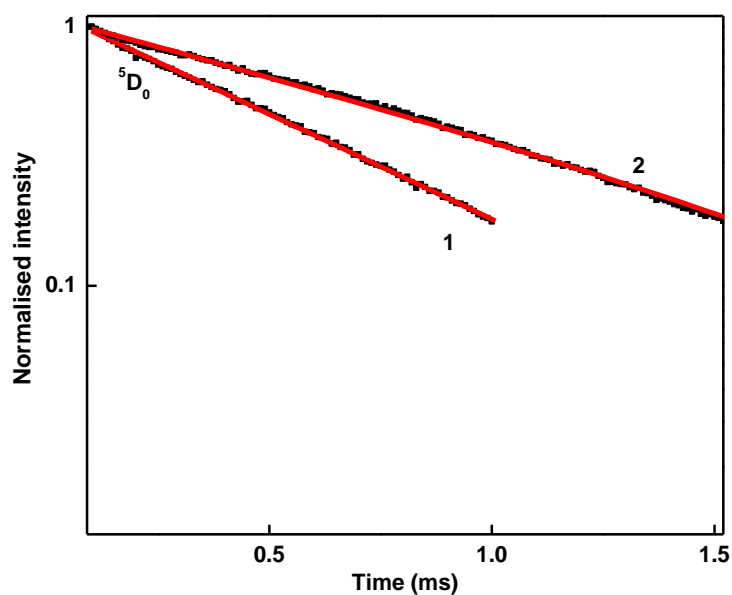


Figure 2.15. Solid state luminescence decay profiles of complexes **1** and **2** monitored at 612 nm.

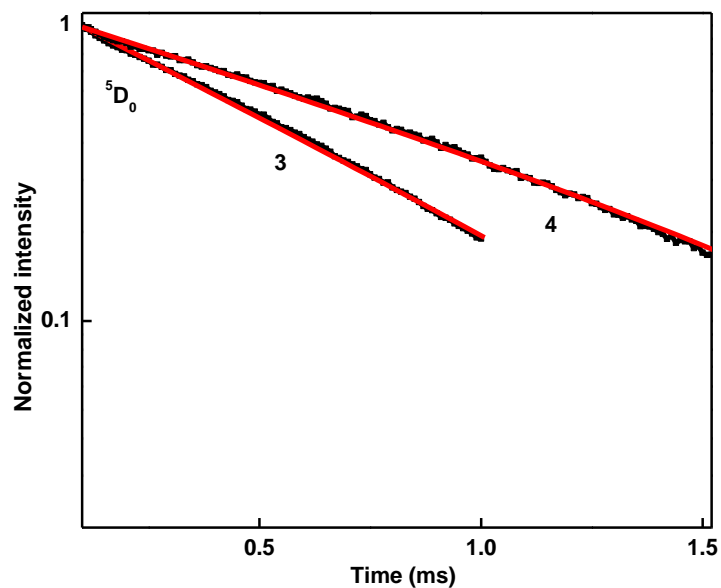


Figure 2.16. Solid state luminescence decay profiles of complexes **3** and **4** monitored at 612 nm.

The lifetime profiles for all the Eu^{3+} complexes are fitted with single exponentials, which indicates the existence of a single chemical environment around the central Eu^{3+} ion in each case. The relatively shorter lifetimes observed for the solvated complexes **1** and **3** may be due to the presence of high frequency oscillators in the solvent molecules, which activate the non-

radiative decay pathways. In the case of the Eu^{3+} ion, the energy gap between the first excited state and the ground state levels is approximately $12,000 \text{ cm}^{-1}$. So, in the presence of solvent molecules, the coupling of Eu^{3+} excited states and the third vibrational overtone of the proximate OH oscillators ($\nu_{\text{OH}} \sim 3300\text{-}3500 \text{ cm}^{-1}$) will be effective, which is responsible for the quenching of luminescence in the solvated complexes **1** and **3**. On the other hand, these non-radiative decay pathways are limited in the complexes **2** and **4**, which thereby exhibit longer life time values.

By analysing the emission spectra in terms of equation (2.5), the luminescence efficiencies and the relation between structure and photophysical properties of Eu^{3+} complexes can be understood in a better way.

$$\Phi_{\text{overall}} = \eta_{\text{sens}} \Phi_{\text{Ln}} = \eta_{\text{sens}} (\tau_{\text{obs}}/\tau_{\text{rad}}) \quad (2.5)$$

where, η_{sens} , is the efficiency of the ligand-to-metal energy transfer, Φ_{overall} and Φ_{Eu} , represent the overall and intrinsic luminescence quantum yields of Eu^{3+} , respectively, τ_{obs} and τ_{rad} are the observed and radiative lifetimes of Eu^{3+} ($^5\text{D}_0$).⁶⁷ Because of the low absorption intensities of direct f-f excitation, the intrinsic quantum yields of Eu^{3+} could not be determined experimentally. Therefore, the radiative lifetime of Eu^{3+} ($^5\text{D}_0$) has been calculated from equation (2.6),⁶⁸

$$1/\tau_{\text{rad}} = A_{\text{MD},0} \times n^3 \times (I_{\text{tot}}/I_{\text{MD}}) \quad (2.6)$$

where, n is the refractive index (1.5), $A_{\text{MD},0}$ represents the spontaneous emission probability for the $^5\text{D}_0 \rightarrow ^7\text{F}_1$ transition in vacuum (14.65 s^{-1}), and $I_{\text{tot}}/I_{\text{MD}}$ implies the ratio of the total integrated intensity of the corrected Eu^{3+}

emission spectrum to the integrated intensity of the magnetic dipole ${}^5\text{D}_0 \rightarrow {}^7\text{F}_1$ transition. The intrinsic quantum yields for Eu^{3+} complexes (Φ_{Eu}) have been calculated from the ratio ($\tau_{\text{obs}}/\tau_{\text{rad}}$) and the values are tabulated in Table 2.4. The overall quantum yields (Φ_{overall}), radiative (A_{RAD}) and nonradiative (A_{NR}) decay rates and energy transfer efficiencies (η_{sens}) are also listed in Table 2.4.

The replacement of solvent molecules by the chelating phosphine oxide molecule results in an approximately 3-fold increase in the overall quantum yield of Eu^{3+} -tris- β -diketonate complexes (from 12 to 34% in complex **2** and 15 to 42% in complex **4**) in the solid state. This significant increase in the overall quantum yields may be due to (i) the removal of quenching effect of the O–H vibrations, which results in the increase of intrinsic quantum yields from 28% (in **1**) and 32% (in **3**) to 64% (in **2**) and 63% (in **4**) and (ii) the enhancement of transfer efficiencies from 43% (in **1**) to 52% (in **2**) and 47% (in **3**) to 66% (in **4**).

Table 2.4. Radiative (A_{RAD}) and non-radiative (A_{NR}) decay rates, ${}^5\text{D}_0$ lifetime (τ_{obs}), intrinsic quantum yield (Φ_{Eu} , %), energy transfer efficiency (η_{sens} , %) and overall quantum yield (Φ_{overall} , %) for complexes **1-4**.

Compound	$A_{\text{RAD}}/\text{s}^{-1}$	$A_{\text{NR}}/\text{s}^{-1}$	$\tau_{\text{obs}}/\mu\text{s}$	Φ_{Eu} , (%)	η_{sens} , (%)	Φ_{overall} , (%)
1	623	1994	382 ± 1	28	43	12
2	755	433	842 ± 1	64	52	34
3	793	1924	368 ± 1	32	47	15
4	757	451	828 ± 1	63	66	42

Determination of the relevant electronic states of the ligands is important to investigate the photoluminescence mechanism of the Eu^{3+} complexes. The singlet (S_1) energy levels of the ligands **L1** and **L2** were estimated by referring

to the upper wavelengths of the UV-vis absorption edges of $\text{Gd}(\mathbf{L1})_3(\text{C}_2\text{H}_5\text{OH})_2$ and $\text{Gd}(\mathbf{L2})_3(\text{C}_2\text{H}_5\text{OH})_2$ complexes, respectively. The triplet (T_1) energy levels of the ligands were calculated by referring to the lower wavelength emission edges of the corresponding phosphorescence spectra of complexes $\text{Gd}(\mathbf{L1})_3(\text{C}_2\text{H}_5\text{OH})_2$ (**5**) and $\text{Gd}(\mathbf{L2})_3(\text{C}_2\text{H}_5\text{OH})_2$ (**6**) (Figure 2.17). The S_1 and T_1 values for **L1** were found to be $24,190 \text{ cm}^{-1}$ and $20,660 \text{ cm}^{-1}$, respectively. The S_1 and T_1 values for **L2** were found to be $24,100 \text{ cm}^{-1}$ and $20,550 \text{ cm}^{-1}$ respectively. The S_1 ($31,850 \text{ cm}^{-1}$) and T_1 ($23,470 \text{ cm}^{-1}$) levels for the ancillary ligand **DDXPO** were taken from our earlier report.⁵⁰ The triplet energy levels of the ligands **L1** and **L2** are found to have significantly higher energy than that of the $^5\text{D}_0$ state of Eu^{3+} , proving that the novel β -diketonate ligands can act as antenna molecules for the photosensitization of the Eu^{3+} ion.⁶⁹ However, the higher $^5\text{D}_1$ emitting state of Eu^{3+} ($18,800 \text{ cm}^{-1}$) appears critically close to the triplet states of the **L1** and **L2** ligands, which can bring about the thermally assisted back-energy transfer from the Eu^{3+} ion.⁷⁰ On the other hand, the triplet energy level of the bidentate **DDXPO** ($23,470 \text{ cm}^{-1}$), is suitable for efficient energy transfer with all the $^5\text{D}_2$, $^5\text{D}_1$ and $^5\text{D}_0$ energy levels of Eu^{3+} ion.

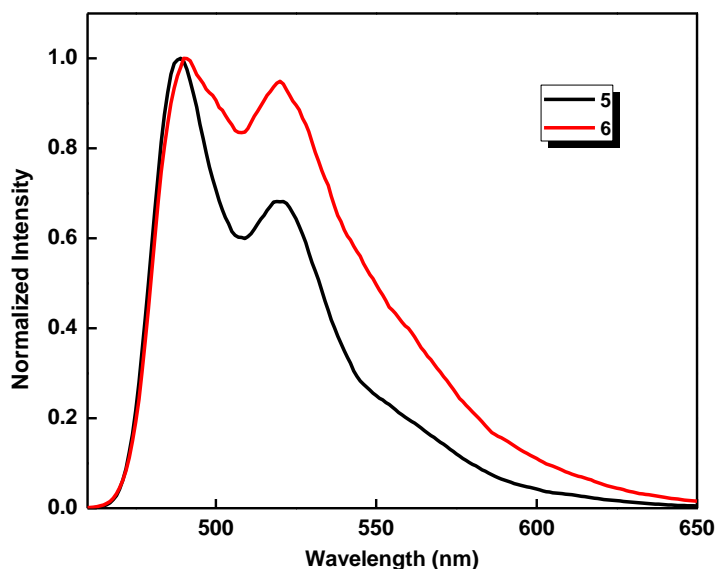


Figure 2.17. 77 K Phosphorescence spectra of complexes 5 and 6.

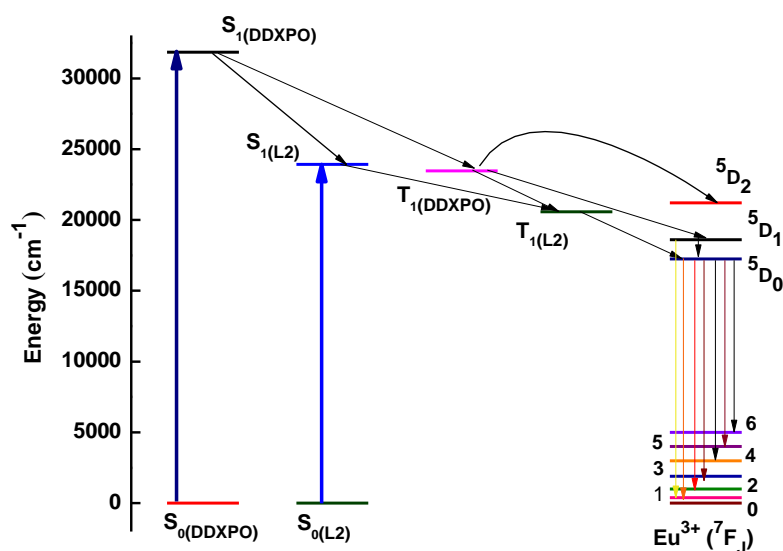


Figure 2.18. Schematic representation of the energy transfer mechanism for complex 4.

Therefore, the photoluminescence mechanism in the Eu^{3+} complexes is proposed to be a ligand sensitized luminescence process, the antenna effect. Based on the preceding observations, the schematic representation of energy level diagrams showing the possible energy transfer mechanism for complex 4 is depicted in Figure 2.18.

2.4.5. Comparison of experimental and theoretical luminescent parameters. The LUMPAC software, developed by Freire and coworkers,⁴⁹ was used to calculate the theoretical luminescent values of intensity parameters (Ω_λ), radiative emission rate (A_{RAD}), nonradiative emission rate (A_{NR}), intrinsic quantum yield (Φ_{Eu}), and overall quantum yield ($\Phi_{overall}$).

The experimental intensity parameters of the complexes **1-4** were calculated from the emission spectra, based on the Judd–Ofelt theory which provides a simple model for reproducing the intensities of f–f transitions within the frame of the crystal-field concept.^{71, 72} The theory assumes that the central metal ion is affected by the nearest neighbour atoms, through a static electric field which is also known as crystal or ligand field. The intensity parameters, Ω_2 and Ω_4 were experimentally calculated from the $^5\text{D}_0 \rightarrow ^7\text{F}_2$ and $^5\text{D}_0 \rightarrow ^7\text{F}_4$ electronic transitions of the corresponding Eu^{3+} ions and describe the interaction between the lanthanide ion and the ligands. The experimental and theoretical values for the intensity parameters (Ω_2 , Ω_4 and Ω_6) are depicted in Table 2.5, and are in excellent agreement with each other. The experimental Ω_6 value could not be calculated due to the absence of $^5\text{D}_0 \rightarrow ^7\text{F}_6$ transition in the emission spectra and hence the intensity parameter Ω_6 can be determined only theoretically. The high values obtained for Ω_2 may be due to the hypersensitive nature of the $^5\text{D}_0 \rightarrow ^7\text{F}_2$ transition and implies that the dynamic coupling mechanism is operative. This also indicates the presence of a highly polarisable chemical environment in the Eu^{3+} complexes. Compared to Ω_2 , Ω_4 is less sensitive to the coordination environment and the relatively low values of Ω_4 point to the rigidity associated with the co-ordination sphere of the synthesized Eu^{3+}

complexes. The theoretical calculations were carried out as described in our recent report.⁷³ The experimental and theoretical values of the radiative (A_{RAD}) and non-radiative (A_{NR}) decay rates, intrinsic quantum yields ($\Phi_{Eu, \%}$) and overall quantum yields ($\Phi_{overall, \%}$) are also summarized in Table 2.5.

Table 2.5. Experimental and theoretical intensity parameters Ω_2 , Ω_4 and Ω_6 , radiative (A_{RAD}) and non-radiative (A_{NR}) decay rates, intrinsic quantum yield ($\Phi_{overall, \%}$) and overall quantum yield ($\Phi_{overall, \%}$) values derived from the optimized Sparkle/PM3 structure.

Compound	Ω_2	Ω_4	Ω_6	A_{RAD}/s^{-1}	A_{NR}/s^{-1}	$\Phi_{Eu, \%}$	$\Phi_{overall, \%}$
1a	17.60	3.09	---	623	1994	28	12
1b	17.59	3.09	0.12	627	1990	24	10
2a	21.60	2.51	---	755	433	64	34
2b	21.57	2.37	0.24	737	451	62	24
3a	23.51	2.71	---	793	1924	32	15
3b	23.51	2.70	0.36	800	1917	30	18
4a	21.10	2.59	---	757	451	63	42
4b	21.11	2.39	0.045	723	485	60	57

The values of the intensity parameters are presented in 10^{-20} cm^2 .
a = experimental, b = theoretical

The intrinsic quantum yield values of the complexes obtained experimentally and theoretically are perfectly matching. In the case of overall quantum yield, even though the experimentally and theoretically calculated values follow the same trend in general, there is a slight variation in the exact figures. This may be due to considerable dependence of the theoretically calculated quantum yield values on the triplet energies of the complexes.

2.5. Conclusions

In this work, we have reported the synthesis, characterization and photophysical properties of a series of carbazole-based fluorinated β -diketonate europium complexes. The novel ligands were designed by introducing a phenyl group or a para methoxy phenyl group on the nitrogen atom of the carbazole ring in complexes **1** and **3**, respectively. Replacement of solvent molecules in **1** and **3** by the ancillary ligand, bidentate phosphine oxide **DDXPO** led to complexes **2** and **4** respectively. The molecular geometries of the designed complexes were optimized by the Sparkle/PM3 model. The suitability of Sparkle/PM3 model was verified by comparing the ground state geometry of our previously reported related complex **A**, with its crystal structure. Complexes **2** and **4** showed remarkable overall quantum yields of 34% and 42% and excellent lifetime values of 842 μs and 828 μs respectively. They also exhibited impressive thermal stabilities up to 325 $^{\circ}\text{C}$. The excitation window was extended from 390 nm into the visible region by the introduction of a phenyl ring on the carbazole ring, giving **1** and **2**, (up to 410 nm) and further by the introduction of an electron donating para-methoxy group onto the phenyl ring in **3** and **4** (up to 420 nm). This shift achieved from near UV to visible blue region is important in the context of biological imaging as long term exposure of near UV light may destroy the cells under study and also the surrounding cells around the target area, in case of *in vivo* experiments. The theoretical luminescent properties of the designed Eu^{3+} complexes were calculated based on the optimized Sparkle/PM3 structure using the LUMPAC software and were in good agreement with the experimental values, proving

the suitability of the Sparkle/PM3 model. Thus, the dramatic improvements in the thermal stabilities, photophysical properties and excitation window, brought about by the introduction of extended conjugation and ancillary ligand; emphasize the significance of molecular engineering of ligand and complexes to achieve desired properties.

2.6. References

1. E. G. Moore, A. P. S. Samuel and K. N. Raymond, *Acc. Chem. Res.*, 2009, **42**, 542-552.
2. J.-C. G. Bunzli and S. V. Eliseeva, *Chem. Sci.*, 2013, **4**, 1939-1949.
3. S. J. Butler, M. Delbianco, L. Lamarque, B. K. McMahon, E. R. Neil, R. Pal, D. Parker, J. W. Walton and J. M. Zwieter, *Dalton Trans.*, 2015, **44**, 4791-4803.
4. D. Geißler, S. Linden, K. Liermann, K. D. Wegner, L. J. Charbonnière and N. Hildebrandt, *Inorg. Chem.*, 2014, **53**, 1824-1838.
5. M. Rajendran, E. Yapici and L. W. Miller, *Inorg. Chem.*, 2014, **53**, 1839-1853.
6. D. Ananias, F. A. A. Paz, D. S. Yufit, L. D. Carlos and J. Rocha, *J. Am. Chem. Soc.*, 2015, **137**, 3051-3058.
7. S. M. Borisov, R. Fischer, R. Saf and I. Klimant, *Adv. Funct. Mater.*, 2014, **24**, 6548-6560.
8. Y. Li, S. Zhang and D. Song, *Angew. Chem. Int. Ed.*, 2013, **52**, 710-713.
9. H. Peng, M. I. J. Stich, J. Yu, L.-n. Sun, L. H. Fischer and O. S. Wolfbeis, *Adv. Mater.*, 2010, **22**, 716-719.
10. B. V. Harbuzaru, A. Corma, F. Rey, J. L. Jordá, D. Ananias, L. D. Carlos and J. Rocha, *Angew. Chem. Int. Ed.*, 2009, **48**, 6476-6479.
11. K. Ai, B. Zhang and L. Lu, *Angew. Chem. Int. Ed.*, 2009, **48**, 304-308.
12. Y. Hasegawa and T. Nakanishi, *RSC Adv.*, 2015, **5**, 338-353.
13. P. P. Lima, F. A. A. Paz, C. D. S. Brites, W. G. Quirino, C. Legnani, M. Costa e Silva, R. A. S. Ferreira, S. A. Júnior, O. L. Malta, M. Cremona and L. D. Carlos, *Org. Electron.*, 2014, **15**, 798-808.
14. J. Wu, J. Wang, J. Lin, Y. Xiao, G. Yue, M. Huang, Z. Lan, Y. Huang, L. Fan, S. Yin and T. Sato, *Sci. Rep.*, 2013, **3**, 2058-2063.
15. M. Pietraszkiwicz, M. Maciejczyk, I. D. W. Samuel and S. Zhang, *J. Mater. Chem. C*, 2013, **1**, 8028-8032.
16. J. Kido and Y. Okamoto, *Chem. Rev.*, 2002, **102**, 2357-2368.
17. S. F. H. Correia, V. de Zea Bermudez, S. J. L. Ribeiro, P. S. Andre, R. A. S. Ferreira and L. D. Carlos, *J. Mater. Chem. A*, 2014, **2**, 5580-5596.
18. A. de Bettencourt-Dias, *Dalton Trans.*, 2007, 2229-2241.
19. H. Kataoka, S. Omagari, T. Nakanishi and Y. Hasegawa, *Opt. Mat.*, 2015, **42**, 411-416.
20. S. Zou, Q. Li and S. Du, *RSC Adv.*, 2015, **5**, 34936-34941.
21. B. Francis, D. B. Ambili Raj and M. L. P. Reddy, *Dalton Trans.*, 2010, **39**, 8084-8092.
22. L. D. Carlos, R. A. S. Ferreira, V. d. Z. Bermudez and S. J. L. Ribeiro, *Adv. Mater.*, 2009, **21**, 509-534.
23. K. Binnemans, *Chem. Rev.*, 2009, **109**, 4283-4374.
24. J.-C. G. Bunzli and C. Piguet, *Chem. Soc. Rev.*, 2005, **34**, 1048-1077.
25. K. Machado, S. Mukhopadhyay, R. A. Videira, J. Mishra, S. M. Mobin and G. S. Mishra, *RSC Adv.*, 2015, **5**, 35675-35682.
26. A. J. Amoroso and S. J. A. Pope, *Chem. Soc. Rev.*, 2015, **44**, 4723-4742.
27. G. F. de Sá, O. L. Malta, C. de Mello Donegá, A. M. Simas, R. L. Longo, P. A. Santa-Cruz and E. F. da Silva Jr, *Coord. Chem. Rev.*, 2000, **196**, 165-195.

28. S. M. Bruno, D. Ananias, F. A. Almeida Paz, M. Pillinger, A. A. Valente, L. D. Carlos and I. S. Goncalves, *Dalton Trans.*, 2015, **44**, 488-492.
29. N. Sabbatini, M. Guardigli and J.-M. Lehn, *Coord. Chem. Rev.*, 1993, **123**, 201-228.
30. J.-M. Lehn, *Angew. Chem. Int. Ed.*, 1990, **29**, 1304-1319.
31. J. Feng and H. Zhang, *Chem. Soc. Rev.*, 2013, **42**, 387-410.
32. S. Raphael, M. L. P. Reddy, K. V. Vasudevan and A. H. Cowley, *Dalton Trans.*, 2012, **41**, 14671-14682.
33. P. He, H. H. Wang, S. G. Liu, J. X. Shi, G. Wang and M. L. Gong, *Inorg. Chem.*, 2009, **48**, 11382-11387.
34. S. Biju, L.-J. Xu, C.-Z. Sun and Z.-N. Chen, *J. Mater. Chem. C*, 2015, **3**, 5775-5782.
35. S. V. Eliseeva and J.-C. G. Bunzli, *Chem. Soc. Rev.*, 2010, **39**, 189-227.
36. J.-C. G. Bunzli, *Chem. Rev.*, 2010, **110**, 2729-2755.
37. C. P. Montgomery, B. S. Murray, E. J. New, R. Pal and D. Parker, *Acc. Chem. Res.*, 2009, **42**, 925-937.
38. M. Irfanullah, D. K. Sharma, R. Chulliyil and A. Chowdhury, *Dalton Trans.*, 2015, **44**, 3082-3091.
39. V. Divya and M. L. P. Reddy, *J. Mater. Chem. C*, 2013, **1**, 160-170.
40. V. Divya, R. O. Freire and M. L. P. Reddy, *Dalton Trans.*, 2011, **40**, 3257-3268.
41. A. Dadabhoy, S. Faulkner and P. G. Sammes, *J. Chem. Soc., Perkin Trans. 2*, 2002, 348-357.
42. A. Dadabhoy, S. Faulkner and P. G. Sammes, *J. Chem. Soc., Perkin Trans. 2*, 2000, 2359-2360.
43. A. D'Aléo, A. Picot, A. Beeby, J. A. Gareth Williams, B. Le Guennic, C. Andraud and O. Maury, *Inorg. Chem.*, 2008, **47**, 10258-10268.
44. M. L. P. Reddy, V. Divya and R. Pavithran, *Dalton Trans.*, 2013, **42**, 15249-15262.
45. V. Divya, V. Sankar, K. G. Raghu and M. L. P. Reddy, *Dalton Trans.*, 2013, **42**, 12317-12323.
46. P. He, H. H. Wang, H. G. Yan, W. Hu, J. X. Shi and M. L. Gong, *Dalton Trans.*, 2010, **39**, 8919-8924.
47. P. He, H. H. Wang, S. G. Liu, J. X. Shi and M. L. Gong, *Appl. Phys. B*, 2010, **99**, 757-762.
48. D. B. A. Raj, B. Francis, M. L. P. Reddy, R. R. Butorac, V. M. Lynch and A. H. Cowley, *Inorg. Chem.*, 2010, **49**, 9055-9063.
49. J. D. L. Dutra, T. D. Bispo and R. O. Freire, *J. Comput. Chem.*, 2014, **35**, 772-775.
50. D. B. Ambili Raj, S. Biju and M. L. P. Reddy, *Dalton Trans.*, 2009, 7519-7528.
51. L. Porrès, A. Holland, L.-O. Pålsson, A. Monkman, C. Kemp and A. Beeby, *J. Fluoresc.*, 2006, **16**, 267-273.
52. L. O. Pålsson and A. P. Monkman, *Adv. Mater.*, 2002, **14**, 757-758.
53. J. C. de Mello, H. F. Wittmann and R. H. Friend, *Adv. Mater.*, 1997, **9**, 230-232.
54. M. S. Wrighton, D. S. Ginley and D. L. Morse, *J. Phys. Chem.*, 1974, **78**, 2229-2233.
55. N. S. S. Kumar, S. Varghese, N. P. Rath and S. Das, *J. Phys. Chem. C*, 2008, **112**, 8429-8437.
56. M. Cölle, J. Gmeiner, W. Milius, H. Hillebrecht and W. Brütting, *Adv. Funct. Mater.*, 2003, **13**, 108-112.

57. S. V. Eliseeva, O. V. Kotova, F. Gumy, S. N. Semenov, V. G. Kessler, L. S. Lepnev, J.-C. G. Bünzli and N. P. Kuzmina, *J. Phys. Chem. A*, 2008, **112**, 3614-3626.
58. M. R. Felício, T. G. Nunes, P. M. Vaz, A. M. P. Botas, P. Ribeiro-Claro, R. A. S. Ferreira, R. O. Freire, P. D. Vaz, L. D. Carlos, C. D. Nunes and M. M. Nolasco, *J. Mater. Chem. C*, 2014, **2**, 9701-9711.
59. D. A. Rodrigues, N. B. da Costa and R. O. Freire, *J. Chem. Inf. Model.*, 2011, **51**, 45-51.
60. A. J. Freeman and J. P. Desclaux, *J. Magn. Magn. Mater.*, 1979, **12**, 11-21.
61. O. L. Malta, S. J. L. Ribeiro, M. Faucher and P. Porcher, *J. Phys. Chem. Solids*, 1991, **52**, 587-593.
62. R. O. Freire, G. B. Rocha and A. M. Simas, *J. Braz. Chem. Soc.*, 2009, **20**, 1638-1645.
63. M. L. P. Reddy and S. Sivakumar, *Dalton Trans.*, 2013, **42**, 2663-2678.
64. A. W. Woodward, A. Frazer, A. R. Morales, J. Yu, A. F. Moore, A. D. Campiglia, E. V. Jucov, T. V. Timofeeva and K. D. Belfield, *Dalton Trans.*, 2014, **43**, 16626-16639.
65. L. Armelao, S. Quici, F. Barigelletti, G. Accorsi, G. Bottaro, M. Cavazzini and E. Tondello, *Coord. Chem. Rev.*, 2010, **254**, 487-505.
66. K. Binnemans, *Coord. Chem. Rev.*, 2015, **295**, 1-45.
67. N. M. Shavaleev, S. V. Eliseeva, R. Scopelliti and J.-C. G. Bünzli, *Inorg. Chem.*, 2010, **49**, 3927-3936.
68. M. H. V. Werts, R. T. F. Jukes and J. W. Verhoeven, *Phys. Chem. Chem. Phys.*, 2002, **4**, 1542-1548.
69. M. Latva, H. Takalo, V.-M. Mikkala, C. Matachescu, J. C. Rodríguez-Ubis and J. Kankare, *J. Lumin.*, 1997, **75**, 149-169.
70. N. Armaroli, G. Accorsi, F. Barigelletti, S. M. Couchman, J. S. Fleming, N. C. Harden, J. C. Jeffery, K. L. V. Mann, J. A. McCleverty, L. H. Rees, S. R. Starling and M. D. Ward, *Inorg. Chem.*, 1999, **38**, 5769-5776.
71. G. S. Ofelt, *J. Chem. Phys.*, 1962, **37**, 511-520.
72. B. R. Judd, *Phys. Rev.*, 1962, **127**, 750-761.
73. J. D. L. Dutra and R. O. Freire, *J. Photochem. Photobiol. A*, 2013, **256**, 29-35.

Chapter 3

Amine Functionalized Silica Nanoparticles Incorporating Covalently Linked Visible Light Excitable Eu³⁺ Complexes: Synthesis, Characterization and Cell Uptake Studies

3.1. Abstract

In this chapter, we synthesized a new bidentate phosphine oxide molecule, 4,6-bis(diphenylphosphoryl)-10H-phenoxazine (DPOXPO), and its corresponding visible light excitable Eu³⁺ complex, Eu(L2)₃(DPOXPO), using our previously designed carbazole-based β-diketone, L2, as primary ligand. Covalent incorporation of the Eu³⁺ complex into the silica nanoparticles was achieved via modification of DPOXPO. The surface amine functionalization of the nanoparticles was carried out using aminopropyltriethoxysilane (APTES). The prepared nanoparticles (Eu@Si-NH₂) are around 30 nm in diameter, monodisperse, stable in aqueous dispersion and also retain the luminescence properties of the incorporated Eu³⁺ complex. The synthesized nanoparticles exhibit promising luminescence quantum yield of 34 % and an excited state lifetime of 537 μs at physiological pH. The photobleaching experiments revealed that the synthesized nanoparticles are more photostable than the parent Eu³⁺ complex. Further, in vitro experiments with Eu@Si-NH₂ nanoparticles on HeLa cells showed that they are biocompatible and can be used for cell uptake studies.

3.2. Introduction

Luminescence based imaging techniques have achieved great attention because of their high sensitivity, versatility and ease of usage in *in vitro* as well as in *in vivo* imaging experiments.¹⁻⁴ The limited optical qualities of organic dyes (weak photostability and low fluorescent quantum yield) and quantum dots (potential cytotoxicity, blinking of fluorescence and complex functionalization strategies) often limit their imaging possibilities and demand the development of better bio-probes.⁵⁻⁸ Because of their attractive characteristics such as high biocompatibility, chemical inertness, optical transparency, high water dispersibility and ease of surface functionalization, silica nanoparticles offer better platform for the preparation of ideal bio-probes.⁹⁻¹¹ Moreover, encapsulation into silica nanoparticles improves the chemical and photo stabilities of the loaded species.¹²⁻¹⁴ The remarkable optical properties of lanthanide ions, such as narrow emission bands, high colour purity, large Stokes shifts and long luminescent decay times, have often been combined with the advantageous characteristics of silica nanoparticles.¹⁵⁻¹⁹ However their use as bio-probes has been restricted due to the low molar absorption coefficients and UV excitation wavelength of lanthanide ions.²⁰⁻²² The development of visible light excitable Eu^{3+} -antenna complexes, which avoid the harmful UV irradiation, and possess high molar absorption coefficients augments their attractiveness in this scenario.²³⁻²⁵ The poor water solubility of these complexes can be overcome by incorporating them into silica nanoparticles which provide better water dispersibility.²⁶⁻²⁸ Hence the past decade has witnessed a surge in the research for the development of

luminescent silica nanoparticles whose optical properties and biocompatibility are promising for various biological applications, by incorporating visible light excitable Eu^{3+} complexes.²⁹⁻³¹

Compared to other preparation methods like impregnation and doping, covalent linking of dye molecules to silica nanoparticles reduces the risk of the dyes being leached out from the nanoparticles.³²⁻³⁴ Furthermore, it improves the homogeneity of the nanoparticles and allows more loading concentrations.³⁵ Previous works concerning the covalent attachment of Eu^{3+} -complexes to the silica nanoparticles have been limited to the modification of primary ligands (β -diketonates or carboxylic acids)³⁶⁻³⁸ or nitrogen based neutral donors.³⁹⁻⁴¹ Compared to nitrogen donor ligands like terpyridine, phenanthroline, etc phosphine oxide molecules are much better candidates as neutral donors for Eu^{3+} ions.^{42, 43} Thanks to the stronger Lewis acid-base interaction of Eu^{3+} ion and phosphoryl oxygen, bidentate phosphine oxide molecules form more rigid and stable complexes with Eu^{3+} ions.⁴⁴ Also the coordinating ability and the charge transport properties of aromatic nitrogen donor ligands like phenanthroline, can be affected by the introduction of substituents on the ring due to the involvement of the lone pair electron on N atoms. However, this is not the case with phosphine oxide molecules, since the groups binding to phosphorus atoms have no influence on the coordinating ability of phosphoryl oxygen.⁴⁵ Therefore modification of phosphine oxide ligands is more flexible and easier than the modification of nitrogen donor ligands. Even though some reports are there in which the hybrid materials were prepared by modifying monodentate phosphine oxide ligands, the

modifications of bidentate phosphine oxide molecules have rarely been explored.^{46, 47}

In this chapter, we have synthesized a novel bidentate phosphine oxide molecule, 4,6-bis(diphenylphosphoryl)-10H-phenoxazine (**DPOXPO**), which can be used as an efficient neutral donor to Eu^{3+} ions. Using our previously reported carbazole-based β -diketonate molecule, **L2**, as primary ligand⁴⁸ and **DPOXPO** as the neutral donor, we have synthesized the corresponding Eu^{3+} complex, **Eu(L2)₃(DPOXPO)**, and investigated its photophysical properties. The newly designed **DPOXPO** has a functional –NH group, so that a variety of substituents can be introduced onto it. We have modified **DPOXPO** by adding a substituted silyl group and then covalently incorporated the corresponding Eu^{3+} complex into silica nanoparticles. The amine functionalization of nanoparticles was done using aminopropyltriethoxysilane (APTES). The synthesized nanoparticles were characterized by FT-IR, TEM, DLS and EDX methods. The surface amine functionalization was confirmed by ζ -potential measurements and fluorescamine test. The photophysical investigations suggest that the synthesized nanoparticles (**Eu@Si–NH2**) retain the excellent luminescence properties of the incorporated Eu^{3+} complexes. Photobleaching experiments of **Eu(L2)₃(DPOXPO)** and **Eu@Si–NH2** reveal that the latter is more photostable than the former. The cell uptake studies on HeLa cells point out that **Eu@Si–NH2** nanoparticles stain the cells and are biocompatible.

3.3. Experimental section

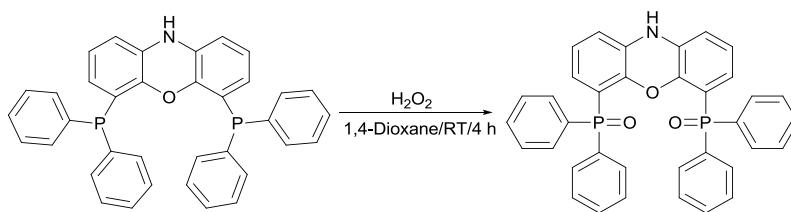
3.3.1. Materials and Instrumentation. Europium(III) nitrate pentahydrate, sodium hydride (60% dispersion in mineral oil), aminopropyltriethoxysilane (APTES) and (3-chloropropyl)trimethoxysilane were procured from Sigma-Aldrich. Tetraethyl orthosilicate (TEOS) and Triton X-100 were purchased from Acros Organics. 4,6-Bis(diphenylphosphino)-10H-phenoxazine was obtained from Alfa Aesar. All the other chemicals used were of analytical reagent grade and used without further purification. Solvents were dried using standard methods. The Eu^{3+} complex $\text{Eu}(\text{L2})_3(\text{C}_2\text{H}_5\text{OH})_2$, was synthesized according to the method described in Chapter 2.⁴⁸

The FT-IR spectra were measured using KBr pellets on a Bruker TENSOR 37 IR FT-IR spectrometer, at ambient temperature operating in the range 4000 to 500 cm^{-1} . A Bruker 500 MHz NMR spectrometer was used to record the ^1H NMR (500 MHz), ^{13}C NMR (125.7 MHz), ^{31}P NMR (202.44 MHz) and ^{29}Si NMR (99.32 MHz) spectra of the newly synthesized compounds in chloroform-d solution. C, H and N elemental analyses were performed with a Perkin-Elmer Series 2 Elemental Analyser 2400. A Thermo Scientific Exactive Benchtop LC/MS Orbitrap Mass Spectrometer was used to record the Electro spray ionization (ESI) mass spectra. HR-TEM-images and EDX-spectra were collected on a FEI Tecnai G2 F20 with an acceleration voltage of 200 kV. The UV-visible absorption spectra of the Eu^{3+} complex (in chloroform solution) and the nanoparticles (in aqueous dispersion) were recorded with a Shimadzu, UV-2450 UV-vis spectrophotometer and the background correction of the spectra has been made using corresponding solvents used. The

photoluminescence (PL) spectra of the Eu^{3+} complex (in chloroform solution) and nanoparticles (in PBS dispersion, at $\text{pH} = 7.4$), were recorded on a Spex-Fluorolog FL22 spectrofluorimeter equipped with a double grating 0.22 m Spex 1680 monochromator and a 450W Xe lamp as the excitation source. The lifetime measurements of complex **1** and nanoparticles were carried out at room temperature using a Spex 1040 D phosphorimeter. The overall quantum yields for the Eu^{3+} complex and nanoparticles were determined under ligand excitation (400 nm), based on the absolute method using a calibrated integrating sphere in a Spex-Fluorolog spectrofluorimeter.⁴⁹ Xe-arc lamp was used to excite the samples placed in the sphere and the quantum yields were determined by comparing the spectral intensities of the lamp and the sample emission as reported in the literature.^{50, 51} Using this experimental setup and the integrating sphere system, the solid-state and film state fluorescence quantum yield of tris-8-hydroxyquinolinolato aluminum (Alq_3) was determined to be 40% and 18% respectively, which is consistent with previously reported values.^{52, 53} Each sample was measured several times under slightly different experimental conditions. The estimated error for the quantum yields is ($\pm 10\%$).^{54, 55}

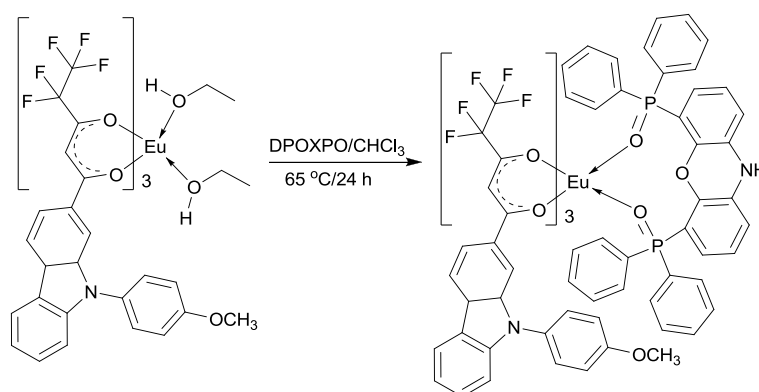
3.3.2. Synthesis of 4,6-bis(diphenylphosphoryl)-10H-phenoxazine (DPOXPO). 4,6-Bis(diphenylphosphino)-10H-phenoxazine (10 mmol) was dissolved in 15 mL of 1,4-dioxane. To this 2 mL of 30% H_2O_2 was added drop-wise and the reaction mixture was then stirred for 4 h at room temperature (Scheme 3.1). 10 mL of water was then added to arrest the reaction and the solution was extracted with dichloromethane (3×20 mL).

The organic layer was washed several times with water to remove excess 1,4-dioxane, dried over anhydrous Na_2SO_4 , filtered and solvent was evaporated. The product was obtained as an off-white powder (yield 99%). Elemental analysis (%): Calcd. for $\text{C}_{36}\text{H}_{27}\text{NO}_3\text{P}_2$ (583.55): C, 74.10; H, 4.66; N, 2.40. Found: C, 73.96; H, 4.49; N, 2.42. ^1H NMR (500 MHz, CDCl_3): δ (ppm) 10.50 (broad, -NH), 7.20 (m, 22 H), 6.50 (m, 2H), 5.98 (m, 2H). ^{31}P NMR (202.44 MHz, CDCl_3): δ (ppm) 30.85. FT-IR (KBr) ν_{max} : 3338 (br), 1193 cm^{-1} (P=O). $m/z = 584.1547$ (M+H) $^+$.



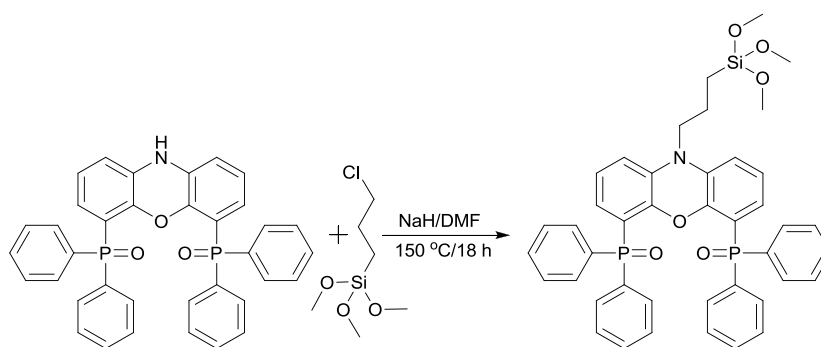
Scheme 3.1. Synthesis of **DPOXPO**.

3.3.3. Synthesis of Eu^{3+} complex, $\text{Eu}(\text{L2})_3(\text{DPOXPO})$. The Eu^{3+} complex, $\text{Eu}(\text{L2})_3(\text{DPOXPO})$, was synthesized by stirring equimolar amounts of $\text{Eu}(\text{L2})_3(\text{C}_2\text{H}_5\text{OH})_2$ and **DPOXPO** in chloroform solution at 65 °C for 24 h (Scheme 3.2). The solvent was then removed and the product was purified by recrystallization from chloroform-hexane mixture (15:85) (yield 90%). $\text{Eu}(\text{L2})_3(\text{DPOXPO})$. ^{31}P NMR (202.44 MHz, CDCl_3): δ (ppm) -91.90. Elemental analysis (%): Calcd. for $\text{C}_{108}\text{H}_{78}\text{EuF}_{15}\text{N}_4\text{O}_{12}\text{P}_2$ (2122.68): C, 61.11; H, 3.70; N, 2.64. Found: C, 61.23; H, 3.64; N, 2.70. FT-IR (KBr) ν_{max} : 3340 (br), 3072, 1616, 1504, 1234, 1144 cm^{-1} . $m/z = 1660.2923$ (M - L2) $^+$.



Scheme 3.2. Synthesis of $\text{Eu}(\text{L}2)_3(\text{DPOXPO})$.

3.3.4. Synthesis of silylated phosphine oxide (Si-DPOXPO). 4,6-Bis(diphenylphosphoryl)-10H-phenoxazine (1 mmol) was dissolved in 10 mL of dry DMF under N_2 atmosphere and the temperature was maintained at 0 °C. Sodium hydride (2 mmol) was added and the orange mixture was stirred for 2 hours while the reaction was allowed to warm to room temperature. 3-Chloropropyltrimethoxysilane (1.9 mmol) was added drop-wise at room temperature. The reaction mixture was then stirred for 18 h at 150 °C. After attaining room temperature the yellowish-brown suspension was filtered and the solvent was removed under reduced pressure. The obtained product was then washed several times with hexane until an off-white powder was obtained (yield 72%). ^1H NMR (500 MHz, CDCl_3): δ (ppm) 7.22 (m, 20 H), 6.66 (m, 2H), 6.49 (m, 2H), 5.97 (m, 2H), 3.61 (s, 9H), 3.49 (t, 2H), 1.80 (m, 2H), 0.72 (t, 2H). ^{31}P NMR (202.44 MHz, CDCl_3): δ (ppm) 31.03. ^{13}C NMR (125 MHz, CDCl_3): δ (ppm) 147.82, 138.24, 134.31, 133.93, 129.12, 128.87, 125.83, 125.51, 124.52, 112.73, 53.77, 47.47, 26.51, 9.21. ^{29}Si NMR (99.32 MHz, CDCl_3): δ (ppm) -42.9 (Figure 3.1). FT-IR (KBr) ν_{max} : 1194, 1115 cm^{-1} .

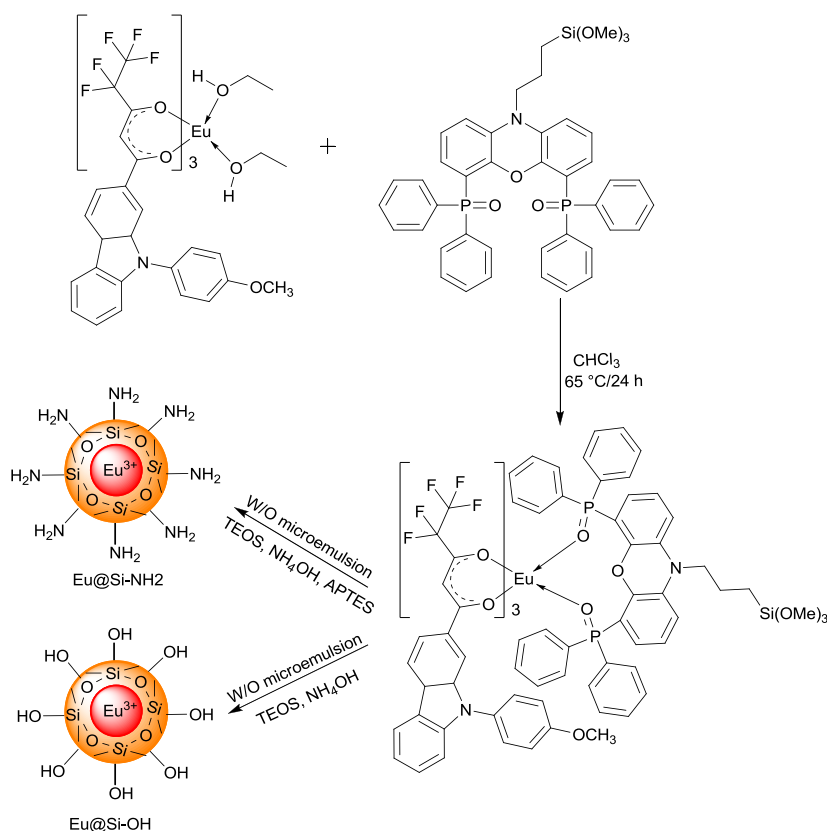


Scheme 3.3. Silylation of **DPOXPO**.

3.3.5. Synthesis of silylated Eu^{3+} complex ($\text{Eu}(\text{L2})_3(\text{Si-DPOXPO})$). 2 mmol of the solvated Eu^{3+} -complex ($\text{Eu}(\text{L2})_3(\text{C}_2\text{H}_5\text{OH})_2$) was dissolved in 20 mL of chloroform. To this **Si-DPOXPO** (2 mmol) was added and the mixture was stirred at 65 °C for 12 h. The solvent was then removed under reduced pressure. The product obtained was then washed with hexane, dried in vacuum and used without further purification.

3.3.6. Synthesis of Eu@Si-NH_2 nanoparticles. The amine functionalized luminescent silica nanoparticles, **Eu@Si-NH_2** , were synthesized by a water-in-oil reverse microemulsion in a one-pot synthesis procedure (Scheme 3.4). A water in oil reverse microemulsion was prepared by mixing 7.5 mL of cyclohexane, 1.82 mL of octanol, 1.78 mL of triton X-100 and 500 μL of water and stirred for 15 minutes. To this 4 mg of the (**$\text{Eu}(\text{L2})_3(\text{Si-DPOXPO})$**) in 1.5 mL of toluene was added and stirred for 30 minutes. 100 μL of TEOS was added to this as a precursor for silica shell formation, followed by 75 μL of aqueous ammonia to catalyse the hydrolysis and condensation of TEOS. For amine functionalization, 10 μL of APTES was added to the reaction mixture and kept for stirring at room temperature for 24 h. The nanoparticles were then

isolated by breaking the microemulsion with the addition of 4 mL of ethanol. The nanoparticles were then separated by centrifugation, washed with a 1:2 mixture of ethanol/water and then with water to remove the surfactants and unreacted Eu^{3+} -complexes. The washing was continued and tested with luminescence measurements until the washings exhibited no emission from unreacted $(\text{Eu}(\text{L}2)_3(\text{Si-DPOXPO}))$. The synthesized nanoparticles are then characterized using Fourier transform infrared spectroscopy (FT-IR), dynamic light scattering (DLS), transmission electron microscopy (TEM), and energy dispersive X-ray spectroscopy (EDX).



Scheme 3.4. Synthesis of luminescent nanoparticles.

3.3.7. Cell imaging experiments and analyses. The luminescent nanoparticles, Eu@Si-NH_2 , were redispersed in autoclaved water at 0.25

mg/mL by sonication for 1 min at 80% amplitude and 0.8 pulse with sonotrode MS7 (Hielscher UP50H). The particles were then diluted with DMEM (cell culture medium, supplemented with 10% fetal calf serum (FCS), 100 U/mL Streptomycin and 100 U/mL Penicillin) to a concentration of 0.1 mg/mL. For CLSM, HeLa cells were seeded one day prior to the experiment at 100000 cells per well in a 4 chamber polystyrene vessel tissue culture treated glass slide. The HeLa cells were incubated for 4 h (or as indicated otherwise) with the **Eu@Si-NH₂** nanoparticle dispersion. Afterwards the cells were washed 3 x with PBS and incubated for 20 min with 3.7% formaldehyde for fixation. The cells were washed again 2 x with PBS before incubation with cellmask (Life Technologies, Carlsbad, USA)) in order to stain the cellular membrane. Afterwards the cells were washed 3 x with PBS and stored overnight in mounting medium before microscopy.

3.3.8. MTT-assays. The cell viability was analysed by the MTT-assay. For MTT-assays the HeLa cells were seeded in 24-well plates. MTT (3-(4,5-dimethylthiazol-2-yl)-2,5-diphenyltetrazolium bromide; Molecular probes, Life Technologies, Carlsbad, USA) was dissolved in PBS (5 mg mL⁻¹) and added to the required amount of cell culture medium to give a final MTT concentration of 1 mg mL⁻¹. The cell culture medium of the cells was replaced by the MTT medium (300 μ L) and incubated for 90 min at 37 °C under 5% CO₂ in humidified atmosphere. Then the MTT medium was removed and the blue precipitate was dissolved in DMSO (300 μ L, each well) and incubated for 30 min. Finally, 100 μ L of each well were taken for photometric analysis at $\lambda = 570$ nm. The absorption of the supernatants of cells treated with **Eu@Si-OH**

and **Eu@Si-NH₂** nanoparticles was normalized to that of the control. In all cases, cells cultivated under the same conditions but without any treatment were used as control.

3.4. Results and discussion

3.4.1. Synthesis and characterisation of DPOXPO and (Eu(L2)₃(DPOXPO)). The bidentate phosphine oxide ligand, **DPOXPO** was synthesized as shown in Scheme 3.1 and characterized well by ¹H, ¹³C and ³¹P NMR, FT-IR, mass spectroscopic methods and by elemental analysis. The downfield shift observed in the ³¹P NMR spectra (from -18.34 ppm to 30.85 ppm) of **DPOXPO** confirms the successful oxidation of the phosphine to phosphine oxide. The solvated complex, **Eu(L2)₃(C₂H₅OH)₂** was synthesized according to the method described in our recent publication.⁴⁸ The synthesis procedure for **(Eu(L2)₃(DPOXPO))**, is depicted in Scheme 3.2. The synthesized complex was characterized using ³¹P NMR, FT-IR, ESI-mass spectroscopic methods and elemental analysis. The ESI-mass and elemental analysis indicated that the **DPOXPO** molecule replaced the solvent molecules from the coordination sphere of the Eu³⁺ ion. In the FT-IR spectra, the P=O stretching frequency of the free DPOXPO ligand was shifted from 1193 to 1144 cm⁻¹ in **(Eu(L2)₃(DPOXPO))**, which confirms the coordination of **DPOXPO** to the Eu³⁺ ion. This was further confirmed by the upfield shift of P=O signal (from 30.85 ppm to -91.90 ppm) in the ³¹P NMR of complex **Eu(L2)₃(DPOXPO)**.

Synthesis and characterisation of Si-DPOXPO and (Eu(L2)₃(Si-DPOXPO)). The silylation of the bidentate phosphine oxide ligand was done following the synthetic route outlined in Scheme 3.3. The silylated ligand (**Si-DPOXPO**) was characterized using ¹H, ¹³C ³¹P and ²⁹Si NMR, FT-IR as well as elemental analysis. Similar to **DPOXPO**, the peak corresponding to the P=O resonance appears at 31.03 ppm in the ³¹P NMR spectrum. In the ²⁹Si NMR spectrum (Figure 3.1) the presence of a peak at 42.9 ppm indicates the successful silylation of **DPOXPO**. In the FT-IR spectrum, the band corresponding to the P=O stretching appears at 1193 cm⁻¹. The elemental analysis further confirms the silylation of **DPOXPO**. Using **Si-DPOXPO** as neutral donor we have synthesized the corresponding Eu³⁺-complex, **(Eu(L2)₃(Si-DPOXPO))**, and used it as the precursor for the synthesis of luminescent nanoparticles without further purification.

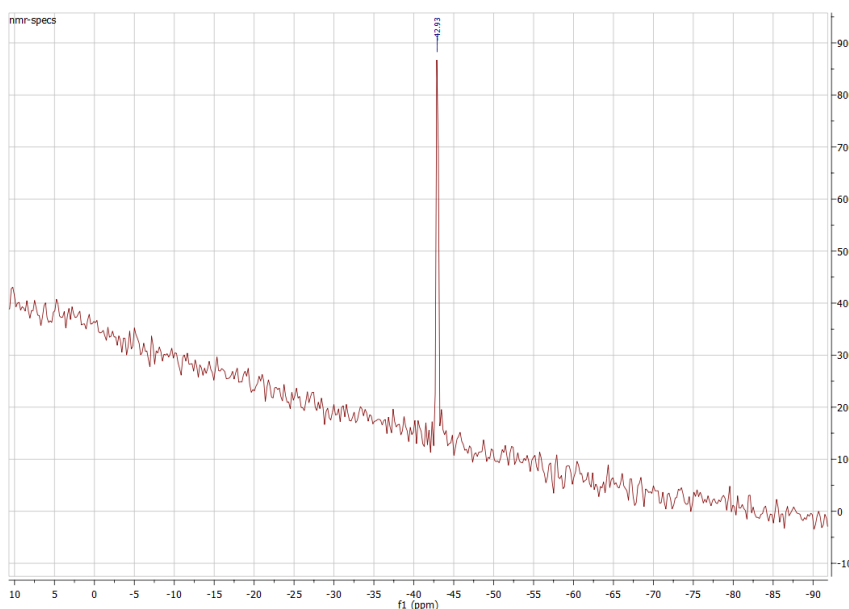


Figure 3.1. ²⁹Si NMR spectrum of **Si-DPOXPO**.

3.4.3. Synthesis and characterisation of nanoparticles. To obtain a homogenous dye distribution and better photostability, the dye molecule has to be covalently linked to the matrix.³⁵ Using the one-pot water-in-oil microemulsion method⁵⁶ we have covalently incorporated the long-wavelength excitable Eu^{3+} complex, **Eu(L2)₃(Si-DPOXPO)** into silica nanoparticles with TEOS as the precursor for silica shell formation (Scheme 3.4). The addition of aqueous ammonia, which catalyses the hydrolysis and condensation of TEOS onto the **Eu(L2)₃(Si-DPOXPO)** conjugate, led to the growth of the silica shell on **Eu(L2)₃(Si-DPOXPO)**. APTES was used to modify the surface of the nanoparticles with $-\text{NH}_2$ groups. The synthesized nanoparticles were characterized using FT-IR, DLS, TEM and EDX methods. In the FT-IR spectra, the broad peak at 3400 cm^{-1} corresponds to the $-\text{OH}$ and $-\text{NH}_2$ groups present on the surface of nanoparticles. The peak at 1092 cm^{-1} with a shoulder peak at 1210 cm^{-1} may be assigned to the asymmetric vibration of the $\text{Si}-\text{O}-\text{Si}$ group.⁵⁷ The characteristic symmetric vibration of $\text{Si}-\text{OH}$ and the asymmetric vibration of $\text{Si}-\text{O}-\text{Si}$ groups are responsible for the peaks observed at 800 cm^{-1} and 952 cm^{-1} respectively. The peak at 467 cm^{-1} , due to the $\text{O}-\text{Si}-\text{O}$ bending vibration, is also present in the FT-IR spectrum of the **Eu@Si-NH₂** nanoparticles. The hydrodynamic diameters of the nanoparticles determined by DLS measurements are found to be 65-70 nm and takes into account their motion and the water sphere around the particles (Figure 3.2). The TEM images indicate that the nanoparticles are monodispersed and have spherical morphology with a particle size around 30-35 nm (Figure 3.3 (a)).

The high water dispersibility of the synthesized nanoparticles can also be seen in Figure 3.3 (b).

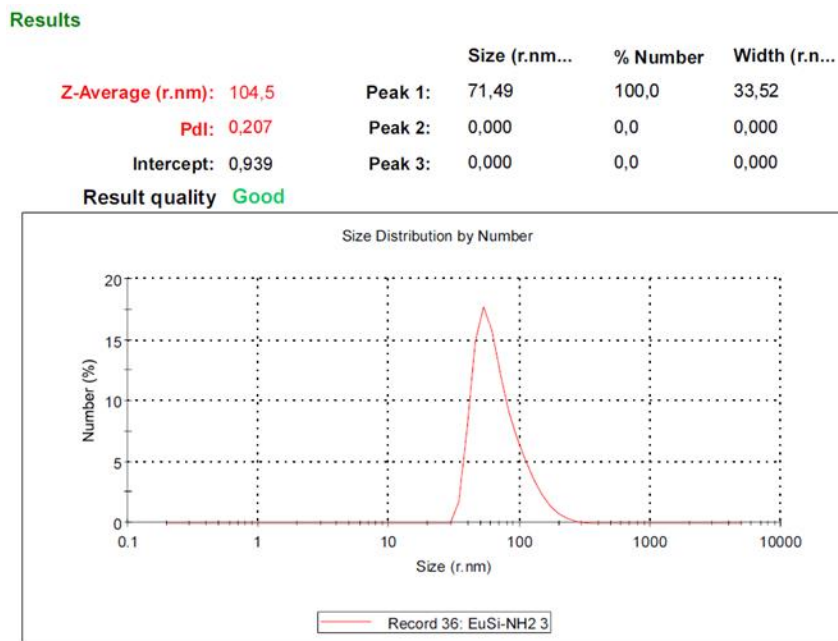


Figure 3.2. DLS particle size distribution of **Eu@Si-NH₂** nanoparticles.

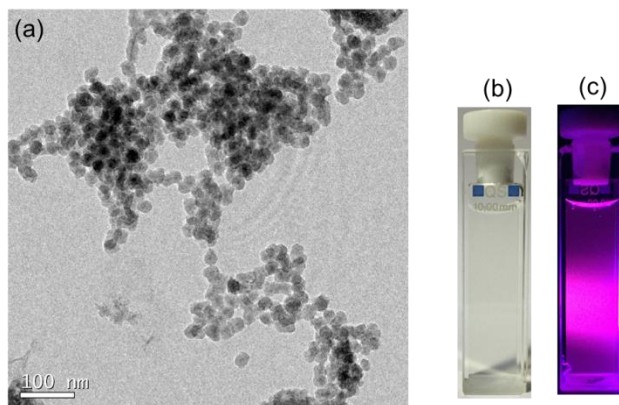


Figure 3.3. (a) TEM images of **Eu@Si-NH₂** nanoparticles, Photograph of the aqueous dispersion of **Eu@Si-NH₂** nanoparticles under (b) normal light and (c) blue light.

Further characterization of the **Eu@Si-NH₂** nanoparticles were done using energy dispersive X-ray (EDX) measurements. As can be seen from Figure

3.4, the peaks corresponding to europium and silicon is present in the EDX spectra.

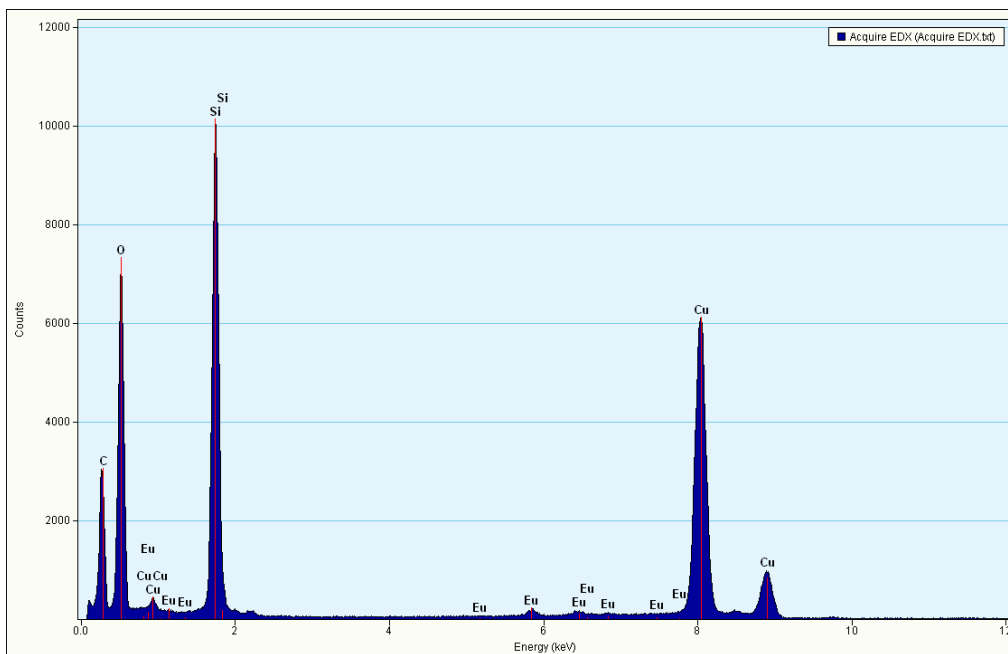


Figure 3.4. EDX spectrum of Eu@Si-NH₂ nanoparticles.

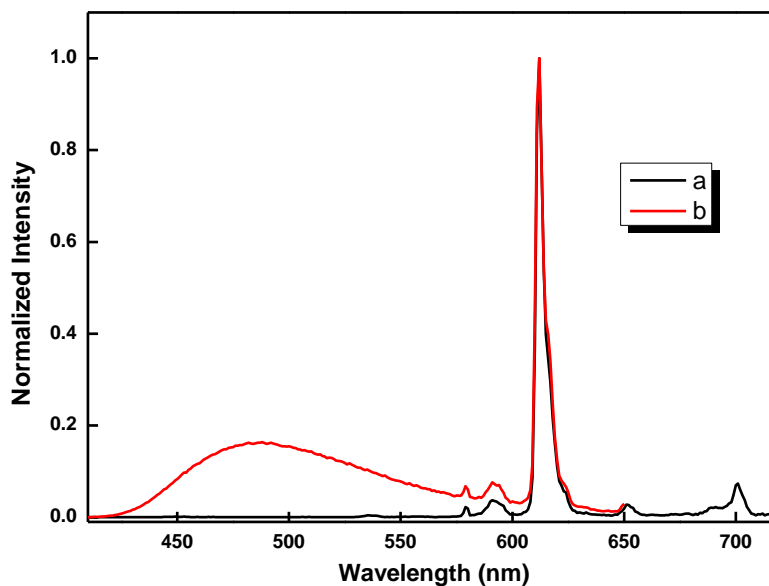


Figure 3.5. Emission spectra of Eu@Si-NH₂ nanoparticles (a) before and (b) after the addition of fluorescamine.

The surface charge of the unmodified (**Eu@Si-OH**) and $-NH_2$ functionalized (**Eu@Si-NH₂**) nanoparticles were determined by measuring the ζ -potential values. The surface charge of **Eu@Si-OH** nanoparticles (-5.8 mV) and that of **Eu@Si-NH₂** nanoparticles (+15.6 mV) confirming the $-NH_2$ functionalization. The $-NH_2$ functionalization was further confirmed by fluorescamine test, in which the **Eu@Si-NH₂** nanoparticles show a broad fluorescence signal with peak maximum around 480 nm (Figure 3.5) following the addition of fluorescamine.^{58, 59}

3.4.4. Photophysical properties

3.4.4.1. UV-visible absorption spectra.

The UV-visible absorption spectra of the ligand **DPOXPO** (in chloroform solution), parent Eu^{3+} complex, **Eu(L₂)₃(DPOXPO)**, (in chloroform solution) and the synthesized nanoparticles, **Eu@Si-NH₂**, (in aqueous dispersion) are depicted in Figure 3.6. The absorption spectra of **Eu(L₂)₃(DPOXPO)** exhibit two distinct broad bands. The band with maxima at around 360-400 nm, corresponds to the electronic transitions of the enolic moiety of the β -diketonate ligand and band in the higher energy 240-280 nm region is attributable to the electronic transitions of the carbazole backbone.^{60, 61} The electronic transitions of the enolic moiety of the β -diketonate ligand (peak at ca. 310-400 nm) and the chelated phosphine oxide (peak at ca. 300-380 nm) units are overlapped in **Eu(L₂)₃(DPOXPO)**. The absorption spectra of **Eu@Si-NH₂** nanoparticles also display two broad bands due to the electronic transitions of the enolic moiety and carbazole ring of the β -diketonate ligands. The absorption bands of the nanoparticles are red shifted compared to that of

the parent complex, which may be due to the change in the environment of the Eu^{3+} complex within the nanoparticles. The scattering effect of the nanoparticles may also contribute towards the red shift of the absorption spectrum.

3.4.4.2. Photoluminescence studies. The room temperature excitation and emission spectra of $\text{Eu}(\text{L2})_3(\text{DPOXPO})$ in chloroform solution and $\text{Eu}@\text{Si-NH2}$ nanoparticles in PBS buffer solution at pH 7.4 are recorded and given in Figure 3.7. The excitation profiles of both parent Eu^{3+} complex and $\text{Eu}@\text{Si-NH2}$ nanoparticles are recorded by monitoring the intense ${}^5\text{D}_0 \rightarrow {}^7\text{F}_2$ transition (612 nm) of Eu^{3+} ion. From the excitation spectra, it is clear that the ligand excitation bands of the $\text{Eu}@\text{Si-NH2}$ nanoparticles match well with that of the parent Eu^{3+} complex. The absence of sharp absorption peaks of Eu^{3+} ions in the excitation spectra indicates that the sensitization *via* ligand excited states are more efficient than the direct excitation of Eu^{3+} ions. The emission spectra of both $\text{Eu}(\text{L2})_3(\text{DPOXPO})$ complex and $\text{Eu}@\text{Si-NH2}$ nanoparticles exhibit the characteristic emission bands due to the intra-configurational ${}^5\text{D}_0 \rightarrow {}^7\text{F}_J$ ($J = 0-4$) transitions of the Eu^{3+} ion, when excited at 400 nm (Figure 3.7).⁶²⁻⁶⁴ The absence of broad ligand emission bands in the emission spectra suggests that sensitization *via* ligand excited states is efficient.⁶⁵ The ${}^5\text{D}_0 \rightarrow {}^7\text{F}_0$, ${}^5\text{D}_0 \rightarrow {}^7\text{F}_1$, ${}^5\text{D}_0 \rightarrow {}^7\text{F}_2$, ${}^5\text{D}_0 \rightarrow {}^7\text{F}_3$ and ${}^5\text{D}_0 \rightarrow {}^7\text{F}_4$ transitions are responsible for the emission peaks centered at 579, 591, 612, 652 and 702 nm, respectively.

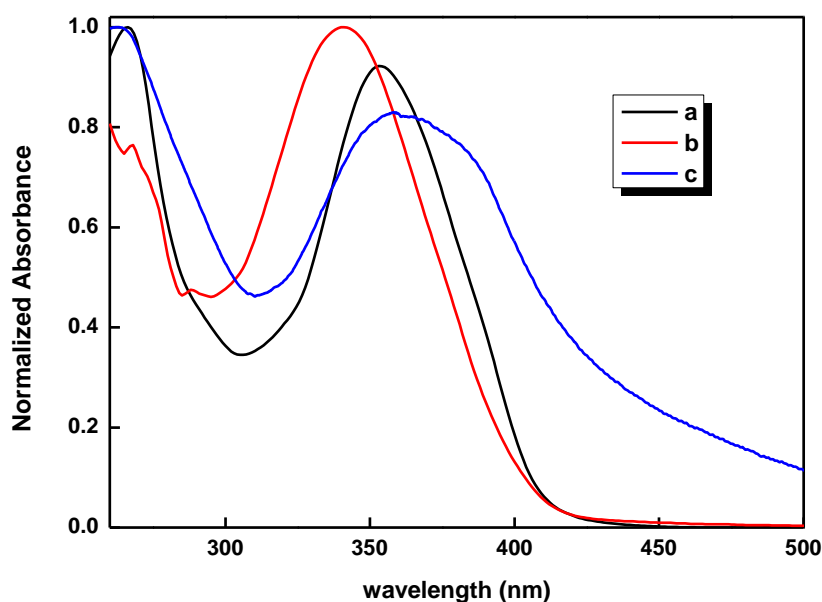


Figure 3.6. Normalized UV-visible absorption spectra of (a) $\text{Eu}(\text{L}2)_3(\text{DPOXPO})$ (in CHCl_3 solution) (b) DPOXPO (in CHCl_3 solution) and (c) Eu@Si-NH_2 nanoparticles (in aq. dispersion).

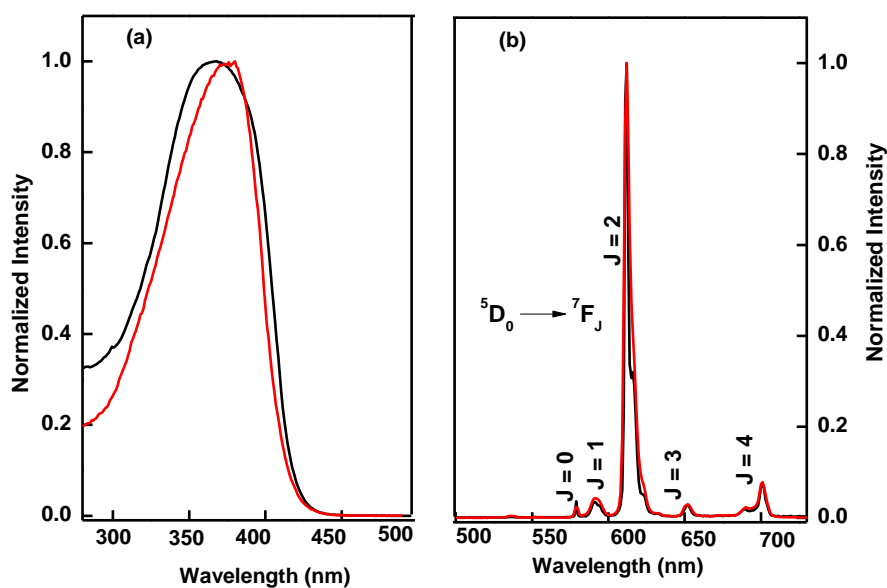


Figure 3.7. Normalized (a) excitation ($\lambda_{em} = 612 \text{ nm}$) and (b) emission ($\lambda_{ex} = 400 \text{ nm}$) spectra of Eu@Si-NH_2 nanoparticles (red) dispersed in PBS solution (pH = 7.4) and $\text{Eu}(\text{L}2)_3(\text{DPOXPO})$ (black) in chloroform solution.

The electric-dipole induced hypersensitive ${}^5\text{D}_0 \rightarrow {}^7\text{F}_2$ transition (612 nm) dominates in both cases which is responsible for the bright red colour of $\text{Eu}(\text{L}2)_3(\text{DPOXPO})$ and Eu@Si-NH_2 .⁶⁶ Visible light excitation of the parent

complex is retained in **Eu@Si-NH₂** nanoparticles as demonstrated in Figure 3.3 (c), where the nanoparticles are excited by blue light. The photophysical studies reveal that the synthesized nanoparticles retain the excellent luminescence properties of the incorporated Eu³⁺ complex.

The absolute quantum yield of the complex, **Eu(L2)₃(DPOXPO)**, was measured in chloroform solution and found to be 42%. The nanoparticles (**Eu@Si-NH₂**) were dispersed in in PBS buffer at pH 7.4 and the luminescence quantum yields were measured to be 34%. This observation further confirms that after incorporation into the nanoparticles, the Eu³⁺-complex maintains its remarkable optical properties.

3.4.4.3. Luminescence decay profiles. The excited state lifetimes of **Eu(L2)₃(DPOXPO)** in chloroform solution and the nanoparticles (**Eu@Si-NH₂**) in PBS buffer solution at pH 7.4 were measured by monitoring the emission peak at 612 nm when excited at 400 nm. The luminescence decay profile of **Eu(L2)₃(DPOXPO)** is depicted in Figure 3.8 and that of **Eu@Si-NH₂** nanoparticles is depicted in Figure 3.9. The single exponential fitting of the decay curves in all compounds indicate the existence of a single coordination environment in the parent Eu³⁺ complex and in the nanoparticles. The excited state lifetime of **Eu(L2)₃(DPOXPO)** is found to be 719 μs, whereas that of **Eu@Si-NH₂** nanoparticles is found to be 537 μs.

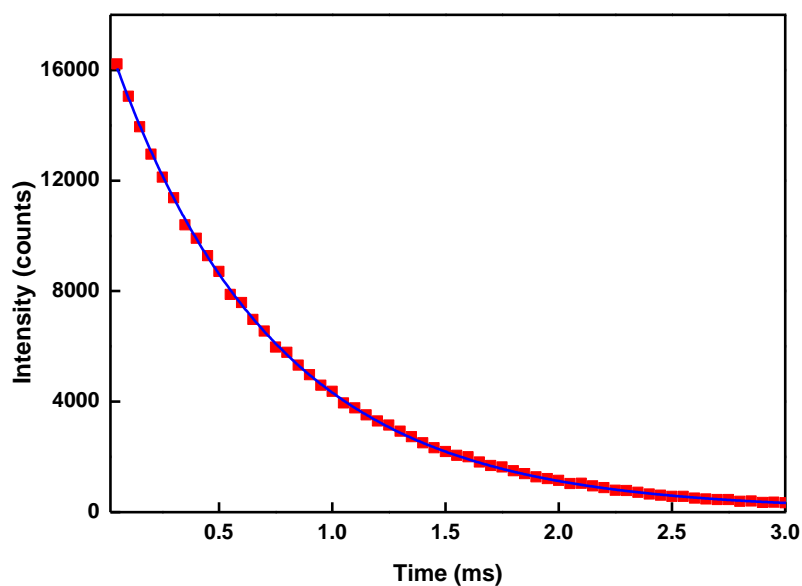


Figure 3.8. Lifetime profile of **Eu(L2)₃(DPOXPO)** in chloroform solution. at room temperature (emission monitored at 612 nm).

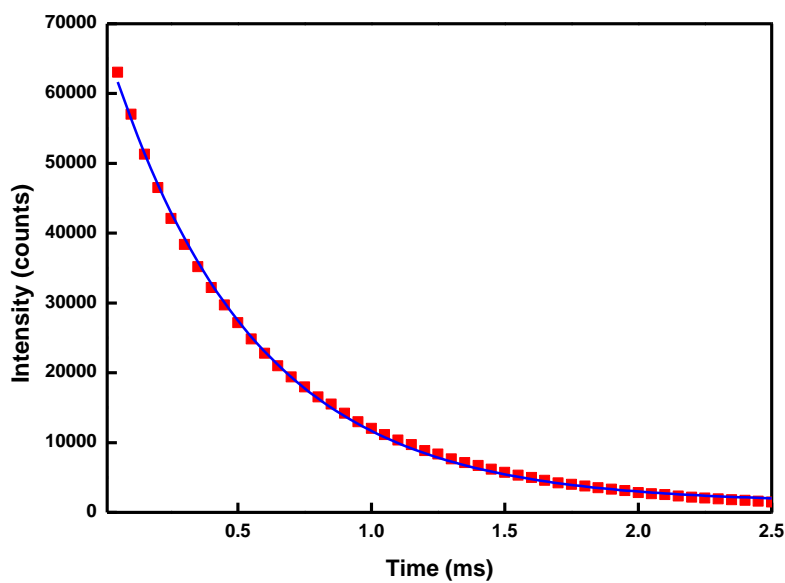


Figure 3.9. Lifetime profile of **Eu@Si-NH₂** nanoparticles dispersed in PBS solution (pH = 7.4) at room temperature (emission monitored at 612 nm).

3.4.5. Photostability studies. The photostabilities of the parent Eu^{3+} complex, **Eu(L2)₃(DPOXPO)**, and the prepared nanoparticles, **Eu@Si-NH₂**, are shown in Figure 3.10. A chloroform solution of **Eu(L2)₃(DPOXPO)** and PBS dispersions of **Eu@Si-NH₂** nanoparticles were used for the studies. The

intensity at 612 nm was monitored at 15 minute time intervals under continuous exposure at 365 nm. The results demonstrated that the parent Eu^{3+} complex, $\text{Eu}(\text{L2})_3(\text{DPOXPO})$, undergoes a photobleaching of more than 60% under continuous irradiation, whereas the photodecomposition of the synthesized nanoparticles, Eu@Si-NH_2 , is less than 15%. This clearly shows that by incorporating into the silica nanoparticles, the photostability of the dye molecules can be improved significantly.

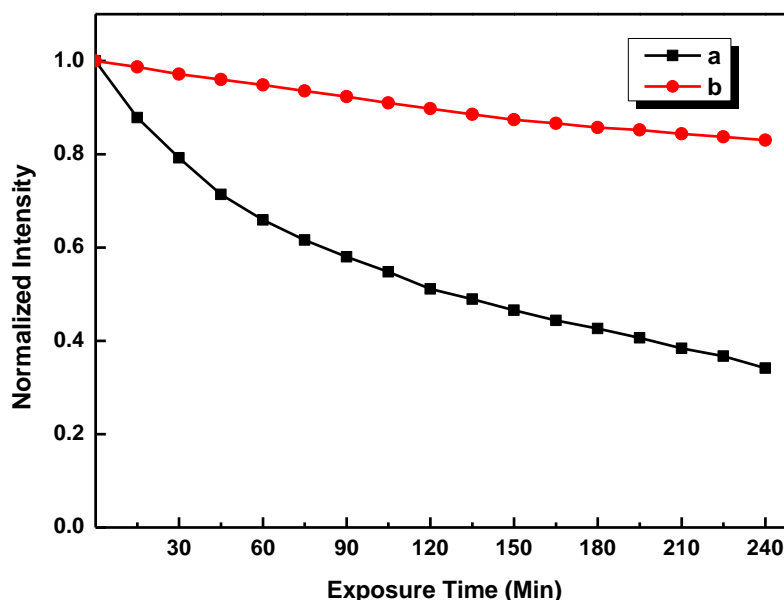


Figure 3.10. Photostability experiments of (a) $\text{Eu}(\text{L2})_3(\text{DPOXPO})$ in CHCl_3 solution and (b) Eu@Si-NH_2 nanoparticles in PBS buffer (pH = 7.4) solution under continuous exposure at 365 nm. The luminescence intensity was monitored at 612 nm in time intervals of 15 minutes.

3.4.6. Cell uptake studies with HeLa cells. The initial cell uptake studies with Eu@Si-NH_2 nanoparticles were carried out using HeLa cells. The CLSM images indicate that Eu@Si-NH_2 nanoparticles stain the cells (Figure 3.11) with most of the particles sticking on the cell wall within 4 h of incubation. This may be due to the electrostatic interaction between the positively charged Eu@Si-NH_2 nanoparticles and the negatively charged cell wall. The

nanoparticles do not display any specificity towards a particular part of the cell.

3.4.7. Cell viability studies. We have also carried out the cell viability studies and the results are shown in Figure 3.12. We have used MTT assay, which monitor the mitochondrial activity for these studies.⁶⁷

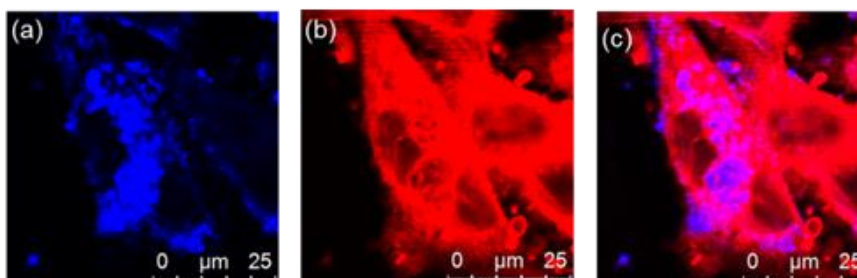


Figure 3.11. Pseudo-colour images of HeLa cells incubated with (a) **Eu@Si-NH₂** nanoparticles (b) cellmask and (c) merged image.

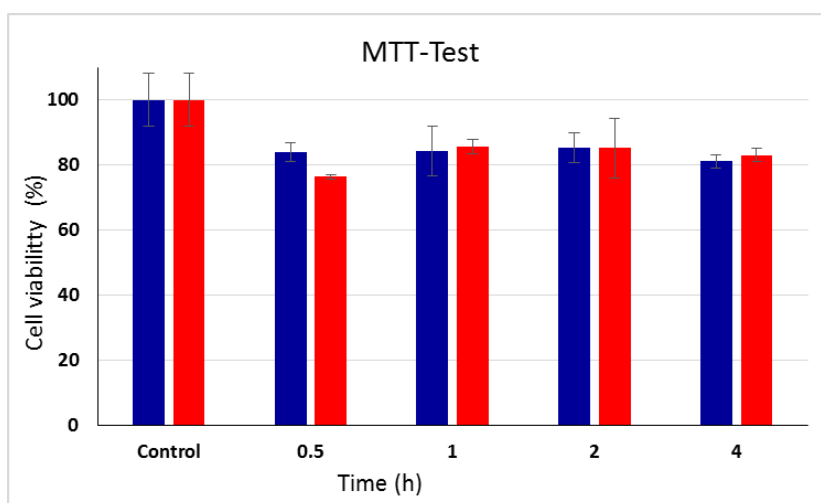


Figure 3.12. Cell viability (%) measured by MTT assay. All results were presented as the mean \pm standard deviation (SD) from three independent experiments with four wells in each. Blue bars correspond to the cell viability of **Eu@Si-OH** nanoparticles and red bars correspond to the cell viability of **Eu@Si-NH₂** nanoparticles

Here the enzyme mitochondrial dehydrogenase cleave the tetrazolium ring of MTT and the pale yellow solution becomes dark-blue because of the formation

of formazan within the living cells. Only active mitochondria contain the enzyme mitochondrial dehydrogenase. As indicated by the MTT-assays more than 80% of the cells are alive after 4 hours of incubation with **Eu@Si-NH₂** nanoparticles, which is desirable for various biological applications.

3.5. Conclusions

In summary, we synthesized a visible light excitable, carbazole-based Eu^{3+} complex (**Eu(L2)₃(DPOXPO)**) using a novel bidentate phosphine oxide molecule, **DPOXPO**, as neutral donor. The **DPOXPO** molecule has a functional $-\text{NH}$ group and by modifying **DPOXPO**, we have covalently incorporated the corresponding Eu^{3+} complex into silica nanoparticles. The amine functionalization of the nanoparticle surface was done for biological studies. Synthesized nanoparticles, **Eu@Si-NH₂**, were of around 30 nm in diameter, monodispersed, dispersible in water and retain the excellent luminescence properties of the incorporated Eu^{3+} complex. The **Eu@Si-NH₂** nanoparticles exhibit a remarkable luminescence quantum yield as high as 34% and an excited state lifetime of 537 μs at physiological pH. Photobleaching studies revealed that the synthesized **Eu@Si-NH₂** nanoparticles are more photostable than the parent Eu^{3+} complex, **Eu(L2)₃(DPOXPO)**. The initial cell uptake studies with HeLa cells revealed that the amine functionalized nanoparticles, **Eu@Si-NH₂**, stain the cells and were found to be biocompatible. So these nanoparticles may find potential use in various biological applications.

3.6. References

1. J. A. Thomas, *Chem. Soc. Rev.*, 2015, **44**, 4494-4500.
2. M. Schäferling, *Angew. Chem. Int. Ed.*, 2012, **51**, 3532-3554.
3. S. V. Eliseeva and J.-C. G. Bunzli, *Chem. Soc. Rev.*, 2010, **39**, 189-227.
4. Y. Liu, D. Tu, H. Zhu, E. Ma and X. Chen, *Nanoscale*, 2013, **5**, 1369-1384.
5. I. L. Medintz, H. T. Uyeda, E. R. Goldman and H. Mattoussi, *Nat. Mater.*, 2005, **4**, 435-446.
6. X. Michalet, F. F. Pinaud, L. A. Bentolila, J. M. Tsay, S. Doose, J. J. Li, G. Sundaresan, A. M. Wu, S. S. Gambhir and S. Weiss, *Science*, 2005, **307**, 538-544.
7. C. Bouzigues, T. Gacoin and A. Alexandrou, *ACS Nano*, 2011, **5**, 8488-8505.
8. U. Resch-Genger, M. Grabolle, S. Cavaliere-Jaricot, R. Nitschke and T. Nann, *Nat. Methods*, 2008, **5**, 763-775.
9. S. W. Bae, W. Tan and J.-I. Hong, *Chem. Commun.*, 2012, **48**, 2270-2282.
10. A. Burns, H. Ow and U. Wiesner, *Chem. Soc. Rev.*, 2006, **35**, 1028-1042.
11. O. S. Wolfbeis, *Chem. Soc. Rev.*, 2015, **44**, 4743-4768.
12. S. Zanarini, E. Rampazzo, L. D. Ciana, M. Marcaccio, E. Marzocchi, M. Montalti, F. Paolucci and L. Prodi, *J. Am. Chem. Soc.*, 2009, **131**, 2260-2267.
13. S. Bonacchi, D. Genovese, R. Juris, M. Montalti, L. Prodi, E. Rampazzo and N. Zaccheroni, *Angew. Chem. Int. Ed.*, 2011, **50**, 4056-4066.
14. H. Ow, D. R. Larson, M. Srivastava, B. A. Baird, W. W. Webb and U. Wiesner, *Nano Lett.*, 2005, **5**, 113-117.
15. S. L. C. Pinho, H. Faneca, C. F. G. C. Geraldese, M.-H. Delville, L. D. Carlos and J. Rocha, *Biomaterials*, 2012, **33**, 925-935.
16. Y.-Y. Li, H. Cheng, Z.-G. Zhang, C. Wang, J.-L. Zhu, Y. Liang, K.-L. Zhang, S.-X. Cheng, X.-Z. Zhang and R.-X. Zhuo, *ACS Nano*, 2008, **2**, 125-133.
17. M. C. Heffern, L. M. Matosziuk and T. J. Meade, *Chem. Rev.*, 2014, **114**, 4496-4539.
18. L. Prodi, E. Rampazzo, F. Rastrelli, A. Speghini and N. Zaccheroni, *Chem. Soc. Rev.*, 2015, **44**, 4922-4952.
19. Y. Zhang, W. Wei, G. K. Das and T. T. Yang Tan, *J. Photochem. Photobiol., C*, 2014, **20**, 71-96.
20. C. P. Montgomery, B. S. Murray, E. J. New, R. Pal and D. Parker, *Acc. Chem. Res.*, 2009, **42**, 925-937.
21. H. Dong, S.-R. Du, X.-Y. Zheng, G.-M. Lyu, L.-D. Sun, L.-D. Li, P.-Z. Zhang, C. Zhang and C.-H. Yan, *Chem. Rev.*, 2015, **115**, 10725-10815.
22. A. J. Amoroso and S. J. A. Pope, *Chem. Soc. Rev.*, 2015, **44**, 4723-4742.
23. V. Divya, V. Sankar, K. G. Raghu and M. L. P. Reddy, *Dalton Trans.*, 2013, **42**, 12317-12323.
24. M. L. P. Reddy, V. Divya and R. Pavithran, *Dalton Trans.*, 2013, **42**, 15249-15262.
25. L. Zhang, L. Tian, Z. Ye, B. Song and J. Yuan, *Talanta*, 2013, **108**, 143-149.
26. C. Gaillard, P. Adumeau, J.-L. Canet, A. Gautier, D. Boyer, C. Beaudoin, C. Hesling, L. Morel and R. Mahiou, *J. Mater. Chem. B*, 2013, **1**, 4306-4312.
27. L. Tian, Z. Dai, L. Zhang, R. Zhang, Z. Ye, J. Wu, D. Jin and J. Yuan, *Nanoscale*, 2012, **4**, 3551-3557.
28. N. T. K. Thanh and L. A. W. Green, *Nano Today*, 2010, **5**, 213-230.

29. J. Wu, G. Wang, D. Jin, J. Yuan, Y. Guan and J. Piper, *Chem. Commun.*, 2008, 365-367.
30. Y. Wu, M. Shi, L. Zhao, W. Feng, F. Li and C. Huang, *Biomaterials*, 2014, **35**, 5830-5839.
31. J. 389 msWu, Z. Ye, G. Wang, D. Jin, J. Yuan, Y. Guan and J. Piper, *J. Mater. Chem.*, 2009, **19**, 1258-1264.
32. R. Kumar, I. Roy, T. Y. Ohulchanskyy, L. N. Goswami, A. C. Bonoiu, E. J. Bergey, K. M. Trampusch, A. Maitra and P. N. Prasad, *ACS Nano*, 2008, **2**, 449-456.
33. L. D. Carlos, R. A. S. Ferreira, V. d. Z. Bermudez and S. J. L. Ribeiro, *Adv. Mater.*, 2009, **21**, 509-534.
34. Z. Wang, X. Hong, S. Zong, C. Tang, Y. Cui and Q. Zheng, *Sci. Rep.*, 2015, **5**, 12602-12611.
35. K. Binnemans, *Chem. Rev.*, 2009, **109**, 4283-4374.
36. A. P. Duarte, M. Gressier, M.-J. Menu, J. Dexpert-Ghys, J. M. A. Caiut and S. J. L. Ribeiro, *J. Phys. Chem. C*, 2012, **116**, 505-515.
37. B. Francis, D. B. Ambili Raj and M. L. P. Reddy, *Dalton Trans.*, 2010, **39**, 8084-8092.
38. D. B. Ambili Raj, S. Biju and M. L. P. Reddy, *J. Mater. Chem.*, 2009, **19**, 7976-7983.
39. A.-C. Franville, D. Zambon, R. Mahiou and Y. Troin, *Chem. Mater.*, 2000, **12**, 428-435.
40. H. R. Li, J. Lin, H. J. Zhang, L. S. Fu, Q. G. Meng and S. B. Wang, *Chem. Mater.*, 2002, **14**, 3651-3655.
41. K. Binnemans, P. Lenaerts, K. Driesen and C. Gorller-Walrand, *J. Mater. Chem.*, 2004, **14**, 191-195.
42. H. Xu, K. Yin and W. Huang, *Chem. Eur. J.*, 2007, **13**, 10281-10293.
43. H. Xu, K. Yin and W. Huang, *ChemPhysChem*, 2008, **9**, 1752-1760.
44. L. J. Charbonnière, R. Ziessel, M. Montalti, L. Prodi, N. Zaccheroni, C. Boehme and G. Wipff, *J. Am. Chem. Soc.*, 2002, **124**, 7779-7788.
45. H. Xu, L.-H. Wang, X.-H. Zhu, K. Yin, G.-Y. Zhong, X.-Y. Hou and W. Huang, *J. Phys. Chem. B*, 2006, **110**, 3023-3029.
46. R. J. P. Corriu, F. Embert, Y. Guari, A. Mehdi and C. Reye, *Chem. Commun.*, 2001, 1116-1117.
47. F. Embert, A. Mehdi, C. Reyé and R. J. P. Corriu, *Chem. Mater.*, 2001, **13**, 4542-4549.
48. B. Francis, C. Heering, R. O. Freire, M. L. P. Reddy and C. Janiak, *RSC Adv.*, 2015, **5**, 90720-90730.
49. L. Porrès, A. Holland, L.-O. Pålsson, A. Monkman, C. Kemp and A. Beeby, *J. Fluoresc.*, 2006, **16**, 267-273.
50. J. C. de Mello, H. F. Wittmann and R. H. Friend, *Adv. Mater.*, 1997, **9**, 230-232.
51. L. O. Pålsson and A. P. Monkman, *Adv. Mater.*, 2002, **14**, 757-758.
52. N. S. S. Kumar, S. Varghese, N. P. Rath and S. Das, *J. Phys. Chem. C*, 2008, **112**, 8429-8437.
53. M. Cölle, J. Gmeiner, W. Milius, H. Hillebrecht and W. Brütting, *Adv. Funct. Mater.*, 2003, **13**, 108-112.
54. S. V. Eliseeva, O. V. Kotova, F. Gumy, S. N. Semenov, V. G. Kessler, L. S. Lepnev, J.-C. G. Bünzli and N. P. Kuzmina, *J. Phys. Chem. A*, 2008, **112**, 3614-3626.
55. M. S. Wrighton, D. S. Ginley and D. L. Morse, *J. Phys. Chem.*, 1974, **78**, 2229-2233.
56. L. Wang, W. Zhao and W. Tan, *Nano Res.*, 2008, **1**, 99-115.

57. L.-F. Alejandro, D. Tristan, D. Silvio, S. Frank, J. M. Artur and J. M. Gerhard, *Nanotechnology*, 2011, **22**, 415501.
58. E. Kaiser, R. L. Colescott, C. D. Bossinger and P. I. Cook, *Anal. Biochem.*, 1970, **34**, 595-598.
59. J. A. Smith, *Anal. Biochem.*, 1976, **74**, 477-483.
60. P. He, H. H. Wang, H. G. Yan, W. Hu, J. X. Shi and M. L. Gong, *Dalton Trans.*, 2010, **39**, 8919-8924.
61. D. B. A. Raj, B. Francis, M. L. P. Reddy, R. R. Butorac, V. M. Lynch and A. H. Cowley, *Inorg. Chem.*, 2010, **49**, 9055-9063.
62. G. F. de Sá, O. L. Malta, C. de Mello Donegá, A. M. Simas, R. L. Longo, P. A. Santa-Cruz and E. F. da Silva Jr, *Coord. Chem. Rev.*, 2000, **196**, 165-195.
63. S. J. Butler, M. Delbianco, L. Lamarque, B. K. McMahon, E. R. Neil, R. Pal, D. Parker, J. W. Walton and J. M. Zwieter, *Dalton Trans.*, 2015, **44**, 4791-4803.
64. S. V. Eliseeva, B. Song, C. D. B. Vandevyver, A.-S. Chauvin, J. B. Wacker and J.-C. G. Bunzli, *New J. Chem.*, 2010, **34**, 2915-2921.
65. B. Makhinson, A. K. Duncan, A. R. Elam, A. de Bettencourt-Dias, C. D. Medley, J. E. Smith and E. J. Werner, *Inorg. Chem.*, 2013, **52**, 6311-6318.
66. K. Binnemans, *Coord. Chem. Rev.*, 2015, **295**, 1-45.
67. N. Lewinski, V. Colvin and R. Drezek, *Small*, 2008, **4**, 26-49.

Chapter 4

Highly Efficient Luminescent Hybrid Materials Covalently Linking with Eu^{3+} Complexes *via* a Novel Fluorinated β -diketonate Ligand

4.1. Abstract

A novel β -diketonate ligand, 1-(3,5-bis(benzyloxy)phenyl)-4,4,5,5,5-pentafluoropentane-1,3-dione (**HBBPPF**), and its corresponding Eu^{3+} ternary complex, **$\text{Eu}(\text{BBPPF})_3(\text{DDXPO})$** [**DDXPO** = 4,5-bis(diphenylphosphino)-9,9-dimethylxanthene oxide], were synthesized, characterized and its photophysical properties (PL) investigated. The synthesized Eu^{3+} complex exhibits intense red emission under UV light excitation with a solid-state quantum yield of 39%. An organic–inorganic mesoporous luminescent hybrid material, **$\text{Eu}(\text{BBPPF-Si})_3(\text{DDXPO})/\text{MCM-41}$** , was also constructed by linking the synthesized Eu^{3+} complex to hexagonal mesoporous MCM-41. The developed hybrid material was characterized by powder X-ray diffraction, nitrogen adsorption-desorption, transmission electron microscopy, dynamic light scattering, FT-IR, ^{29}Si NMR and ^{13}C NMR solid-state techniques, and photoluminescence spectroscopy. **$\text{Eu}(\text{BBPPF-Si})_3(\text{DDXPO})/\text{MCM-41}$** exhibits an efficient intramolecular energy transfer process from the silylated β -diketonate to the central Eu^{3+} , namely, the “antenna effect”, which favours a strong luminescence intensity (quantum yield = 43%).

4.2. Introduction

The exceptional photophysical properties of trivalent lanthanide ions (Ln^{3+}) have inspired vigorous research activities owing to a wide range of potential applications in the fields of solid state lighting,^{1, 2} telecommunication,^{3, 4} and bio-medical analysis.⁵⁻⁷ Unfortunately, because of the Laporte and spin forbidden nature of 4f-4f transitions the molar absorption coefficients of Ln^{3+} ions are very small (less than $10 \text{ M}^{-1} \text{ cm}^{-1}$). This weak absorbance can, however, be overcome by coordinating chromophore-containing organic ligands to the Ln^{3+} ion which, upon irradiation, absorb energy and transfer the absorbed energy to the metal center, typically *via* the ligand triplet excited state, thereby populating the Ln^{3+} emitting levels in a process known as the “antenna effect”.^{8, 9} The ligand sensitized luminescence of lanthanide complexes were first described by Weissman *et al.* in 1942.¹⁰ Since then, numerous compounds of lanthanide ions, in particular Eu^{3+} and Tb^{3+} , with various organic ligands, have been developed and their crystal structures and luminescence properties have been described in detail.¹¹⁻¹⁷ β -Diketonate ligands containing high-energy oscillators, such as C–H and O–H groups, are able to quench the Ln^{3+} excited states nonradiatively, thereby leading to lower luminescence intensities and shorter excited-state lifetimes. The replacement of C–H groups with C–F groups is important in the syntheses of lanthanide complexes with efficient photoluminescence properties. It is well known that the replacement of C–H oscillators in a β -diketonate ligand with lower-energy C–F oscillators, lowers the vibration energy of the ligand, which in turn decreases the energy loss caused by ligand vibration and enhances the luminescence intensity of the corresponding lanthanide ion.¹⁸⁻²² Further, due to the heavy-atom effect, which facilitates intersystem crossing, the lanthanide-centered

luminescence properties are enhanced.^{23, 24} To achieve this goal, herein, a new β -diketonate ligand, 1-(3,5-bis(benzyloxy)phenyl)-4,4,5,5,5-pentafluoropentane-1,3-dione (**HBBPPF**) was synthesized, which contains a polyfluorinated alkyl group, as well as larger conjugated bis(benzyloxy)phenyl unit and utilized as an efficient photosensitizer for Eu^{3+} luminescence.

Lanthanide β -diketonate complexes have been excluded from practical use in various fields of optoelectronics because of their poor thermal stability and mechanical properties.²⁵ In order to circumvent these limitations, the lanthanide complexes should be incorporated into inorganic or organic/inorganic matrices such as sol-gel silica, mesoporous materials, polymers etc.²⁶⁻²⁹ Nowadays, the incorporation of luminescent Ln^{3+} complexes in solid matrices with controlled structural organization is of widespread interest in materials science as it affords functional materials with a variety of optical properties. In this framework, excellent reviews on different strategies toward lanthanide-incorporated hybrid materials have been recently reported in the literature.^{25, 30, 31} Extensive work has been carried out on the covalent grafting of lanthanide complexes with β -diketonates,³²⁻³⁶ aromatic carboxylic acids,³⁷⁻³⁹ and heterocyclic ligands such as 2,2'-bipyridine and 1,10-phenanthroline,⁴⁰⁻⁴² into ordered mesoporous silica hosts. These studies have indicated that the thermal stability and mechanical properties of the incorporated complexes are improved by the host silica matrix. However, the synthesis and the optical properties of MCM-41 mesoporous materials covalently bonded with Eu^{3+} complexes by modified fluorinated β -diketonates have not been fully explored. Recently, Reddy and co-workers reported a highly luminescent Eu^{3+} complex containing organosilyl 4,4,5,5,5-pentafluoro-1-(naphthalen-2-yl)pentane-1,3-dionate

ligands grafted on silica nanoparticles in the presence of 4,7-diphenyl-1,10-phenanthroline as a co-ligand.⁴³

Given the important potential applications of Eu^{3+} complexes and the fascinating advantages of fluorinated β -diketonates, we were prompted to design a novel β -diketonate ligand, 1-(3,5-bis(benzyloxy)phenyl)-4,4,5,5,5-pentafluoropentane-1,3-dione (**HBBPPF**), which contains a polyfluorinated alkyl group, and its corresponding Eu^{3+} ternary complex in the presence of a bidentate phosphine oxide, 4,5-bis(diphenylphosphino)-9,9-dimethylxanthene oxide (**DDXPO**), and to evaluate its photophysical properties. Here, we also report on the synthesis and characterization of 1-(3,5-bis(benzyloxy)-phenyl)-4,4,5,5,5-pentafluoropentane-1,3-dione functionalized mesoporous hybrid material **Eu(BBPPF-Si)₃(DDXPO)/MCM-41**, in which **HBBPPF** was covalently bonded to the framework of MCM-41. The synthesized luminescent hybrid material was characterized well, and its photophysical properties were investigated. The photophysical properties of the developed hybrid material, **Eu(BBPPF-Si)₃(DDXPO)/MCM-41**, are found to be superior to that of parent Eu^{3+} complex, **Eu(BBPPF-Si)₃(DDXPO)**.

4.3. Experimental section

4.3.1. Materials and Instrumentation. Europium(III) nitrate hexahydrate, 99.9% (Treibacher); gadolinium(III) nitrate hexahydrate, 99.9% (Aldrich); 3,5-dihydroxyacetophenone, 97% (Aldrich); benzyl bromide, 98% (Aldrich); potassium carbonate, 98% (Merck); methyl pentafluoropropionate, 99% (Aldrich); sodium hydride, 60% dispersion in mineral oil (Aldrich); (3-isocyanatopropyl)-triethoxysilane, 95% (Alfa Aesar) and mesostructured hexagonal silica, MCM-41

(Aldrich) were purchased from commercial sources and used without further purification. **DDXPO** has been synthesized in our laboratory according to the method described earlier.²² All the other chemicals used were of analytical reagent grade.

FT-IR spectra were obtained as KBr pellets using a Perkin-Elmer Spectrum One FT-IR Spectrometer. Elemental analyses for C, H and N were performed with a Perkin-Elmer Series 2 Elemental Analyzer 2400. ¹H NMR (500 MHz) and ¹³C NMR (125 MHz) spectra were recorded by using a Bruker 500 MHz NMR spectrometer relative to tetramethylsilane (TMS) as internal standard. Solid state ²⁹Si and ¹³C NMR spectra were obtained on a Bruker DRX 500 spectrometer (the measurements were obtained in natural abundance at frequencies of 75.47 and 59.61 MHz for carbon and silicon, respectively). The mass spectra were recorded on a JEOL JSM 600 fast atom bombardment (FAB) high-resolution mass spectrometer (FAB-MS). X-Ray powder diffraction using Ni-filtered Cu-K α radiation with a Philips X'pert Pro diffractometer. Data were collected by step scanning from 2 to 20° (2 θ). Nitrogen (N₂) adsorption/desorption isotherms were measured by using a Micromeritics Gemini 2375 V5.01 analyzer with nitrogen. The samples were outgassed for 4 h at 120 °C before the measurements. Surface areas were calculated by the Brunauer–Emmett–Teller (BET) method and pore sizes by the Barrett–Joyner–Halenda (BJH) methods. The transmission electron microscopy (TEM) study of the morphology of the nanoparticles was carried out with a JEOL 2010 (200 kV). A pinch of material was suspended in ethanol. Then, a carbon-coated copper grid was dipped in the solution and allowed to dry at room temperature. Average particle sizes were determined by statistical calculations based on the TEM images. The

dynamic light scattering experiment was conducted using Malvern Instruments zetasizer nano Zis Model no: ZEN 3600 to determine the hydrodynamic diameter of the hybrid material. Optical reflectance and UV absorption studies were carried out with an UV-vis spectrometer (Shimadzu UV-2450). The excitation and emission spectra of the samples were recorded on a Spex-Fluorolog FL322 spectrofluorimeter equipped with a double grating 0.22 m Spex 1680 monochromator and a 450 W Xe lamp as the excitation source operating in the front face mode. The lifetime measurements were carried out at room temperature using a Spex 1040 D phosphorimeter. The overall quantum yields ($\Phi_{overall}$) were measured using a calibrated integrating sphere in a SPEX Fluorolog Spectrofluorimeter. The Xe-arc lamp was used to excite the samples placed in the sphere. Samples were prepared by drop casting the material placed between two quartz cover slips. The quantum yield was determined by comparing the spectral intensities of the lamp and the sample emission as reported in the literature. Using this experimental setup and the integrating sphere system,⁴⁴ the solid-state emission quantum yield of standard material, tris-8-hydroxyquinolinolato aluminum (Alq₃), was determined to be 40%,⁴⁵⁴⁶ which is consistent with previously reported values. Each sample was measured several times under slightly different experimental conditions. The estimated error for quantum yields is ($\pm 10\%$).⁴⁷

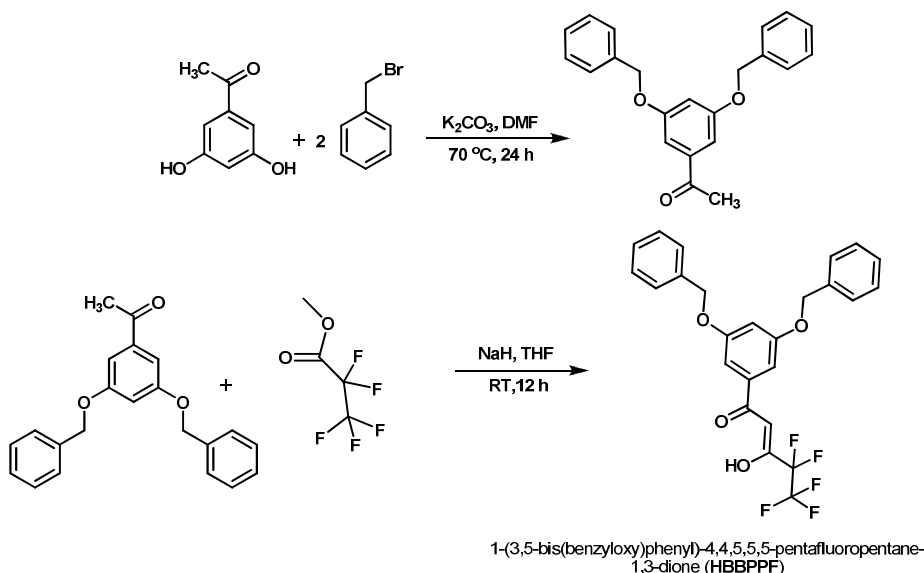
4.3.2 Synthesis of the ligand and Ln³⁺ complexes. The method of synthesizing the ligand 1-(3,5-bis(benzyloxy)phenyl)-4,4,5,5,5-pentafluoropentane-1,3-dione, (**HBBPPF**), is outlined in Scheme 4.1.

4.3.2.1. Synthesis of 1-(3,5-bis(benzyloxy)phenyl)ethanone. 3,5-Dihydroxyacetophenone (1.6 mmol) and potassium carbonate (3.3 mmol) were

dissolved in DMF (30 mL) and stirred at 75 °C for 1 h. To this, benzyl bromide (3.2 mmol) was added and refluxed for 24 h. The resultant reaction mixture was then poured in to cold water. The precipitate obtained was washed well with water, dried and recrystallized from a chloroform-hexane (25:75) mixture (yield = 80%). ¹H NMR (500 MHz, CDCl₃): δ (ppm) 7.32-7.26 (m, 8H), 7.22 (t, 2H, *J* = 7.25 Hz), 7.09 (d, 2H, *J* = 2.5 Hz), 6.70 (t, 1H, *J* = 2.25), 4.94 (s, 4H), 2.43 (s, 3H). ¹³C NMR (125 MHz, CDCl₃): δ (ppm) 197.69, 160.03, 139.10, 136.48, 128.72, 128.23, 127.67, 107.42, 106.89, 70.35, 26.77. MS (FAB) *m/z* = 332.14 (M)⁺.

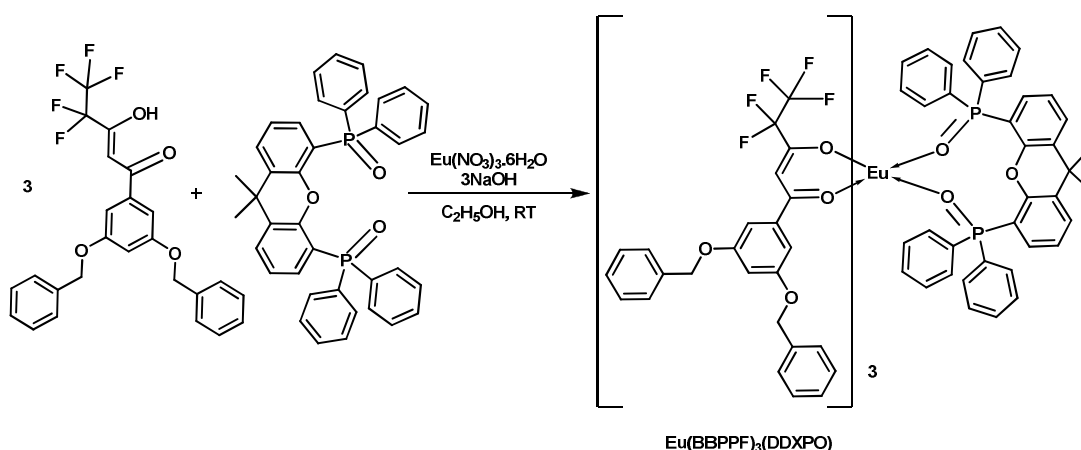
4.3.2.2. Synthesis of 1-(3,5-bis(benzyloxy)phenyl)-4,4,5,5,5-pentafluoropentane-1,3-dione (HBBPPF). The ligand **HBBPPF** was synthesized by a modified method of typical Claisen condensation procedure. 1-(3,5-Bis(benzyloxy)phenyl)ethanone (1 mmol) and methyl pentafluoropropionate (1 mmol) were added into 20 mL of dry THF and stirred for 10 min at 0 °C. To this, sodium hydride (2.5 mmol) was added in inert atmosphere and stirred for 12 h. The reaction mixture was then quenched with water, 2 M HCl (20 mL) added, and the solution was extracted with dichloromethane (3 × 20 mL). The organic layer was dried over Na₂SO₄, and the solvent was evaporated. The product was then purified by utilizing silica gel column chromatography by using a mixture of chloroform and hexane as the eluent (30:70) to obtain a yellow solid as the product (yield 73%). Elemental analysis (%): calc. for C₂₅H₁₉F₅O₄ (478.41): C 62.76, H 4.00; found: C 63.04, H 4.04; ¹H NMR (500 MHz, CDCl₃): δ (ppm) 15.31 (broad, 1H, enol -OH), 7.44–7.39 (m, 10H), 7.16 (d, 2H, *J* = 2 Hz), 6.85 (t, 1H, *J* = 2.25 Hz), 6.54 (s, 1H), 5.09 (s, 4H). ¹³C NMR (125 MHz, CDCl₃): δ (ppm) 186.13, 178.01, 160.23, 136.10, 134.86, 128.74, 128.33, 127.62,

107.38, 106.79, 94.12, 70.47. FT-IR (KBr) ν_{max} : 3435, 2927, 1581, 1450, 1170, 1018 cm^{-1} . MS (FAB) $m/z = 478.58$ (M)⁺.



Scheme 4.1. Synthesis of ligand HBBPPF.

4.3.2.3. Synthesis of Eu(BBPPF)₃(DDXPO). To an ethanolic solution of HBBPPF (0.6 mmol), NaOH (0.6 mmol) was added and stirred for 5 min. To this mixture, a saturated ethanolic solution of Eu(NO₃)₃·6H₂O (0.2 mmol) was added drop wise followed by the addition of an ethanolic solution of DDXPO (0.2 mmol) and stirred for 24 h. The product was obtained after solvent evaporation and was purified by recrystallization from a chloroform-hexane mixture. The method of synthesizing the complex is outlined in Scheme 4.2. Unfortunately, efforts to grow single crystals of complex were not fruitful. Elemental analysis (%): calc. for C₁₁₄H₈₆F₁₅O₁₅P₂Eu (2194.83): C 62.38, H 3.95; found: C 62.67, H 4.07. MS(FAB) $m/z = 1718.87$ (M+H-HBBPPF)⁺. FT-IR (KBr) ν_{max} : 2927, 2851, 1590, 1502, 1210, 1173, 1158, 1030 cm^{-1} .

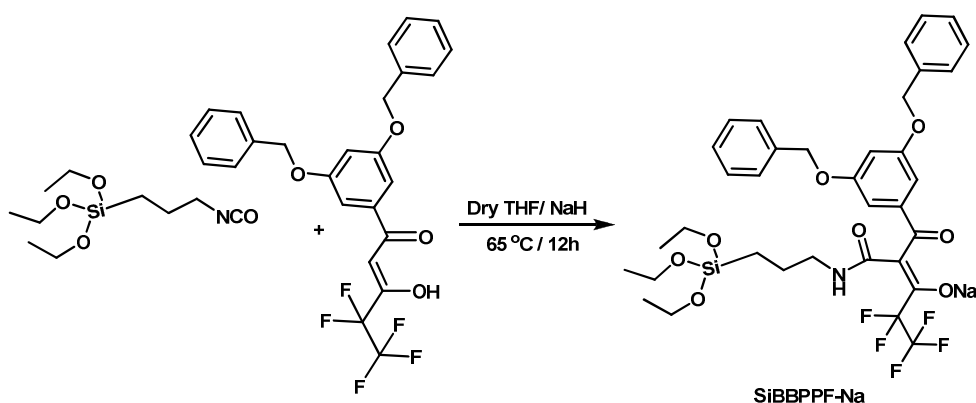
Scheme 4.2. Synthesis of $\text{Eu}(\text{BBPPF})_3(\text{DDXPO})$.

4.3.2.4. Synthesis of sodium-1-(3,5-bis(benzyloxy)phenyl)-4,4,5,5,5-pentafluoro-1-oxo-2-((3-(triethoxysilyl)propyl)carbamoyl)pent-2-en-3-olate (SiBBPPF-Na).

The method of synthesizing the ligand, sodium-1-(3,5-bis(benzyloxy)phenyl)-4,4,5,5,5-pentafluoro-1-oxo-2-((3-(triethoxysilyl)propyl)carbamoyl)pent-2-en-3-olate, **SiBBPPF-Na** is outlined in Scheme 4.3. 1 mmol of the β -diketone ligand, **HBBPPF**, was dissolved in dry THF, and 2.5 mmol of NaH (60%) was added to the solution and refluxed at 65 °C with stirring. Two hours later, 1 mmol of (3-isocyanatopropyl)triethoxysilane was added dropwise into the refluxing solution. The whole mixture was heated at 65 °C under argon atmosphere for 8 h. After isolation and purification (washing with 3 x 30 mL hexane), the sodium salt of **SiBBPPF** was obtained as a yellow solid, which was used without further purification (yield 62%).

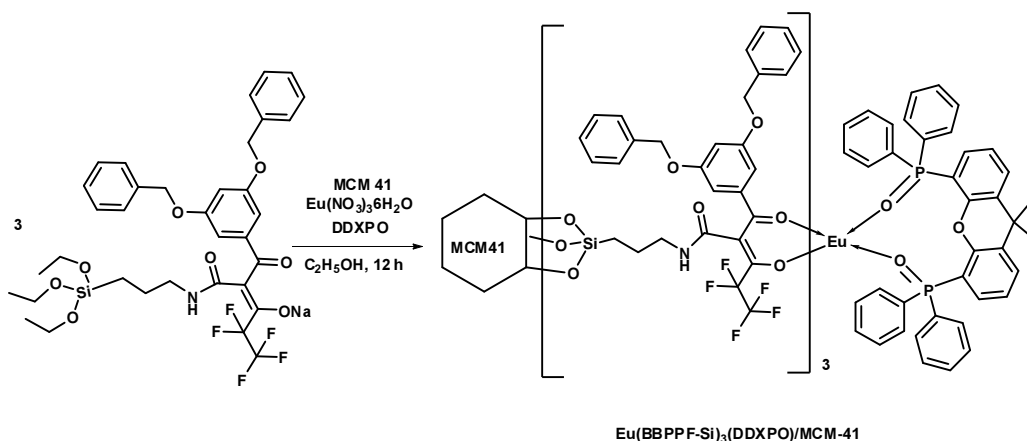
^1H NMR (500 MHz, CDCl_3): δ (ppm) 7.56 (q, 4H, $J = 3.33$), 7.51–7.47 (m, 6H), 7.09 (d, 2H, $J = 2.5$ Hz), 6.82 (t, 1H, $J = 2.25$) 5.96 (broad, NH), 5.28 (s, 4H), 3.62 (q, 6H, $J = 7.12$ Hz), 3.15–3.05 (m, 2H), 1.64–1.62 (m, 2H), 1.20 (t, 9H, $J = 7.25$ Hz), 0.71–0.58 (t, 2H, $J = 2$ Hz). ^{13}C NMR: δ (ppm) 10.22, 24.50, 42.89, 61.68, 69.37, 92.29,

105.39, 128.05, 137.07, 159.86, 171.60, 184.44, 188.58. FT-IR (KBr) ν_{max} : 3400, 2927, 2860, 1643, 1586, 1409, 1217, 1059, 784, 738 cm^{-1} .



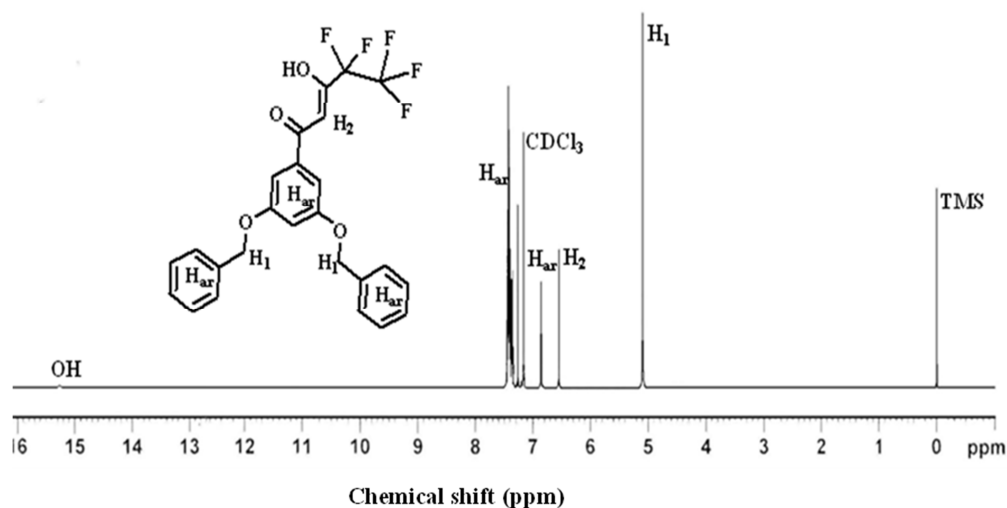
Scheme 4.3. Synthesis of SiBBPPF-Na.

4.3.2.5. Synthesis of luminescent hybrid material, Eu(BBPPF-Si)₃(DDXPO)/MCM-41. The method of synthesizing the luminescent hybrid material is described in Scheme 4.4. **SiBBPPF-Na** (3.5 mmol) was dissolved in 20 mL of ethanol with constant stirring. An appropriate amount of MCM-41 (molar ratio of MCM-41: **SiBBPPF-Na** = 1:3) was then added to the solution. Six hours later, $\text{Eu}(\text{NO}_3)_3 \cdot 6\text{H}_2\text{O}$ (1.17 mmol) and **DDXPO** (1.17 mmol) were added and stirred vigorously in air atmosphere at room temperature for 48 h. Finally, the solid product was recovered by centrifugation, washed with ethanol, dried at 80 °C. This hybrid material with mesoporous MCM-41 covalently bonded to luminescent Eu^{3+} complex is represented as **Eu(BBPPFSi)₃(DDXPO)/MCM-41**. FT-IR (KBr) ν_{max} : 3435, 2927, 2857, 1643, 1593, 1409, 1246, 1217, 1174, 1085, 784, 750, 699 cm^{-1} . The solid-state ^{29}Si and ^{13}C NMR spectral data are described in the "Results and discussion" section.

Scheme 4.4. Synthesis of Eu(BBPPF-Si)₃(DDXPO)/MCM-41.

4.4. Results and discussion

4.4.1. Synthesis and characterization of ligand (HBBPPF) and Eu³⁺ complex (Eu(BBPPF)₃(DDXPO)). The ligand 1-(3,5-bis(benzyloxy)phenyl)-4,4,5,5,5-pentafluoropentane-1,3-dione was synthesized in a two-step process according to the method described in Scheme 4.1 with an overall yield of 59%. The designed ligand was characterized by ¹H NMR, ¹³C NMR (Figures 4.1 and 4.2), FAB-MS and elemental analysis.

Figure 4.1. ¹H NMR spectrum of HBBPPF.

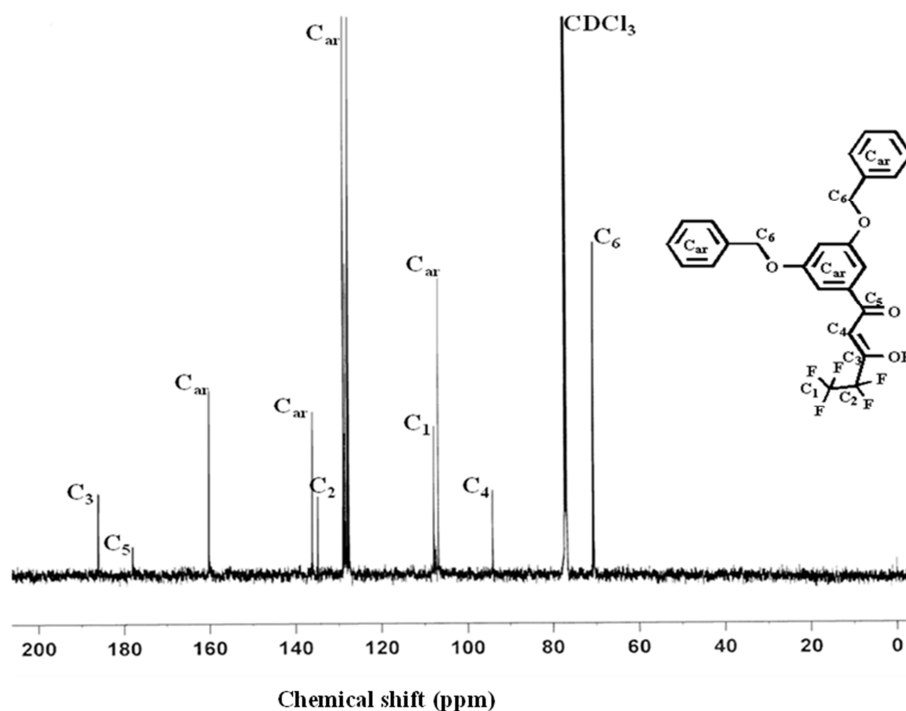


Figure 4.2. ^{13}C NMR spectrum of **HBBPPF**.

The synthetic procedure for **Eu(BBPPF)₃(DDXPO)** is illustrated in Scheme 4.2. The elemental analysis and FAB-MS data of the developed Eu^{3+} complex imply that Eu^{3+} ion has reacted with the β -diketonate ligand, **HBBPPF**, in a metal-to-ligand mole ratio of 1:3 and one molecule of bidentate phosphine oxide, **DDXPO**, is also present in the coordination sphere. In the FT-IR spectra, the carbonyl stretching frequency of **HBBPPF** (1581 cm^{-1}) has been shifted to higher wave numbers in **Eu(BBPPF)₃(DDXPO)** (1590 cm^{-1}) indicating the coordination of the carbonyl oxygen to the Eu^{3+} ion. Further, the P=O stretching frequency of **DDXPO**, 1190 cm^{-1} has been shifted to 1173 cm^{-1} in **Eu(BBPPF)₃(DDXPO)** confirms the coordination of **DDXPO** to the Eu^{3+} ion. In addition, the absence of broadband in the region $3000\text{--}3500\text{ cm}^{-1}$ suggests that there is no solvent molecules present in **Eu(BBPPF)₃(DDXPO)**.

4.4.2. Synthesis and characterization of SiBBPPF-Na and luminescent hybrid material, Eu(BBPPF-Si)₃(DDXPO)/MCM-41. The silylated β -diketonate ligand (SiBBPPF-Na) and the corresponding luminescent hybrid material, Eu(BBPPF-Si)₃(DDXPO)/MCM-41 were synthesized as shown in Schemes 4.3 and 4.4, respectively. The structure of the modified ligand, SiBBPPF-Na has been confirmed by ¹H NMR (CDCl₃) (Figure. 4.3) and solid-state ¹³C NMR spectroscopic methods (Figure. 4.4). A broad peak at δ 5.96 ppm in the ¹H NMR and the peak at δ 171.60 ppm in the ¹³C NMR spectra indicates the formation of amide –CO–NH– linkages in the SiBBPPF-Na ligand. The propyl chain in the ligand gives peaks at 0.58–3.15 ppm in the ¹H NMR spectrum and 10.22–42.89 ppm in the ¹³C NMR spectrum. The purity of the product was confirmed by the absence of signal at δ 6.54 ppm characteristic of the free H in between the two carbonyl groups in the ¹H NMR spectrum. The ²⁹Si NMR spectrum of unmodified MCM-41 displays two broad overlapping resonances at δ = –101.4 and –110.6 ppm, which correspond to Q₃ and Q₄ species of the silica framework [Q_n = Si(OSi)_n(OH)_{4–n}] (Figure 4.5). A weak shoulder is also observed at δ = –91.9 ppm for the Q₂ species. The Q₃ sites are associated with single Si–OH groups that include both free and hydrogen-bonded silanols, and the Q₂ sites correspond to geminal silane diols.^{48, 49} The ²⁹Si NMR spectrum of Eu(BBPPF-Si)₃(DDXPO)/MCM-41 exhibited four peaks (Figure. 4.6). The first one, at δ –57.29 ppm, which was assigned to the silicon atom of the silylating agent, bound to one hydroxyl group, forming the structure RSi(OSi)₂(OH), represented as T₂ signal. The second peak, at –66.05 ppm, was assigned to RSi(OSi)₃ (T₃ signal).⁵⁰ The presence of T₂ and T₃ signals confirms that the organic groups have been covalently bonded to the silica matrix. The other two peaks, at –101.44

and -111.14 ppm, were attributed to pure surface signals and were assigned, respectively, to (i) $\text{Si}(\text{OSi})_3\text{OH}$, corresponding to the Q_3 signal, and (ii) $\text{Si}(\text{OSi})_4$, corresponding to the Q_4 signal.^{50, 51}

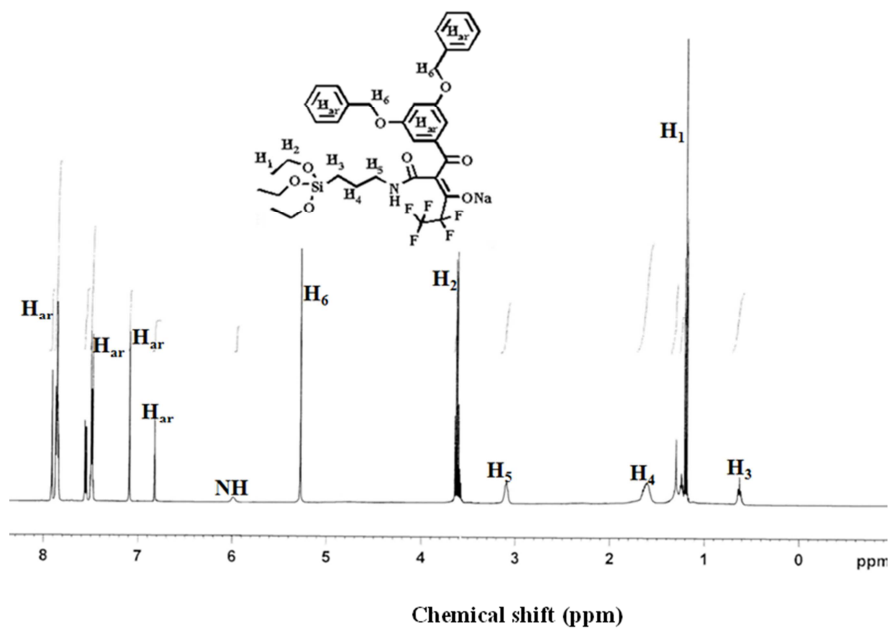


Figure 4.3. ^1H NMR spectrum of SiBBPPF-Na.

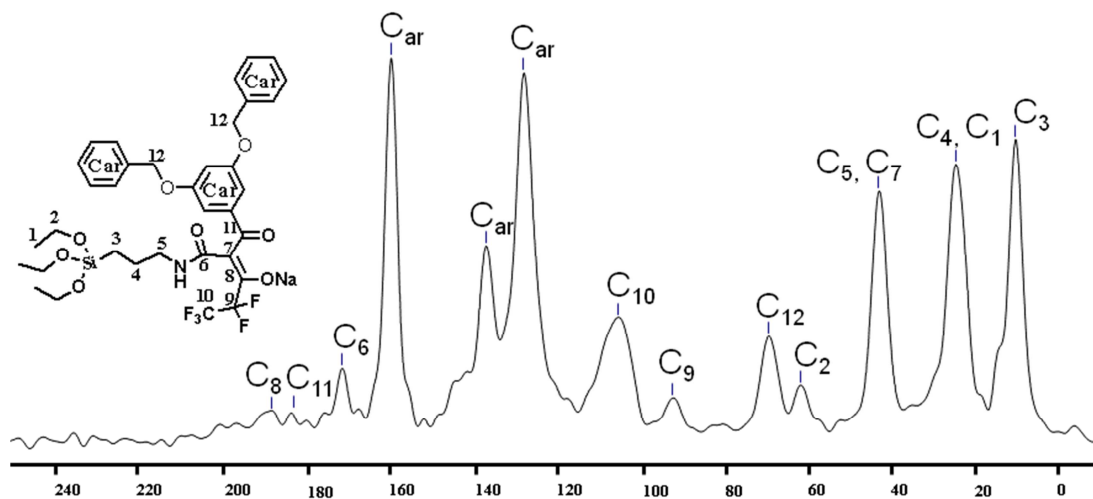


Figure 4.4. Solid-state ^{13}C NMR spectrum of SiBBPPF-Na.

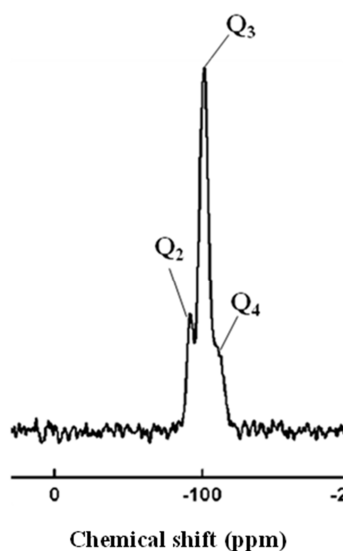


Figure 4.5. Solid-state ^{29}Si NMR spectrum of MCM-41.

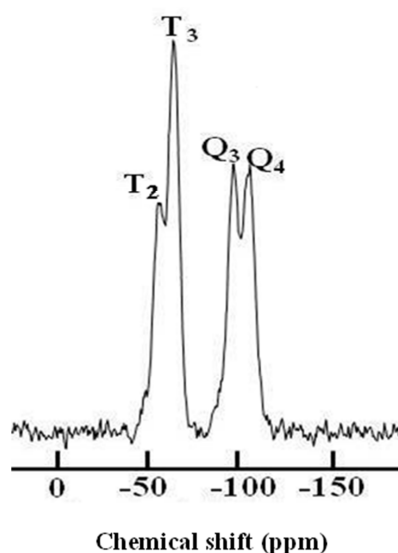


Figure 4.6. Solid-state ^{29}Si NMR spectrum of $\text{Eu}(\text{SiBBPPF})_3(\text{DDXPO})/\text{MCM-41}$.

The FT-IR spectrum of **SiBBPPF-Na** contains no characteristic band at 2270 cm^{-1} ascribed to the vibration of R-NCO terminal group indicating that the grafting reaction was complete (Figure 4.7). In addition, bands located at 2927 and 2860 cm^{-1} represents the absorption of $-\text{CH}_2-$ groups in the benzyloxy groups of the β -diketone together with the stretching vibration of methylene groups of 3-(triethoxysilyl)-propylisocyanate. The presence of the amide group in **SiBBPPF-Na** was confirmed

by the appearance of new bands at 3400 (ν NH), 1643 cm^{-1} (ν NHCO) and 1409 cm^{-1} (δ NH). The FT-IR spectrum of **SiBBPPF-Na** shows the stretching vibration absorption bands at 1217 cm^{-1} (ν C–Si) and at 1059 cm^{-1} (ν Si–O), characteristic of the trialkoxysilyl functional group, derived from the cross-linking reagent 3-(triethoxysilyl)-propylisocyanate (TESPIC) proving that it was successfully grafted onto the β -diketone ligand. The FT-IR spectrum of **Eu(BBPPF-Si)₃(DDXPO)/MCM-41** (Figure 4.8) consists of a broad band located in the region 1046-1140 cm^{-1} (ν_{as} , Si–O) and a band at 784 cm^{-1} (ν_s , Si–O) (ν represents stretching, δ in plane bending, ν_s symmetric, and ν_{as} asymmetric vibrations) which demonstrates the successful hydrolysis and co-polycondensation reactions of ligand and MCM-41. Furthermore, the peak at 1643 cm^{-1} originating from the –CONH– group of **SiBBPPF-Na**, can also be observed in Figure 4.8, which is consistent with the fact that the carbonyl groups of the amide linkage in the grafted ligand remain the same after hydrolysis and condensation reactions, confirming that the two carbonyl groups of the β -diketones are coordinated to the Eu^{3+} ions, not the carbonyl groups of the TESPIC.^{52, 53} In addition, the carbonyl stretching frequency of the β -diketone group of **SiBBPPF-Na** is blue shifted from 1586 cm^{-1} to 1593 cm^{-1} in the Eu^{3+} complex incorporated hybrid material indicating that this group is involved in complexation with Eu^{3+} ions. Similar to the parent complex, **Eu(BBPPF)₃(DDXPO)**, the P=O stretching peak is observed at 1174 cm^{-1} for the developed luminescent hybrid material indicating that the coordination environment around the Eu^{3+} ion is similar to that of **Eu(BBPPF)₃(DDXPO)**.²²

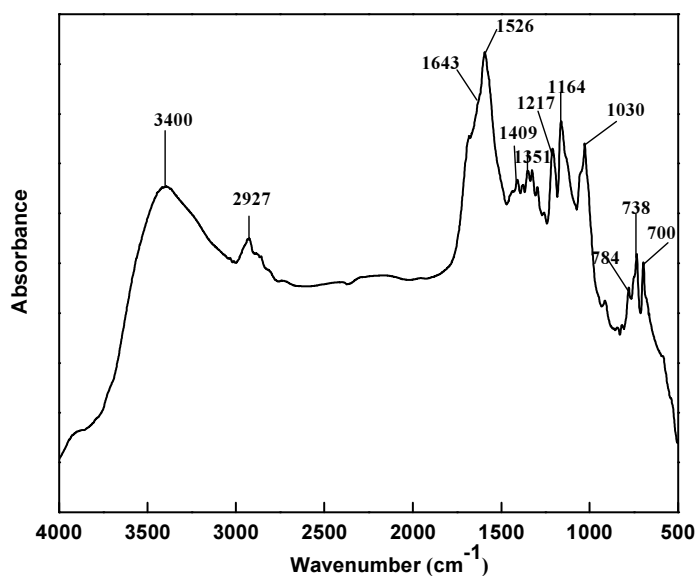


Figure 4.7. FT-IR spectrum of SiBBPPF-Na.

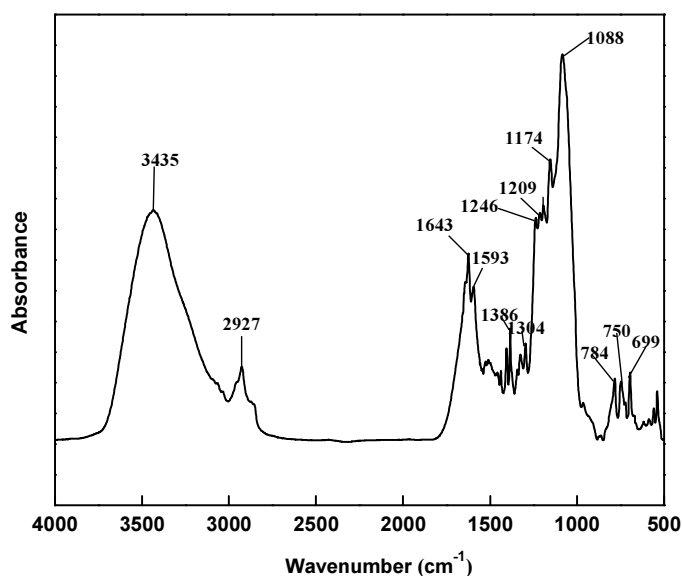


Figure 4.8. FT-IR spectrum of Eu(SiBBPPF)₃(DDXPO)/MCM-41.

The XRD pattern of the Eu³⁺ complex incorporated hybrid material along with MCM-41 is shown in Figure 4.9. The periodic nature of the product was confirmed by XRD analysis. The XRD pattern of MCM-41 used for the synthesis of hybrid material is characteristic of a well-ordered hexagonal mesoporous phase.⁵⁴⁻⁵⁶ The Bragg peaks indexed as (100), (110) and (200) are still observed in the XRD pattern

of the hybrid luminescent material and the gradual broadening of peaks reveals that the structure ordering has been decreased due to the introduction of the bulky **Eu(BBPPF-Si)₃(DDXPO)** fragment inside the channels of the mesoporous materials.^{50, 57}

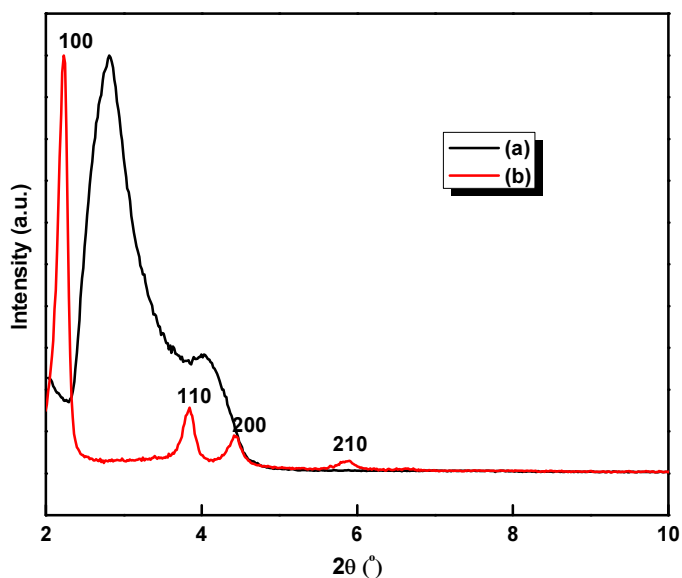


Figure 4.9. X-ray diffraction patterns of (a) **Eu(SiBBPPF)₃(DDXPO)/MCM-41** and (b) MCM-41.

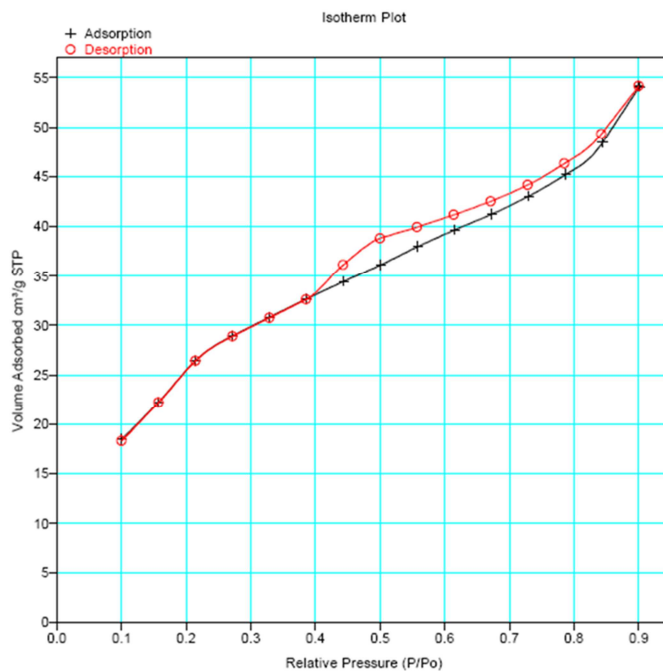


Figure 4.10. N₂ adsorption-desorption isotherms for **Eu(SiBBPPF)₃(DDXPO)/MCM-41**.

The N₂ adsorption-desorption isotherm of **Eu(BBPPF-Si)₃(DDXPO)/MCM-41** is shown in Figure 4.10, which displays Type IV isotherm with H4-type hysteresis loops at high relative pressure according to the IUPAC classification,^{50, 58} characteristic of mesoporous materials with highly uniform size distributions. The specific surface area and pore size have been calculated using Brunauer-Emmett-Teller (BET) and Barrett-Joyner-Halenda (BJH) methods, respectively. It is clear from the N₂ adsorption-desorption data that the MCM-41 is having a high BET surface area (1009 m²/g) and a large pore volume (0.81 cm³/g), indicative of its potential use as a host matrix for luminescent materials. The introduction of luminescent Eu³⁺ complex into the MCM-41, has decreased the BET surface area (105 m²/g) and pore volume (0.08 cm³/g), which further confirms the successful incorporation of the Eu³⁺ complexes into the channels of mesoporous MCM-41.

From the dynamic light scattering (DLS) measurements it is clear that the developed hybrid material has an average hydrodynamic diameter of 39 nm (Figure 4.11). The TEM image (Figure 4.12) of **Eu(BBPPF-Si)₃(DDXPO)/MCM-41** shows that the particle shape is almost spherical with dimensions less than 60 nm. However, some aggregation did occur, as can be seen from the TEM image. The quite uniform frameworks observed demonstrate that homogeneous, molecular-based hybrid materials were obtained which contains a functional bridging aminopropyl silane group with strong chemical bonds between the inorganic and organic phases. Compared to hybrid materials with doped lanthanide complexes, which generally experiencing phase separation phenomena, the two phases in the hybrid materials with chemical covalent bonds (Si-O) can exhibit their distinct properties together.⁵⁹ It should be noted that the diameter reading obtained from TEM images is slightly

larger than that shown in DLS data due to the different measuring mechanisms behind these two methods. The TEM image of the developed hybrid material indicates that the monodispersity of the nanosized MCM-41 units were conserved even after the incorporation of luminescent Eu^{3+} complexes.

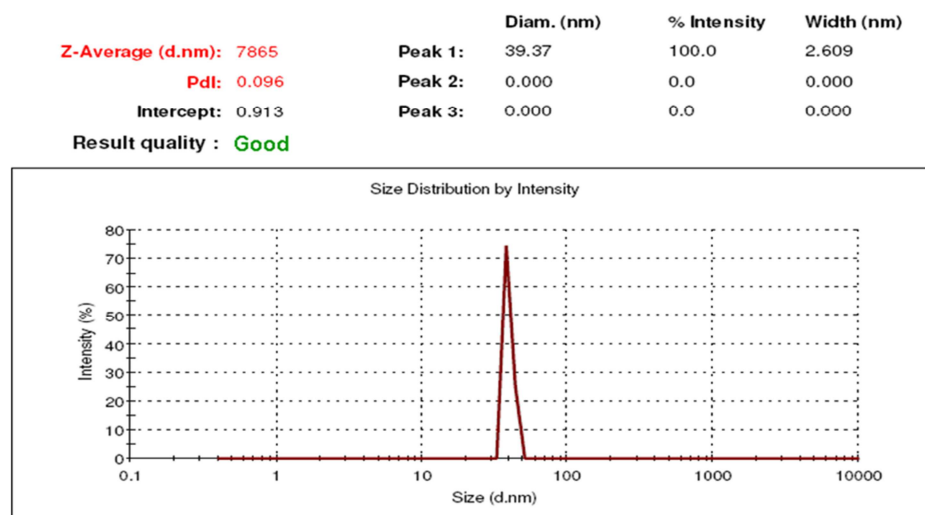


Figure 4.11. DLS particle size distribution curve of $\text{Eu}(\text{SiBBPPF})_3(\text{DDXPO})/\text{MCM-41}$.

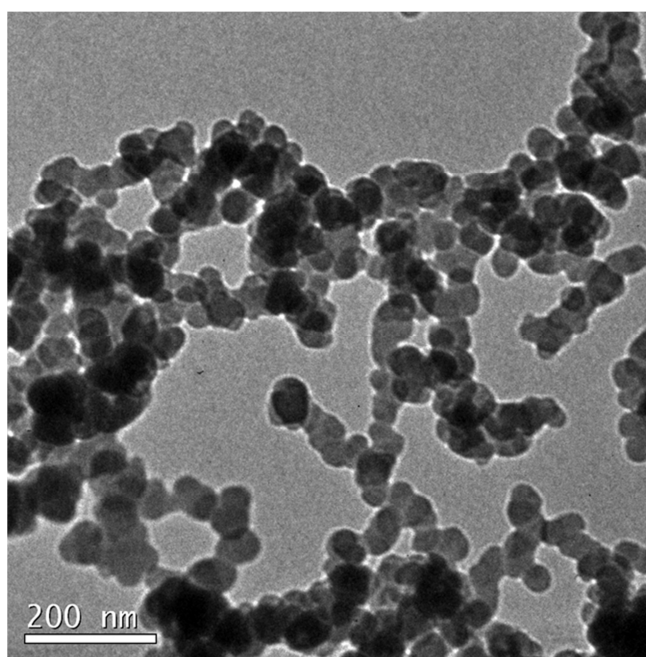


Figure 4.12. TEM picture of $\text{Eu}(\text{SiBBPPF})_3(\text{DDXPO})/\text{MCM-41}$.

4.4.3. Photophysical studies

The solid-state room-temperature excitation and emission spectra of the parent complex, **Eu(BBPPF)₃(DDXPO)**, and the hybrid material, **Eu(BBPPF-Si)₃(DDXPO)/MCM-41**, were recorded and are shown in Figure 4.13. The excitation spectra of the Eu^{3+} complex and the resulting hybrid material **Eu(BBPPF-Si)₃(DDXPO)/MCM-41**, are similar, which are obtained by monitoring the corresponding emission wavelength of the Eu^{3+} ions at 612 nm. For both spectra, a broad band ranging 250 to 460 nm can be seen, which is ascribed to the electronic transitions of the ligands. A series of sharp lines assigned to transitions between the ${}^7\text{F}_{0,1}$ and ${}^5\text{D}_{2-1}$ are also seen in the solid state excitation spectra of the complex and hybrid material.^{12, 14, 60} However, these transitions are weaker than the absorption of the organic ligands and are overlapped by broad excitation band, which proves that luminescence sensitization *via* excitation of the ligand, is much more efficient than the direct excitation of Eu^{3+} ions.^{8, 9}

The solid state emission spectra of the parent complex, **Eu(BBPPF)₃(DDXPO)**, and the hybrid material, **Eu(BBPPF-Si)₃(DDXPO)/MCM-41**, exhibit the characteristic narrow emission bands arising from the intra-configurational ${}^5\text{D}_0 \rightarrow {}^7\text{F}_J$ ($J = 0-4$) transitions of the Eu^{3+} ion.⁶¹ A weak green emission band at 536 nm, corresponding to the high energy transition of ${}^5\text{D}_1 \rightarrow {}^7\text{F}_1$ (inset in Figure 4.13), is also observed in the emission spectra.¹² No ligand-based emission is observed in the emission spectra, indicating an efficient ligand-to-metal energy transfer process in both the parent complex and the hybrid material. The five narrow emission peaks centered at 579, 592, 612, 652 and 700 nm, assigned to ${}^5\text{D}_0 \rightarrow {}^7\text{F}_0$, ${}^5\text{D}_0 \rightarrow {}^7\text{F}_1$, ${}^5\text{D}_0 \rightarrow {}^7\text{F}_2$, ${}^5\text{D}_0 \rightarrow {}^7\text{F}_3$, and ${}^5\text{D}_0 \rightarrow {}^7\text{F}_4$ transitions of Eu^{3+} ion, respectively.⁶¹ Among the

peaks, the emission at 612 nm from the ${}^5D_0 \rightarrow {}^7F_2$ induced electronic dipole transition is the strongest, suggesting the Eu^{3+} ions does not have an inversion center.⁶² Moreover, the presence of only one sharp peak in the region of the ${}^5D_0 \rightarrow {}^7F_0$ transition at 579 nm indicates the existence of a single chemical environment around the Eu^{3+} ion of point group symmetry C_s , C_n , or C_{nv} .^{63, 64} The experimental data on the parent Eu^{3+} complex and developed hybrid material indicate that the magnetic dipole transition ${}^5D_0 \rightarrow {}^7F_1$ of Eu^{3+} is largely independent of the ligand field and therefore can be used as an internal standard to account for the ligand differences.^{61, 65} The electric dipole transition ${}^5D_0 \rightarrow {}^7F_2$, so called hypersensitive transition, is sensitive to the symmetry of the coordination sphere. The intensity ratio of the electric dipole transition to the magnetic dipole transition in the lanthanide complex measures the symmetry of the coordination sphere. The relative luminescence intensity ratios ${}^5D_0 \rightarrow {}^7F_2/{}^5D_0 \rightarrow {}^7F_1$ (red/orange ratio) for all materials are listed in Table 4.1. For the parent complex, **Eu(BBPPF)₃(DDXPO)**, the intensity ratio of the transitions of ${}^5D_0 \rightarrow {}^7F_2/{}^5D_0 \rightarrow {}^7F_1$ (I_{21}) is 11.74 (Table 4.1.). This intensity ratio increases to 12.40 in the developed hybrid material, **Eu(BBPPF-Si)₃(DDXPO)/MCM-41**. In short, the incorporation of luminescent Eu^{3+} complex into the pores of mesoporous material, MCM-41, resulted in an enhancement in the intensity of the hypersensitive transition, ${}^5D_0 \rightarrow {}^7F_2$, observed at 612 nm. This behavior is consistent with that observed for similar luminescent Eu^{3+} complexes reported in the literature.²⁵

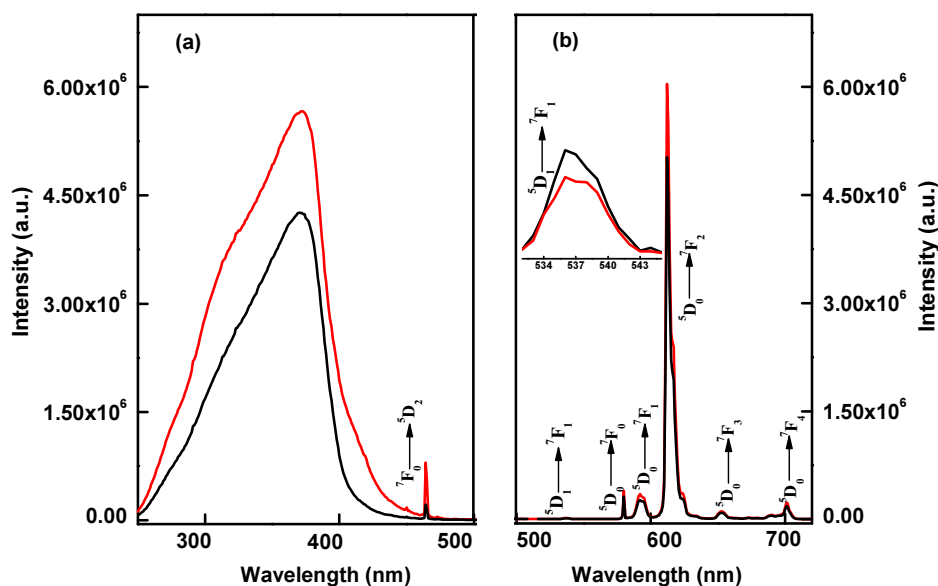


Figure 4.13. Solid state room temperature (a) excitation and (b) emission for **Eu(BBPPF)₃(DDXPO)** (red) and **Eu(BBPPF-Si)₃(DDXPO)/MCM-41** (black) ($\lambda_{ex} = 371$ nm, $\lambda_{em} = 612$ nm). ⁵D₁ → ⁷F₁ transition in the emission spectrum is shown in inset.

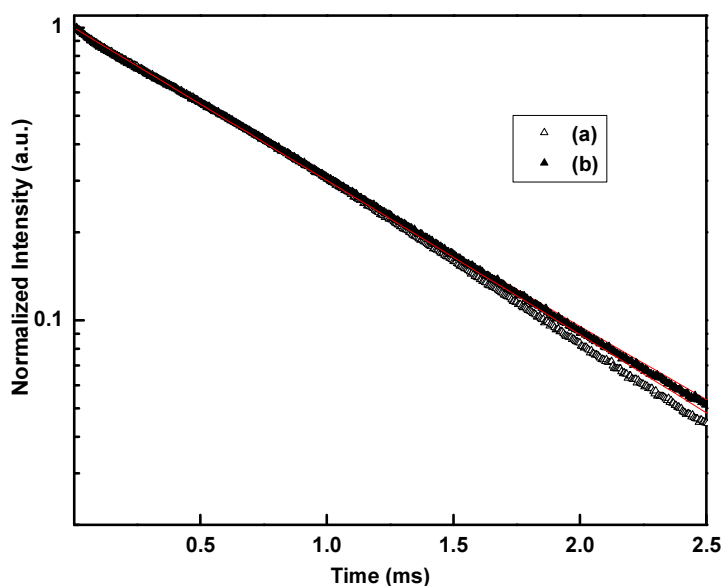


Figure 4.14. Experimental luminescence decay profiles of (a) **Eu(BBPPF)₃(DDXPO)** and (b) **Eu(BBPPF-Si)₃(DDXPO)/MCM-41** monitored at 612 nm and excited at their maximum emission wave lengths.

The luminescence decay times (τ) for **Eu(BBPPF)₃(DDXPO)** and **Eu(BBPPF-Si)₃(DDXPO)/MCM-41** were measured at room-temperature by monitoring the most intense emission line at 612 nm and an excitation wavelength of 371 nm, which

is shown in Figure 4.14. The lifetime profiles for both the parent complex, **Eu(BBPPF)₃(DDXPO)**, and the hybrid material, **Eu(BBPPF-Si)₃(DDXPO)/MCM-41**, are fitted with single exponentials, indicating that all Eu³⁺ ions occupy the same average coordination environment.⁶¹ The luminescence lifetime was calculated to be 829 ± 1 and 855 ± 1 μs for the complex, **Eu(BBPPF)₃(DDXPO)**, and the hybrid material, **Eu(BBPPF-Si)₃(DDXPO)/MCM-41**, respectively, which are also listed in Table 4.1. The shorter lifetime value observed for **Eu(BBPPF)₃(DDXPO)** indicates that the nonradiative transition probability is higher in it than that in **Eu(BBPPF-Si)₃(DDXPO)/MCM-41**.

The efficiency of photoluminescence can be expressed in terms of luminescence quantum yield, Φ , which is defined as the ratio of the number of photons emitted to the number of photons absorbed per unit time. For luminescent Eu³⁺ complexes, the overall luminescence quantum yield, $\Phi_{overall}$, upon the excitation of the organic ligands can be determined by the ligand sensitization efficiency, η_{sens} , and the intrinsic quantum yield, Φ_{Eu} , of the Eu³⁺ ion.⁶⁶⁻⁶⁸

$$\Phi_{overall} = \eta_{sens} \Phi_{Eu} \quad (4.1)$$

Φ_{Eu} can be calculated as:

$$\Phi_{Eu} = \left(\frac{A_{RAD}}{A_{RAD} + A_{NR}} \right) = \frac{\tau_{obs}}{\tau_{RAD}} \quad (4.2)$$

The radiative lifetime (τ_{RAD}) can be calculated using equation 4.3,¹² assuming that the energy of the ⁵D₀ → ⁷F₁ transition (MD) and its oscillator strength are constant

$$A_{RAD} = \frac{1}{\tau_{RAD}} = A_{MD,0} n^3 \left(\frac{I_{TOT}}{I_{MD}} \right) \quad (4.3)$$

where, $A_{MD,0}$ (14.65 s^{-1}) is the spontaneous emission probability of the ${}^5D_0 \rightarrow {}^7F_1$ transition in vacuo, I_{TOT}/I_{MD} is the ratio of the total area of the corrected Eu^{3+} emission spectrum to the area of the ${}^5D_0 \rightarrow {}^7F_1$ band and n is the refractive index of the medium. An average refractive index of 1.5 was considered.

The overall quantum yield ($\Phi_{overall}$), radiative (A_{RAD}) and non-radiative (A_{NR}) decay rates, intrinsic quantum yield (Φ_{Eu}) and energy transfer efficiency (η_{sens}) of the parent complex, **Eu(BBPPF)₃(DDXPO)**, and the hybrid material, **Eu(BBPPF-Si)₃(DDXPO)/MCM-41**, were summarized in Table 4.1. It is clear from Table 4.1 that, intrinsic quantum yield of **Eu(BBPPF-Si)₃(DDXPO)/MCM-41** ($\Phi_{Eu} = 66\%$) is higher than that of pure **Eu(BBPPF)₃(DDXPO)** ($\Phi_{Eu} = 61\%$), which can be ascribed to substitution of the silanol with covalently bonded **HBBPPF** groups in the pores of MCM-41, resulting in the decrease of the nonradiative multiphonon relaxation of Eu^{3+} ions by coupling to -OH vibrations and nonradiative transition rate. This clearly demonstrates the modifications in the Eu^{3+} ion local environment as **Eu(BBPPF-Si)₃(DDXPO)** is covalently bonded to the mesoporous MCM-41. Moreover, the absolute quantum yields ($\Phi_{overall}$) estimated for **Eu(BBPPF)₃(DDXPO)** and **Eu(BBPPF-Si)₃(DDXPO)/MCM-41**, 39% and 43%, respectively, are well consistent with the above results. These values are comparable to our recent report on europium(III) complex ($\Phi_{overall} = 43\%$) containing organosilyl 4,4,5,5,5-pentafluoro-1-(naphthalen-2-yl)pentane-1,3-dionate ligands grafted on silica nanoparticles in the presence of 4,7-diphenyl-1,10-phenanthroline as a co-ligand⁴³ or much higher than those when europium(III) complexes with other fluorinated β -diketonate ligands^{69, 70} incorporated into mesoporous silica materials.

Table 1. Radiative (A_{RAD}) and non-radiative (A_{NR}) decay rates, 5D_0 lifetime (τ_{obs}), intrinsic quantum yield (Φ_{Eu} , %), energy transfer efficiency (η_{sens} , %) and overall quantum yield ($\Phi_{overall}$, %) for complexes 1-4.

Compound	A_{RAD}/s^{-1}	A_{NR}/s^{-1}	$\tau_{obs}/\mu s$	Φ_{Eu} , (%)	η_{sens} , (%)	$\Phi_{overall}$, (%)
1	623	1994	382 ± 1	28	43	12
2	755	433	842 ± 2	64	52	34
3	793	1924	368 ± 1	32	47	15
4	757	451	828 ± 2	63	66	42

Based on the measurements of the absolute quantum yields, the corresponding chromaticity coordinates (x, y) are also obtained (Figure 4.15), which can quantify the emission features. The emission of the parent complex **Eu(BBPPF)₃(DDXPO)** and that of the hybrid material, **Eu(BBPPF-Si)₃(DDXPO)/MCM-41**, lies in the red spectral region, with coordinates of (0.66, 0.34) and these coordinates are equal or very close to those of the well-known standard red phosphor $Y_2O_3:Eu$ (0.66, 0.33).⁷¹

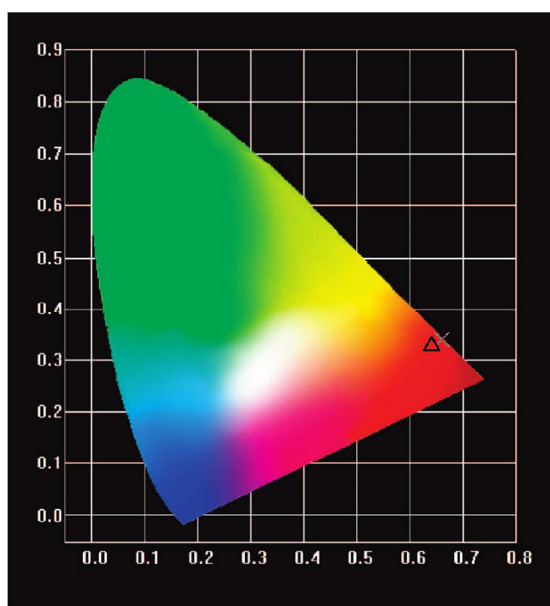


Figure 4.15. CIE (x,y) chromaticity diagram showing the emission colour coordinates of **Eu(BBPPF-Si)₃(DDXPO)/MCM-41**.

4.4.4. Intramolecular energy transfer in the Eu^{3+} complexes

It is well documented that in the ternary europium(III) β -diketonate complexes, the ancillary ligands often play a major role in absorbing and transferring energy to the primary β -diketonate ligand or to the central Eu^{3+} ion.⁷² For an effective energy transfer to occur, the overlap between the emission spectrum of the donor and the absorption spectrum of the acceptor is essential.³⁶ It is evident from Figure 4.16 that the room temperature emission spectrum of chelating ligand (**DDXPO**) is overlapped by the absorption spectrum of the **HBBPPF** in the region 375 to 450 nm, and hence nearly all the radiation from the singlet state of **DDXPO** can be absorbed by the **HBBPPF** ligand. The large area overlap of room temperature emission spectrum of **HBBPPF** with that of low-temperature phosphorescence spectrum of **Gd(DDXPO)(NO₃)₃** in the region 400–600 nm, indicates that energy transfer from singlet state (S_1) of **HBBPPF** to the triplet state (T_1) of **DDXPO** is effective (Figure 4.16). The overlap of low-temperature phosphorescence spectra of **Gd(DDXPO)(NO₃)₃** and **Gd(BBPPF)₃(H₂O)(C₂H₅OH)** again highlights that the ancillary ligand can transfer energy to the T_1 of **HBBPPF**, which subsequently transfers energy to the 5D_0 state of the Eu^{3+} ion. Finally, the Eu^{3+} ion emits when transition to the ground state occurs. Apart from the above energy transfer pathways, the overlap of room-temperature emission and low temperature phosphorescence spectra of **DDXPO** and **HBBPPF**, indicates that effective intersystem crossing process takes place between S_1 and T_1 of the ligands.

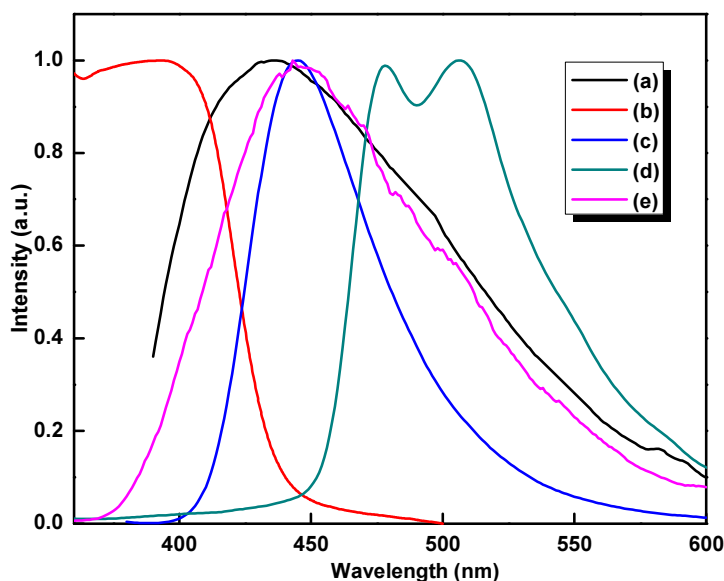


Figure 4.16. (a) Room-temperature emission spectrum of **DDXPO**, (b) UV-vis absorption spectra of **HBBPPF**, (c) room-temperature emission spectrum of **HBBPPF**, (d) 77 K phosphorescence spectra of **Gd(BBPPF)₃(H₂O)(C₂H₅OH)**, (e) 77 K phosphorescence spectra of **Gd(DDXPO)(NO₃)₃**. All spectra are in solid state and normalized to a constant intensity at the maximum.

To demonstrate the energy transfer process of the Eu^{3+} complex, **Eu(BBPPF)₃(DDXPO)**, the energy levels of relevant electronic states of the ligands have been determined. The S_1 and T_1 energy levels of **HBBPPF** were estimated by referring to higher wavelengths of UV-vis absorption edges (Figure 4.17) and the lower wavelength emission edges of phosphorescence spectra of complex **Gd(BBPPF)₃(H₂O)(C₂H₅OH)** (Figure 4.18). The S_1 and T_1 of **HBBPPF** are found to be $26,580$ and $21,230 \text{ cm}^{-1}$, respectively. The S_1 ($31,850 \text{ cm}^{-1}$) and T_1 ($23,470 \text{ cm}^{-1}$) levels of **DDXPO** has taken from our earlier publication.²² The triplet energy level of **SiBBPPF-Na** was found to be same as that of **HBBPPF**, indicating that silylation of the β -diketone ligand does not significantly change its electronic states (Figure 4.18).

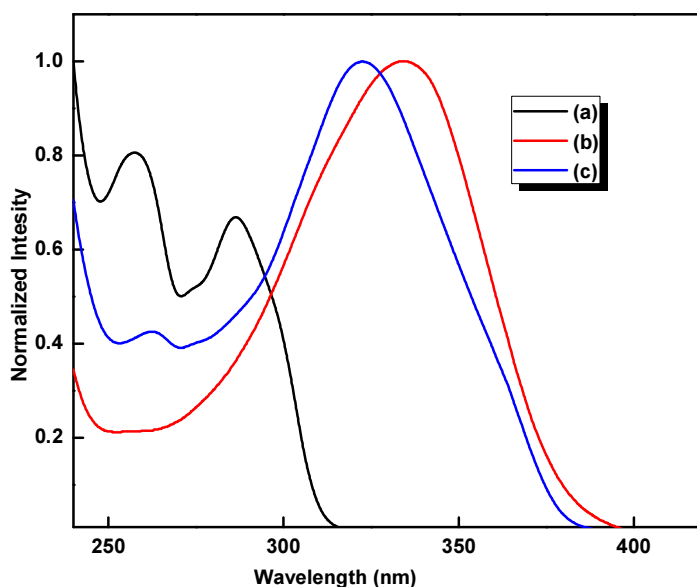


Figure 4.17. UV absorption spectra of DDXPO, HBBPPF and $\text{Eu}(\text{BBPPF})_3(\text{DDXPO})$ in acetonitrile solution ($c = 2 \times 10^{-5}$ M). All spectra are normalized to a constant intensity at the maximum.

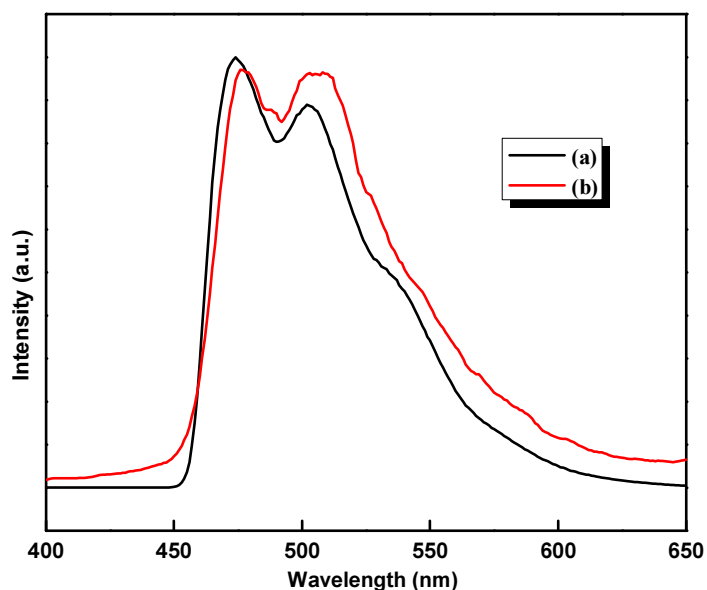


Figure 4.18. Phosphorescence spectra of (a) $\text{Gd}(\text{SiBBPPF})_3(\text{H}_2\text{O})(\text{C}_2\text{H}_5\text{OH})$ and (b) $\text{Gd}(\text{BBPPF})_3(\text{H}_2\text{O})(\text{C}_2\text{H}_5\text{OH})$ at 77K.

The triplet energy level of the **HBBPPF** ligand ($21,230 \text{ cm}^{-1}$) is found to be energetically compatible for an efficient energy transfer process between both the $^5\text{D}_0$ ($17,250 \text{ cm}^{-1}$) and $^5\text{D}_1$ ($18,800 \text{ cm}^{-1}$) emitting levels of Eu^{3+} ion. On the other

hand, 5D_2 emitting state of Eu^{3+} ($21,200 \text{ cm}^{-1}$) is found to be critically close to the triplet state of the **HBBPPF** ligand, which can lead to the thermally assisted back-energy transfer from the central core.⁷³ However, the triplet energy level of the chelating phosphine oxide, **DDXPO** ($23,470 \text{ cm}^{-1}$) is found to be compatible for efficient energy transfer with all the 5D_2 , 5D_1 and 5D_0 energy levels of Eu^{3+} ion. Based on the preceding observations, the schematic representation of energy level diagrams showing the possible energy transfer pathways for the complex, **Eu(BBPPF)₃(DDXPO)**, is depicted in Figure 4.19.

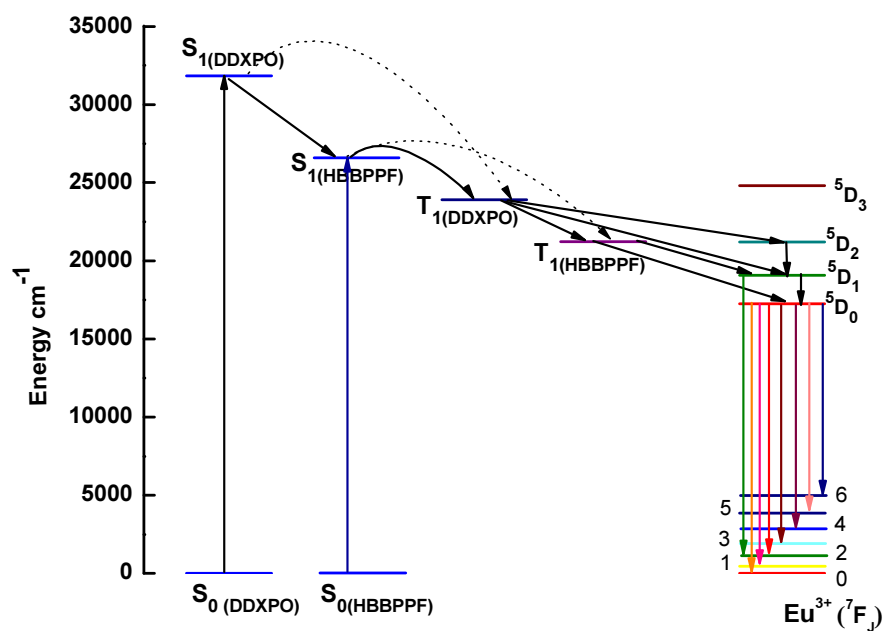


Figure 4.19. Schematic energy level diagram and energy transfer processes for **Eu(BBPPF)₃(DDXPO)**.

4.5. Conclusions

In summary, a highly luminescent Eu^{3+} ternary complex has been covalently immobilized in the ordered MCM-41 mesoporous host through modification of a novel polyfluorinated β -diketonate, 1-(3,5-bis(benzyloxy)phenyl)-4,4,5,5,5-pentafluoropentane-1,3-dione with 3-(triethoxysilyl)propyl isocyanate by a co-condensation route. The designed mesoporous inorganic-organic hybrid material was fully characterized by various techniques, and its photophysical properties were evaluated. The photophysical properties of the developed hybrid material, **Eu(BBPPF-Si)₃(DDXPO)/MCM-41**, revealed that luminescence occurs through intramolecular energy transfer from the modified bidentate polyfluorinated β -diketonate and chelating phosphine oxide ligands to the central Eu^{3+} ions. The hybrid material exhibits higher $^5\text{D}_0$ quantum efficiency ($\Phi_{\text{Eu}} = 66\%$), absolute quantum yield ($\Phi_{\text{overall}} = 43\%$) and longer lifetime ($\tau = 0.86$ ms) values as compared to that of the parent europium(III) ternary complex, **Eu(BBPPF)₃(DDXPO)**. In addition, the present reported values are found to be superior to that of europium(III) ternary complex, $\text{Eu}(\text{tta})_3(\text{phen})$ covalently bonded with mesoporous material SBA-15 ($\Phi_{\text{Eu}} = 45\%$; $\Phi_{\text{overall}} = 22\%$; $\tau = 0.52$ ms)⁷⁰ and ethyl[3-(2-pyridyl)-1-pyrazolyl]acetate functionalized MCM-41 mesoporous hybrid material, $\text{Eu}(\text{NTA})_3(\text{ethyl}[3-(2\text{-pyridyl})\text{-1-pyrazolyl]acetate})$, ($\Phi_{\text{Eu}} = 21\%$; $\Phi_{\text{overall}} = 15\%$; $\tau = 0.23$ ms)⁶⁹ reported so far in the literature. Most importantly, the current designed luminescent mesoporous hybrid material shows high colour purity, thus rendering as an excellent candidate for use in various photonic applications.

4.6. References

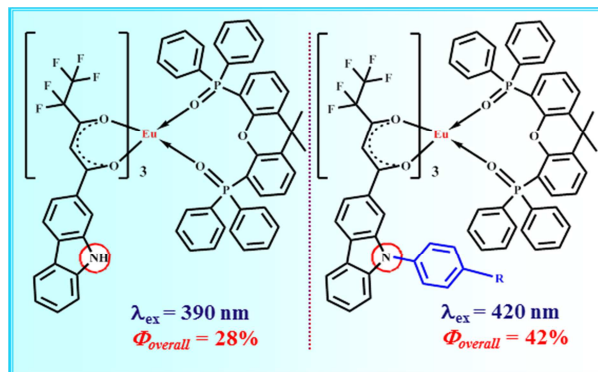
1. J. Kido and Y. Okamoto, *Chem. Rev.*, 2002, **102**, 2357-2368.
2. J.-C. G. Bünzli and C. Piguet, *Chem. Soc. Rev.*, 2005, **34**, 1048-1077.
3. K. Kuriki, Y. Koike and Y. Okamoto, *Chem. Rev.*, 2002, **102**, 2347-2356.
4. A. Polman and F. C. J. M. van Veggel, *Journal of the Optical Society of America B*, 2004, **21**, 871-892.
5. C. P. Montgomery, B. S. Murray, E. J. New, R. Pal and D. Parker, *Acc. Chem. Res.*, 2009, **42**, 925-937.
6. J.-C. G. Bünzli, *Chem. Rev.*, 2010, **110**, 2729-2755.
7. S. V. Eliseeva and J.-C. G. Bünzli, *Chem. Soc. Rev.*, 2010, **39**, 189-227.
8. J.-M. Lehn, *Angew. Chem. Int. Ed.*, 1990, **29**, 1304-1319.
9. N. Sabbatini, M. Guardigli and J.-M. Lehn, *Coord. Chem. Rev.*, 1993, **123**, 201-228.
10. S. I. Weissman, *J. Chem. Phys.*, 1942, **10**, 214-217.
11. N. M. Shavaleev, S. V. Eliseeva, R. Scopelliti and J.-C. G. Bünzli, *Chem. Eur. J.*, 2009, **15**, 10790-10802.
12. S. Biju, M. L. P. Reddy, A. H. Cowley and K. V. Vasudevan, *Cryst. Growth Des.*, 2009, **9**, 3562-3569.
13. S. Sivakumar, M. L. P. Reddy, A. H. Cowley and K. V. Vasudevan, *Dalton Trans.*, 2010, **39**, 776-786.
14. S. Biju, D. B. A. Raj, M. L. P. Reddy and B. M. Kariuki, *Inorg. Chem.*, 2006, **45**, 10651-10660.
15. A. R. Ramya, M. L. P. Reddy, A. H. Cowley and K. V. Vasudevan, *Inorg. Chem.*, 2010, **49**, 2407-2415.
16. P. N. Remya, S. Biju, M. L. P. Reddy, A. H. Cowley and M. Findlater, *Inorg. Chem.*, 2008, **47**, 7396-7404.
17. J. M. Stanley, X. Zhu, X. Yang and B. J. Holliday, *Inorg. Chem.*, 2010, **49**, 2035-2037.
18. O. Moudam, B. C. Rowan, M. Alamiry, P. Richardson, B. S. Richards, A. C. Jones and N. Robertson, *Chem. Commun.*, 2009, 6649-6651.
19. L.-N. Sun, J.-B. Yu, G.-L. Zheng, H.-J. Zhang, Q.-G. Meng, C.-Y. Peng, L.-S. Fu, F.-Y. Liu and Y.-N. Yu, *Eur. J. Inorg. Chem.*, 2006, **2006**, 3962-3973.
20. H. J. Batista, A. V. M. de Andrade, R. L. Longo, A. M. Simas, G. F. de Sá, N. K. Ito and L. C. Thompson, *Inorg. Chem.*, 1998, **37**, 3542-3547.
21. D. B. A. Raj, B. Francis, M. L. P. Reddy, R. R. Butorac, V. M. Lynch and A. H. Cowley, *Inorg. Chem.*, 2010, **49**, 9055-9063.
22. D. B. Ambili Raj, S. Biju and M. L. P. Reddy, *Dalton Trans.*, 2009, 7519-7528.
23. N. S. Baek, M. K. Nah, Y. H. Kim and H. K. Kim, *J. Lumin.*, 2007, **127**, 707-712.
24. G. A. Hebbink, L. Grave, L. A. Woldering, D. N. Reinhoudt and F. C. J. M. van Veggel, *J. Phys. Chem. A*, 2003, **107**, 2483-2491.
25. K. Binnemans, *Chem. Rev.*, 2009, **109**, 4283-4374.
26. L. Armelao, G. Bottaro, S. Quici, M. Cavazzini, M. C. Raffo, F. Barigelletti and G. Accorsi, *Chem. Commun.*, 2007, 2911-2913.
27. P. Escribano, B. Julian-Lopez, J. Planelles-Arago, E. Cordoncillo, B. Viana and C. Sanchez, *J. Mater. Chem.*, 2008, **18**, 23-40.

28. S. Quici, C. Scalera, M. Cavazzini, G. Accorsi, M. Bolognesi, L. Armelao and G. Bottaro, *Chem. Mater.*, 2009, **21**, 2941-2949.
29. C. Peng, H. Zhang, J. Yu, Q. Meng, L. Fu, H. Li, L. Sun and X. Guo, *J. Phys. Chem. B*, 2005, **109**, 15278-15287.
30. L. D. Carlos, R. A. S. Ferreira, V. d. Z. Bermudez and S. J. L. Ribeiro, *Adv. Mater.*, 2009, **21**, 509-534.
31. J. Feng and H. Zhang, *Chem. Soc. Rev.*, 2013, **42**, 387-410.
32. Q. Xu, L. Li, X. Liu and R. Xu, *Chem. Mater.*, 2002, **14**, 549-555.
33. B. Yan and Q.-M. Wang, *Cryst. Growth Des.*, 2008, **8**, 1484-1489.
34. E. DeOliveira, C. R. Neri, O. A. Serra and A. G. S. Prado, *Chem. Mater.*, 2007, **19**, 5437-5442.
35. Y. Li, B. Yan and H. Yang, *J. Phys. Chem. C*, 2008, **112**, 3959-3968.
36. H. Li, W. Cheng, Y. Wang, B. Liu, W. Zhang and H. Zhang, *Chem. Eur. J.*, 2010, **16**, 2125-2130.
37. D. Dong, S. Jiang, Y. Men, X. Ji and B. Jiang, *Adv. Mater.*, 2000, **12**, 646-649.
38. H. Zhang, Y. Xu, W. Yang and Q. Li, *Chem. Mater.*, 2007, **19**, 5875-5881.
39. F. Liu, L. Fu, J. Wang, Z. Liu, H. Li and H. Zhang, *Thin Solid Films*, 2002, **419**, 178-182.
40. A.-C. Franville, D. Zambon, R. Mahiou and Y. Troin, *Chem. Mater.*, 2000, **12**, 428-435.
41. H. R. Li, J. Lin, H. J. Zhang, L. S. Fu, Q. G. Meng and S. B. Wang, *Chem. Mater.*, 2002, **14**, 3651-3655.
42. K. Binnemans, P. Lenaerts, K. Driesen and C. Gorller-Walrand, *J. Mater. Chem.*, 2004, **14**, 191-195.
43. D. B. Ambili Raj, S. Biju and M. L. P. Reddy, *J. Mater. Chem.*, 2009, **19**, 7976-7983.
44. M. S. Wrighton, D. S. Ginley and D. L. Morse, *J. Phys. Chem.*, 1974, **78**, 2229-2233.
45. M. Cölle, J. Gmeiner, W. Milius, H. Hillebrecht and W. Brütting, *Adv. Funct. Mater.*, 2003, **13**, 108-112.
46. N. S. S. Kumar, S. Varghese, N. P. Rath and S. Das, *J. Phys. Chem. C*, 2008, **112**, 8429-8437.
47. S. V. Eliseeva, O. V. Kotova, F. Gumy, S. N. Semenov, V. G. Kessler, L. S. Lepnev, J.-C. G. Bünzli and N. P. Kuzmina, *J. Phys. Chem. A*, 2008, **112**, 3614-3626.
48. W. H. Zhang, X. B. Lu, J. H. Xiu, Z. L. Hua, L. X. Zhang, M. Robertson, J. L. Shi, D. S. Yan and J. D. Holmes, *Adv. Funct. Mater.*, 2004, **14**, 544-552.
49. M. Jia, A. Seifert and W. R. Thiel, *Chem. Mater.*, 2003, **15**, 2174-2180.
50. S. M. Bruno, A. C. Coelho, R. A. S. Ferreira, L. D. Carlos, M. Pillinger, A. A. Valente, P. Ribeiro-Claro and I. S. Gonçalves, *Eur. J. Inorg. Chem.*, 2008, **2008**, 3786-3795.
51. C. Tiseanu, V. I. Parvulescu, M. U. Kumke, S. Dobroiu, A. Gessner and S. Simon, *J. Phys. Chem. C*, 2009, **113**, 5784-5791.
52. X.-F. Qiao and B. Yan, *Inorg. Chem.*, 2009, **48**, 4714-4723.
53. X. Qiao and B. Yan, *J. Phys. Chem. B*, 2008, **112**, 14742-14750.
54. C. T. Kresge, M. E. Leonowicz, W. J. Roth, J. C. Vartuli and J. S. Beck, *Nature*, 1992, **359**, 710-712.
55. Y.-S. Lin, Y. Hung, J.-K. Su, R. Lee, C. Chang, M.-L. Lin and C.-Y. Mou, *J. Phys. Chem. B*, 2004, **108**, 15608-15611.

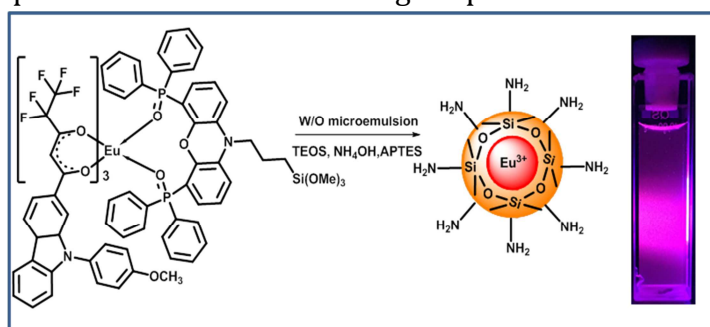
56. J. S. Beck, J. C. Vartuli, W. J. Roth, M. E. Leonowicz, C. T. Kresge, K. D. Schmitt, C. T. W. Chu, D. H. Olson and E. W. Sheppard, *J. Am. Chem. Soc.*, 1992, **114**, 10834-10843.
57. S. Gago, J. A. Fernandes, J. P. Rainho, R. A. Sá Ferreira, M. Pillinger, A. A. Valente, T. M. Santos, L. D. Carlos, P. J. A. Ribeiro-Claro and I. S. Gonçalves, *Chem. Mater.*, 2005, **17**, 5077-5084.
58. M. Kruk and M. Jaroniec, *Chem. Mater.*, 2001, **13**, 3169-3183.
59. S. Cousinié, M. Gressier, C. Reber, J. Dexpert-Ghys and M.-J. Menu, *Langmuir*, 2008, **24**, 6208-6214.
60. D. B. A. Raj, S. Biju and M. L. P. Reddy, *Inorg. Chem.*, 2008, **47**, 8091-8100.
61. K. Binnemans, *Coord. Chem. Rev.*, 2015, **295**, 1-45.
62. P. Lenaerts, K. Driesen, R. Van Deun and K. Binnemans, *Chem. Mater.*, 2005, **17**, 2148-2154.
63. J. Kai, D. F. Parra and H. F. Brito, *J. Mater. Chem.*, 2008, **18**, 4549-4554.
64. M.-S. Liu, Q.-Y. Yu, Y.-P. Cai, C.-Y. Su, X.-M. Lin, X.-X. Zhou and J.-W. Cai, *Cryst. Growth Des.*, 2008, **8**, 4083-4091.
65. G. F. de Sá, O. L. Malta, C. de Mello Donegá, A. M. Simas, R. L. Longo, P. A. Santa-Cruz and E. F. da Silva Jr, *Coord. Chem. Rev.*, 2000, **196**, 165-195.
66. M. Xiao and P. R. Selvin, *J. Am. Chem. Soc.*, 2001, **123**, 7067-7073.
67. S. Quici, M. Cavazzini, G. Marzanni, G. Accorsi, N. Armaroli, B. Ventura and F. Barigelletti, *Inorg. Chem.*, 2005, **44**, 529-537.
68. S. Comby, D. Imbert, A.-S. Chauvin, J.-C. G. Bünzli, L. J. Charbonnière and R. F. Ziessel, *Inorg. Chem.*, 2004, **43**, 7369-7379.
69. S. M. Bruno, R. A. Sá Ferreira, L. D. Carlos, M. Pillinger, P. Ribeiro-Claro and I. S. Gonçalves, *Microporous Mesoporous Mater.*, 2008, **113**, 453-462.
70. X. Guo, H. Guo, L. Fu, R. Deng, W. Chen, J. Feng, S. Dang and H. Zhang, *J. Phys. Chem. C*, 2009, **113**, 2603-2610.
71. R. A. Sá Ferreira, M. Karmaoui, S. S. Nobre, L. D. Carlos and N. Pinna, *ChemPhysChem*, 2006, **7**, 2215-2222.
72. H. Xu, L.-H. Wang, X.-H. Zhu, K. Yin, G.-Y. Zhong, X.-Y. Hou and W. Huang, *J. Phys. Chem. B*, 2006, **110**, 3023-3029.
73. N. Armaroli, G. Accorsi, F. Barigelletti, S. M. Couchman, J. S. Fleming, N. C. Harden, J. C. Jeffery, K. L. V. Mann, J. A. McCleverty, L. H. Rees, S. R. Starling and M. D. Ward, *Inorg. Chem.*, 1999, **38**, 5769-5776.

Summary of the Thesis

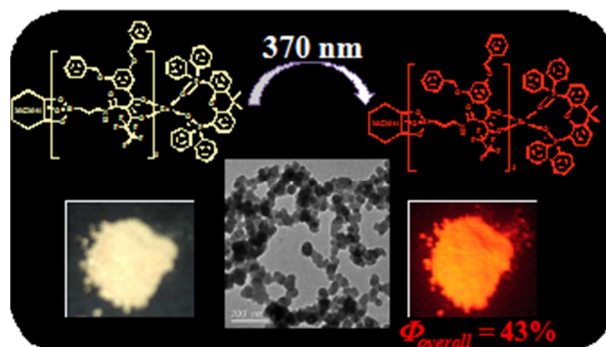
Tuning of excitation wavelength from UV to visible region: In the first working chapter, molecular engineering is successfully employed in achieving remarkable improvements in the thermal stabilities, photophysical properties and in extending the excitation window into the visible region for the novel carbazole-based Eu^{3+} - β -diketonate complexes. This shift achieved from near UV to visible blue region is important in the context of biological imaging as long term exposure of near UV light may destroy the cells under study and also the surrounding cells around the target area, in case of *in vivo* experiments.



Visible light excitable luminescent silica nanoparticles: A novel bidentate phosphine oxide molecule was synthesized and used as neutral donor for carbazole-based Eu^{3+} - β -diketonate complexes in the second working chapter. The resulted Eu^{3+} -complex was then used for the development of photostable and water dispersible luminescent silica nanoparticles which were used for bio-imaging studies with HeLa cells. The interesting photophysical properties of the developed biocompatible nanoparticles make them ideal for various biological applications.



Eu^{3+} -based luminescent hybrid material: In the third working chapter, an organic-inorganic mesoporous hybrid material was constructed by linking a novel Eu^{3+} - β -diketonate complex into the mesoporous MCM-41. The developed hybrid material exhibited superior photophysical properties such as better colour purity, luminescence quantum yield and excited state lifetime compared to the parent Eu^{3+} -complex, thus rendering as an excellent candidate for use in various photonic applications.



Papers Presented at Conferences

1. V. Divya, **Biju Francis**, Ricardo O. Friere and M. L. P. Reddy, “Highly efficient visible light excited red emitting materials for OLED applications”, STAR 2011, Munnar, Kerala, India.
2. **Biju Francis**, Ambili Raj D. B. and M. L. P. Reddy, “Structure-property relationship in luminescent europium complexes: Tuning of excitation energy towards visible light” 15th CRSI-NSC & 7th CRSI-RSC Symposium 2013, Banaras Hindu University, Varanasi, India.

List of Publications

1. Highly efficient luminescent hybrid materials covalently linking with europium(III) complexes *via* a novel fluorinated β -diketonate ligand: synthesis, characterization and photophysical properties, **Biju Francis**, D. B. Ambili Raj and M. L. P. Reddy. *Dalton Trans.*, 2010, **39**, 8084–8092.
2. Highly Luminescent Poly(Methyl Methacrylate)-Incorporated Europium Complex Supported by a Carbazole-Based Fluorinated β -Diketonate Ligand and a 4,5-Bis(diphenylphosphino)-9,9-dimethylxanthene Oxide Co-Ligand, D. B. Ambili Raj, **Biju Francis**, M. L. P. Reddy, Rachel R. Butorac, Vincent M. Lynch, and Alan H. Cowley. *Inorg. Chem.*, 2010, **49**, 9055–9063.
3. Achieving visible light excitation in carbazole based Eu^{3+} - β -diketonate complexes *via* molecular engineering, **Biju Francis**, Christian Heering, Ricardo O. Freire, M. L. P. Reddy and Christoph Janiak. *RSC Adv.*, 2015, **5**, 90720–90730.
4. Amine functionalized silica nanoparticles incorporating covalently linked visible light excitable Eu^{3+} complexes: Synthesis, characterization and cell uptake studies, **Biju Francis**, Bernhard Neuhaus, M. L. P. Reddy, Mathias Epple and Christoph Janiak. *Manuscript to be communicated*.